Title

The role of caveolin-associated microdomains in adult cardiac myocytes : cAMP and cytoskeletal assembly

Author

Head, Brian P.

Publication Date

2005

Peer reviewed|Thesis/dissertation

UNIVERSITY OF CALIFORNIA, SAN DIEGO

The role of caveolin-associated microdomains in
adult cardiac myocytes:
cAMP and cytoskeletal assembly

A dissertation submitted in partial satisfaction of the requirements for
the degree of Doctor of Philosophy

in

Molecular Pathology
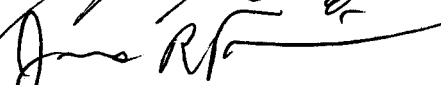

by

Brian P. Head

Committee in charge:

> Professor Paul A. Insel, chair
> Professor Marilyn G. Farquhar
> Professor James R. Feramisco
> Professor David M. Roth
> Professor Wolfgang H. Dillmann

2005

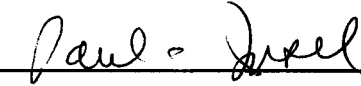This dissertation of Brian P. Head is approved, and is

acceptable in quality and form for publication on microfilm:

_____

_____

_____

_____

_____
                                                    Chair

University of Calfornia, San Diego

2005

TABLE OF CONTENTS

LIST OF ABBREVIATIONS

adenylyl cyclase, AC

adult cardiac fibroblast, ACF

β-adrenergic receptor, β-AR

buoyant fraction, BF

cardiac myocyte, CM

caveolin, Cav

colchicine, Colch

cytochalasin D, CD

dihydropyridine receptor, DHPR

G protein-coupled receptor, GPCR

heavy fraction, HF

human coronary artery smooth muscle cell, hCASMC

methyl-β-cyclodextran, MβCD

muscarinic receptor, M-mAChR

nocodazole, Nocod

opioid receptor, OR

phosphorylated caveolin, P-Cav

phosphorylated p38 mitogen-activated protein kinase, P-p38

phosphorylated Src tyrosine kinase, P-Src

ryanodine receptor, RyR

sarcoplasmic reticulum, SR

transverse tubule, T-tubule

LIST OF FIGURES

ACKNOWLEDGEMENT

This dissertation is dedicated to my Father, Patrick (b. 1932, d. 2003), and to my Mother, Eleanor (b. 1937). I am forever thankful to them for their words of encouragement, teachings of morality and integrity, and for their passionate pursuit of true knowledge.

The James Feramisco Laboratory

I would like to thank the UCSD Cancer Center Digital Imaging Shared Resource, in particular Julie Sherman and Steve McMullen for their technical assistance. I also would like to thank Dr. James Feramisco for his guidance and advice regarding technical approaches for immunofluorescence and deconvolution microscopy. Because of Jim's guidance I was able to ask the right questions, approach them with the proper experimental techniques, and use the best software available to analyze my data most appropriately.

The David M. Roth Laboratory

I would like to thank Dr. David M. Roth for his patience to teach me how to isolate adult cardiac myocytes. This is an extremely difficult technique that takes a lot of research, experimental trouble shooting, and overall patience. If it were not for Dave and Jeff Drum, the scientific material that fueled this thesis would have never been available.

The Wolfgang H. Dillmann Laboratory

I would like to thank Dr. Dillmann for his time and availability to be a member of my thesis committee. Dr. Dillmann is an expert in myocyte biology and his comments and advice during my major proposition examination and towards my dissertation was greatly appreciated.

The Marilyn G. Farquhar Laboratory

I would like to thank Ingrid Niesman for all of her technical assistance with both fluorescence and electron microscopy. Ingrid generated all the electron microscopic images for this dissertation. Ingrid was very helpful and supportive with my work and both efficient and professional with her ideas and approaches. In regards to Dr. Farquhar, there are few better teachers out there than her. Marilyn was very generous with her time and advice regarding my project. She taught me how to ask cell biological questions and how to answer them with the correct approaches. In addition, she showed me the correct manner in which to critically examine the literature in addition to my own results. I know that very few are as fortunate as I was to learn and receive advice from Dr. Farquhar.

The Paul A. Insel Laboratory

I am greatly indebted to all of the members of the Insel lab for their support, advice, and technical assistance during the five plus years I attended UCSD's Molecular Pathology Graduate Program. I especially would like to thank Paul himself, for allowing me the opportunity to work and conduct my thesis in his lab. Paul taught me that there is a lot

more than just accumulating data. He taught me how to convey my points both on paper and in front of an audience. He also allowed me great independence with my project, including pursuing research ideas that were always of interest to me, even prior to joining his lab. Paul was always supportive with collaborations with others and believed no ideas were impossible to pursue. Paul always enjoyed engaging in scientific dialogue and discussions and never refused anyone's input. In Dr. Insel's lab I learned a great amount of pharmacology, cell biology and physiology, and how these fields of study are applicable to molecular pathology.

Publications

The text of Chapter Two is a reprint of the material as it appears in Journal of Biological Chemistry. I was the primary author and the co-authors listed in this publication directed and supervised the research which forms the basis for this chapter.

The text of Chapter Four has been submitted for publication. I was the primary author and the co-authors listed in this publication directed and supervised the research which forms the basis for this chapter.

VITA

1994   B.A., Georgetown University

1996-2001   M.S., University of San Diego

2000-2005   Ph.D., University of California, San Diego

PUBLICATIONS

Head BP, Patel HH, Niesman IR, Roth DM, Farquhar MG, and Insel PA. Cytoskeletal components regulate expression of caveolae, caveolin phosphorylation and cAMP production. Submitted to *J Biol Chem.*

Patel HH, Head BP, Petersen HN, Niesman IR, Feramisco JR, Farquhar MG, Gross GJ, Insel PA, and Roth DM. Protection of adult rat cardiomyocytes from ischemic cell death: role of caveolar microdomains and opioid receptors. Submitted to *American Journal of Physiology*.

Insel PA, Head BP, Patel HH, Roth DM, Niesman IR, Farquhar MG, and Bundey R. Compartmentation of G-protein-coupled receptors and their signaling components in lipid rafts and caveolae. *Biochem Soc Transact.* (In press).

Insel PA, Head BP, Ostrom RS, Patel HH, Swaney JS, Tang C-M, Roth DM. Caveolae and lipid rafts: G-protein-coupled receptor signaling microdomains in cardiac myocytes. *Annals of NY Acad Sci,* 1047: 166-172, 2005.

Head BP, Patel HH, Lai NC, Niesman IR, Roth DM, Farquhar MG, and Insel PA. 2005. G-protein coupled receptor signaling components localize in both sarcolemmal and intracellular Caveolin-3-associated microdomains in adult rat cardiac myocytes. *J Biol Chem.* 280: 31036-31044, 2005.

Ostrom RS, Liu X, Head BP, Gregorian C, Seasholtz TM, Insel PA. 2002. Localization of adenylyl cyclase isoforms and G protein-coupled receptors in vascular smooth muscle cells: expression in caveolin-rich and noncaveolin domains. *Mol Pharmacol.* 62:983-9.

Lai NC, Roth DM, Gao MH, Fine S, Head BP, Zhu J, McKirnan MD, Kwong C, Dalton N, Urasawa K, Roth DA, Hammond MD. 2000. Intracoronary delivery of adenovirus encoding adenylyl cyclase VI increases left ventricular function and cAMP-generating capacity. *Circulation.* 102:2396-2401.

Head BP, Graham JB, Shabetai R, Lai NC. 2001. Regulation of cardiac function in the horn shark by changes in pericardial fluid volume mediated through the pericardioperitoneal canal. *Fish Physiol. Biochem*. 24:141-148.

ABSTRACTS

Peterson HN, Patel HH, Head BP, Roth DM, Insel PA. 2005. Expression and distribution of caveolin-1, -2, and –3 in adult rat and mouse cardiac myocytes. *FASEB* 19 (4): A663.

Head BP, Patel HH, Roth DM, Insel PA. 2005. Cytoskeletal disruption alters localization of caveolin and GPCR signaling components in caveolin-enriched membranes of adult cardiac myocytes. *FASEB* 19 (4): A1530.

Head BP, Patel HH, Roth DM, Insel PA. Ischemic preconditioning of adult rat cardiomyocytes: role of caveolar microdomains and opioid receptor sub-types. *Anesth Analg* 98: SCA 52, 2004.

Head BP, Roth DM, Niesman IR, Farquhar MG, Insel PA. 2004. Caveolin-3, a muscle specific caveolae marker, is present on the sarcolemma, within intracellular vesicles and in the core of fibers in adult cardiac myocytes. Molecular Cell Biology of Lipid Domains-*Keyston Symposia*. Abstract 208.

Head BP, Ostrom RS, Ander AN, Roth DM, Insel PA. 2002. Caveolar microdomains concentrate signal transduction of β_1-adrenergic receptors, but not β_2-adrenergic receptors in adult rat cardiac myocytes. *Circulation*, 106 (19): II-48.

Head BP, Graham JB, Lai NC. 2000. Pericardial pressure return in the California horn shark. *FASEB* 14 (4): A436

Lai NC, Roth DM, Gao MH, Head BP, Zhu J, Hammond HK (1999) Intracoronary delivery of an adenovirus expressing adenylylcyclase VI is associated with marked global changes in LV function and cardiac output in conscious pigs. *Circulation,* 100 (18): I-107 #550.

ABSTRACT OF THE DISSERTATION

The role of caveolin-associated microdomains in adult cardiac myocytes:

cAMP and cytoskeletal assembly

by

Brian Patrick Head

Doctor of Philosophy in Molecular Pathology

University of California, San Diego, 2005

Professor Paul A. Insel, Chair

Caveolae-localized signaling microdomains are proposed sites that concentrate G protein-coupled receptors (GPCR), heterotrimeric G-proteins, GPCR/G-protein-regulated effector molecules, and gaseous enzymes involved in generating free radicals and antioxidants, such as heme oxygenase (HO) and nitric oxide synthase (NOS), in a confined region, so as to facilitate coordinated and rapid generation of second messengers and regulation of cell function. The effectiveness of these signaling cascades is dependent upon the organization and location of key signaling proteins within the plasma membrane. Caveolae, "little caves", a subset of lipid rafts, are cholesterol- and sphingolipid- enriched 50-100 nm invaginations of the plasma membrane that contain isoforms of the structural protein caveolin (Cav-1, -2, and –3). Defining the localization and interaction of GPCR and gaseous signaling components in normal adult cardiac myocytes (CM) is thus essential for understanding signaling cascades that regulate developmental and pathological

changes in the heart. Microtubules and microfilaments help regulate plasma membrane topography but their role in compartmentation of caveolar-resident signaling components involved in cAMP production has not been defined. The present study used adult rat cardiac myocytes (CM) to investigate whether 1) GPCR, G-proteins, effector enzymes, and gaseous signaling components (heme oxygenae (HO) and endothelial nitric oxide synthase (eNOS)) involved in free radical generation, localize with caveolin in both sarcolemmal and intracellular membrane regions, and 2) if cytoskeletal disruption influences localization of caveolin (Cav) and expression of caveolae, thereby altering the distribution of G protein-coupled receptor (GPCR) signaling components and cAMP production. The observed distribution of GPCRs, G-proteins, and AC with Cav-3 on both sarcolemmal and intracellular regions defines unique cellular microdomains for regulation and signaling by hormones and drugs in the adult heart. The localization of HO-1 and eNOS with caveolin, and the close apposition between caveolae and mitochondria suggests that caveolae in addition to being sites that generate gaseous signaling components (i.e. CO and NO) may also be sites for generation of antioxidants (biliverdin), and thus "sinks" for free radicals in adult CM. Disruption microtubules and microfilaments alters the expression of caveolae, phosphorylation state of caveolins, and ability of caveolins to blunt GPCR-AC signal transduction.

Chapter 1

Introduction
Caveolae, Caveolins, and Compartmentation

PLASMA MEMBRANE AND LIPID RAFTS (CAVEOLAE)

For several decades, the fluid mosaic model theorized by Singer and Nicolson [1] provided the foundation for understanding the structure of cellular membranes. This model viewed membrane proteins as "icebergs" floating in a "sea" of lipids. However, work over the past decade has demonstrated that the plasma membrane is not a random ocean of lipids, but rather a region in which there are discrete structures that organize proteins within the bilayer. These lipid structures within the membrane are termed lipid rafts.
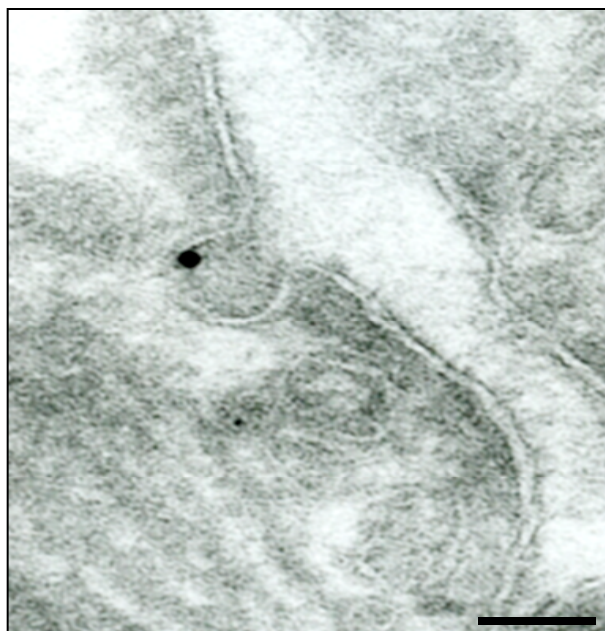
Fig. 1-1. Immunoelectron microscopy reveals immunogold lebeling of Cav-3 (10 nm) on a flask like invagination of the sarcolemmal membrane in isolated adult rat ventricular cardiac myoyctes. Scale bar 0.05 μm.

Today, we know the plasma membrane to exist as a lipid bilayer with both liquid-disordered and liquid-ordered domains. In the liquid-disordered state, the phospholipids

are capable of lateral diffusion, while the liquid-ordered domains generate a more rigid

bilayer organization. In the latter state the movement of phospholipids is confined due to

the arrangement of glycosphingolipids, sphingomyelin, and cholesterol into lipid rafts [2].

A subset of lipid rafts termed caveolae, or "little caves" are cholesterol and sphingolipid

enriched invaginations of the plasma membrane 50-100 nm in size (Fig. 1-1) [3-5]. These

lipid rafts are insoluble in detergent buffers and are more buoyant than the remaining

plasma membrane due to their cholesterol content, which allows them to be isolated

through density gradient purification techniques [6-8]. Agents used to remove cholesterol,

such as filipin and β-cyclodextrin, create a loss of morphologically identifiable caveolae,

which eventually leads to the removal of the structural protein, caveolin, from the

flattened plasma membrane [9, 10]. Caveolin, the structural protein that is essential for

caveolae formation, is present in three isoforms [11, 12] and has been implicated in signal

transduction [13-17], specialized endocytic uptake [18], calcium homeostasis [19-21], and

transverse tubule (T-tubule) formation during myocyte development [11]. The multiplicity

of suggested roles for caveolin raises the question of whether variations in the cellular

distribution and function of caveolin are cell-type-dependent.

GPCR COMPARTMENTATION AND CYCLIC AMP

There exists a large body of evidence demonstrating caveolin-associated

compartmentation of components involved in 3', 5' cycle adenosine monophosphate

production (cAMP) in cardiac tissue and non-cardiac cell types [22-24]. More specifically,

components involved in GPCR signaling, i.e. certain receptors, G-proteins and G-protein

regulated effectors, cAMP-dependent protein kinase (PKA), enzymes involved in

generating gaseous signaling molecules and antioxidants (i.e., NO, CO, biliverdin) have

been shown to localize with caveolin in the plasma membrane of numerous cell types [5, 14,

25-32]. The "caveolin/lipid raft signaling hypothesis" proposes that compartmentation of

signaling molecules in caveolae is a mechanism for temporal and spatial signal transduction

and cross-talk among signaling pathways [15]. In spite of substantial data from *neonatal*

cardiac myocytes and other non-striated myocyte cells supporting this notion [16, 33], little

is known about the potentially different roles that caveolin plays as a scaffold for

signaling components in *mature/adult* cardiac cells and whether such components exist in

non-surface sarcolemmal membrane locations.
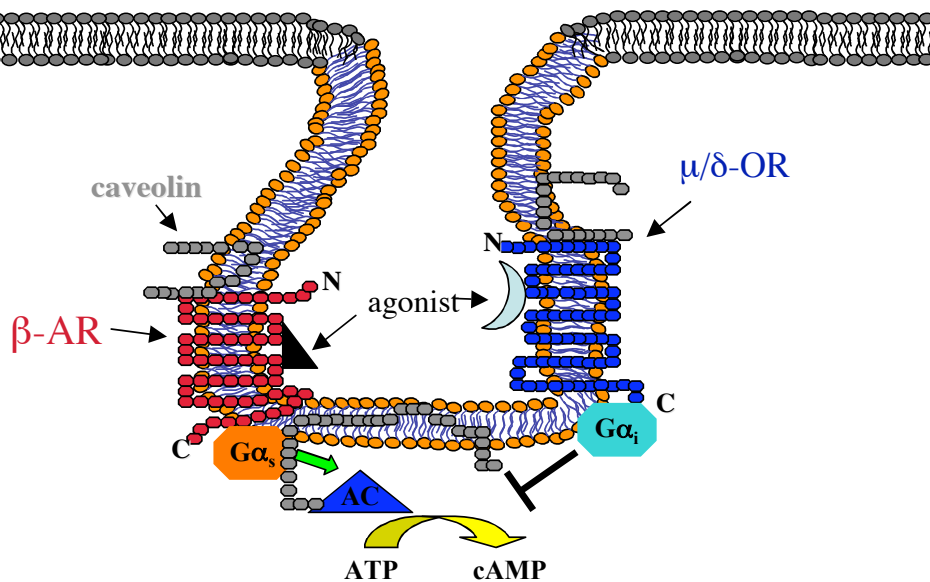
Fig. 1-2. Schematic depicting GPCR signaling components involved in regulating cAMP formation localizing to a caveolar microdomain.

The sympathetic nervous system, with its release of norepinephrine as a neurotransmitter, and circulating catecholamines stimulate cardiac β-adrenergic receptors (β-AR). Under normal physiological conditions, cAMP elevation through stimulation of the β-AR-$G\alpha_s$-AC pathway increases both rate (chronotropy) and force of contraction (inotropy) and force of relaxation (lusitropy) (Fig. 1-2). This signaling pathway is considered the principal physiological mechanism for production of the second messenger cAMP in the mammalian heart, in particular by cardiac myocytes. The effectiveness of this signaling cascade is dependent upon the location and compartmentation of these key signaling proteins within the sarcolemmal caveolin-associated microdomains [9, 34, 35]. In essence a heartbeat occurs when an excitation induces a change in membrane potential, or action potential (A.P.) resulting in a transient increase in intracellular $[Ca^{2+}]$ that drives interactions between contractile proteins and subsequent cardiac myocyte contraction.

Calcium influx into and efflux from the cell is regulated by signaling proteins and channels within the sarcolemmal (plasma) membrane and intracellular membranes [36]. Ca^{2+} entry triggers Ca^{2+} release from the sarcoplasmic reticulum (SR) via ryanodine receptors (RyR), which allows calcium to bind the myofilament protein troponin C, which then switches on the contractile machinery. This movement of calcium among organelles and its linkage to myocyte contractility is termed the excitation-contraction coupling (ECC) (Fig. 1-3). To achieve cardiac relaxation, Ca^{2+} dissociates from the contractile proteins and is exported out of the cytosol by four pathways: SR Ca^{2+}-ATPase, sarcolemmal Na/Ca exchange, sarcolemmal Ca^{2+}-ATPase (a.k.a. mitochondrial Ca^{2+} uniport). The

effectiveness of this signaling cascade is dependent upon numerous factors; these include

levels of expression of the membrane components in the signaling pathway as well as

their location within these membranes. Several studies have shown that caveolin not only

localizes with β-AR, Gα_s, and AC in the sarcolemma of adult cardiac cells, but in addition

localizes with calcium channels (i.e., DHPR, RyR) near the T- tubule/sarcoplasmic

reticulum junction (dyad), suggesting that there are multiple populations of caveolin that

localize receptors and ion channels involved in intracellular calcium regulation [37-41].
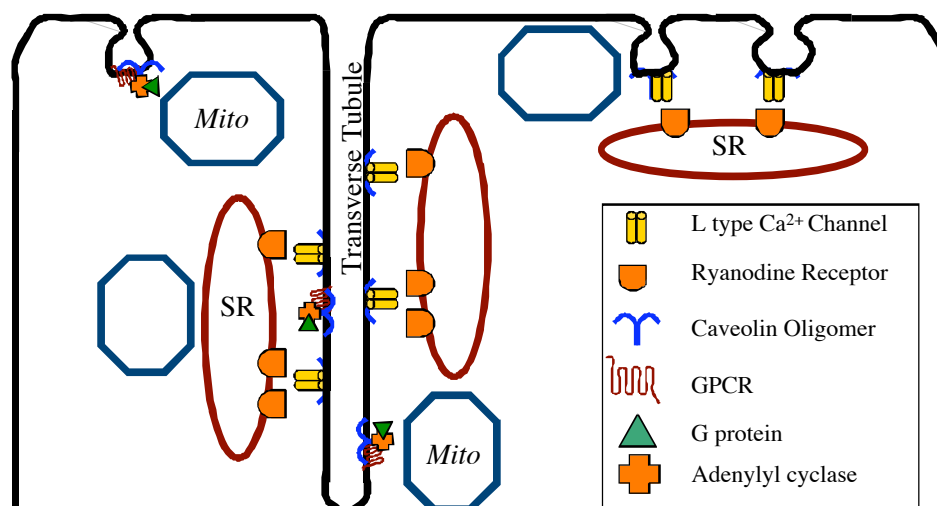
Fig. 1-3. Schematic showing caveolin oligomers scaffolding L-type Ca^{2+} channels proximal to the ryanodine receptor and sarcoplasmic reticulum in both sarcolemmal caveolae and T-tubule regions.

CAVEOLIN

Caveolin is the structural protein that is essential for caveolar formation and is

present in three isoforms [11]. Caveolin-1 and –2 (Cav-1 or –2) are found primarily in

endothelial, epithelial, smooth muscle cells, and fibroblasts. Cav-1 and Cav-2 form

hetero-oligomers of approximately 15 monomers following synthesis of Cav-1 in the endoplasmic reticulum (ER) and prior to transport to the Golgi apparatus [42]. Cav-2 is dependent upon Cav-1 for localization to caveolae, and in the absence of Cav-1, Cav-2 remains in the Golgi apparatus [43, 44]. Cav-3, the muscle specific isoform, is found exclusively in skeletal and cardiac myocytes, with the exception of certain smooth muscle cells, and forms homo-oligomer complexes [45]. Rybin et al. (2003) showed that both Cav-2 and Cav-3 are present in buoyant membrane fractions isolated from neonatal and two month old rat cardiac myocytes, yet there is still dispute over whether all caveolin subtypes are expressed in adult cardiac myocytes. All three isoforms possess a structural motif (FEDVIAEP) that remains conserved across species [46]. The importance of Cav-3 in caveolar formation as well as its association with T-tubules during muscle development has been emphasized [11]. In addition, studies conducted on adult rat skeletal and cardiac myocytes demonstrated the association between Cav-3 and surface sarcolemmal membrane and in the core of the fibers, more specifically I-band/A-band interface and T-tubules [40, 47], indicating that caveolin is present on both the surface sarcolemmal membrane and in non-surface sarcolemmal membrane regions. Knowledge of the cellular distribution of caveolin in various cell types is of critical importance, considering that there is evidence that suggests redistribution of caveolin isoforms during aging and pathological changes in the heart and non-cardiac cells [48, 49].

Investigating caveolin has been of considerable interest because of this scaffold-protein's ability to undergo covalent modifications (i.e., phosphorylation) following

cellular stress or insulin stimulation [50-53]. Several studies have established that Cav-1 is phosphorylated on tyrosine-14 (Tyr^{14}) by members of Src tyrosine kinase. Moreover, Cav-2 is phosphorylated on Tyr^{19} and Tyr^{27} by Src tyrosine kinase on serine 23 and 36 (Ser^{23}, Ser^{36}) by casein kinase 2 [54-56]. To date there is no evidence for Cav-3 phosphorylation; the possible tyrosine phosphorylation of Cav-3 is an interesting hypothesis that needs to be tested, especially as this modification might contribute to cardiac myocyte physiology.

KNOCKOUT OF CAVEOLIN

Studies have demonstrated that mice deficient in Cav-1 display a complete loss in morphologically identifiable caveolae in tissues that normally express the Cav-1 protein, in addition to primary cells isolated from Cav-1 knockout mice [10, 57-59]. Because caveolin serves as a binding partner for lipids and proteins, its absence may alter membrane organization and caveolar biogenesis. An example of this is well demonstrated in the Cav-1 null mice in terms of the effect on Cav-2 protein levels, which are reduced to less than 10% of wild-type levels, suggesting that Cav-2 is dependent upon Cav-1 for heteromultimeric association and trafficking to plasma membrane [60]. The absence of morphologically distinct caveolae impairs nitric oxide and calcium signaling in the cardiovascular system, resulting in impaired endothelium-dependent relaxation, contractility, and maintenance of myogenic tone [59]. A lack of caveolae was observed in lung, adipose tissue, diaphragm, kidney, and heart. In striated muscle cells (i.e., cardiac

and skeletal) that lack Cav-1, Cav-3 is still expressed and caveolar morphology was retained, however abnormal cardiac function such as an enlarged right ventricular cavity, decreased systolic function, myocyte hypertrophy, and hyperactivation of the p44/42 MAPK (Erk 1/2) cascade in cardiac tissue has been detected [59, 61], suggesting a role for Cav-1 in regulating MAP kinase signaling in cardiac muscle.

CAVEOLAE AND THE CYTOSKELETON

The cytoskeleton which is composed of three systems – intermediate filaments, microtubules, and microfilaments – contributes to the structural organization of the cytoplasm and plays a key role in the topography of the plasma membrane in animal cells [62-64]. Microtubules and microfilaments have nucleotide-binding and hydrolyzing activity, while intermediate filaments have no known enzymatic activity. Intermediate filaments are cytoskeletal 'identity cards' that serve to distinguish one cell type from another [65]. For example, vimentin marks intermediate filaments in mesenchymal cells, while proteins such as desmin, synemin, syncolin, and nestin identify the same cytoskeletal network in muscle cells [62]. Experiments involving disruption of vimentin-containing intermediate filaments result in disassembly of both microtubules and microfilaments, and demonstrate that intermediate filaments are vital for stabilizing crosstalk between microtubules and microfilaments [66].

Intermediate filaments interact and demonstrate motility along microtubules through association with molecular motors such as kinesin and dynein. Disruption of

microtubules with colchicine results in reorganization of vimentin-containing intermediate filaments, indicating dependence of intermediate filaments on proper microtubule formation [67]. Following disruption of microtubules, some components of intermediate filaments continue to move, implicating microfilaments as an alternative mode of transport [68]. Intermediate filaments interact with microfilaments primarily via myosin. Treatment with cytochalasin D, an agent that disrupts microfilaments through actin depolymerization, results in disruption of keratin-based intermediate filaments [69], consisten with the interaction between intermediate filaments and microfilaments. In mature cardiac and skeletal myocytes, the end capping proteins of actin-myosin filaments (e.g. CapZ, a-actinin, telethonin) from opposing sarcomeres overlap and contribute to the formation of the highly ordered Z-discs. Z-discs cross-link myofilaments in an organized 3-dimensional lattice and are located at the interface of the sarcomere, sarcoplasmic reticulum (SR), sarcolemma, and cytoskeleton [70]. Interestingly, intracellular signaling components, such as protein kinase A, protein kinase C and calcineurin, interact with subcellular structures and cardiac Z-discs via anchoring proteins [70], in addition to being compartmentalized to caveolae [34, 71].

Several studies have demonstrated a connection between caveolar-related cellular processes and the cytoskeleton [72-76]. Ligand-triggered endocytosis of caveolae involve rearrangement of the actin cytoskeleton, suggesting that caveolae serve as sites for actin "tail" formation [72, 75]. Additional work has demonstrated that caveolae are anchored to the cell surface by cortical actin filaments [74, 77], and that F-actin spikes stem from

organized rosette-like clusters of caveolae/lipid raft microdomains termed Cav-actin [78].

Another group that investigated whether there is a connection between caveolae and the

actin cytoskeleton identified the F-actin cross-linking protein filamin as a ligand for

caveolin and showed that the actin network is directly involved in the spatial organization

of caveolin-associated microdomains (Fig. 1-4) [73].
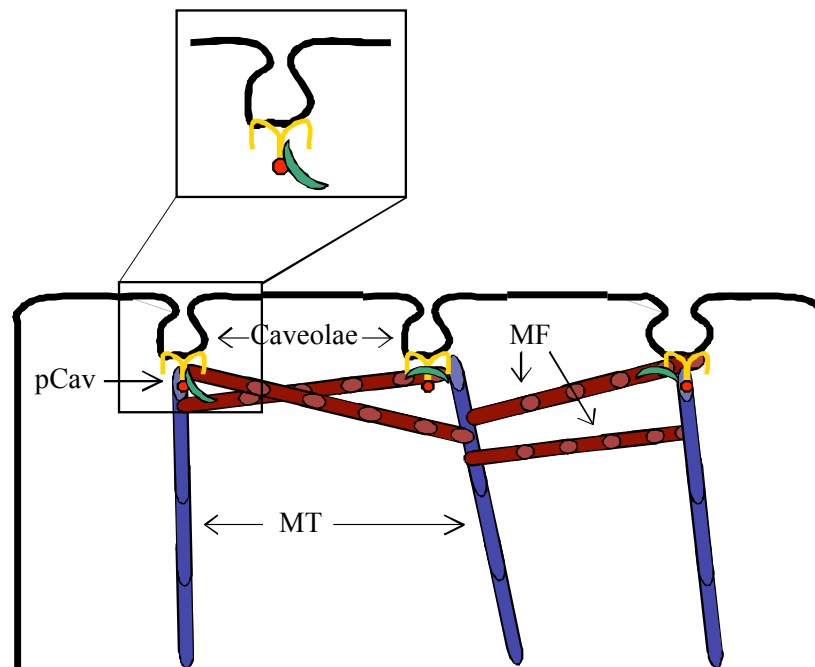
Fig. 1-4. Schematic showing microtubules (MT; blue rods) and microfilaments (MF; brown rods) interacting with phosphorylated (red circle) caveolin (yellow anchors) (P-Cav) oligomers in plasmalemmal caveolae. Filamin, a known ligand for caveolin and F-actin cross-linking protein, is represented by the green crescent. Inset represents magnified view of caveolar microdomain with phosphorylated caveolin and filamin.

Recently, there have been conflicting findings with regard to the role of

cytoskeletal changes, more specifically microtubule alterations, in cardiac myocyte

contraction and heart failure. One study that investigated myocardium experiencing

pressure-overload cardiac hypertrophy revealed that myocardial microtubule content was increased [79, 80, 81] and that microtubule disruption increased contraction in failing myocytes [82, 83]. In normal cardiac myocytes (neonatal and adult) and smooth muscle cells microtubule disruption results in changes in heart rate and contraction [84-88], Ca^{2+} current [89, 90], and β-AR responsiveness [91, 92]. In contrast to these findings, others have shown no affect with colchicine, an agent that depolymerizes tubulin, on contraction of normal and failing myocytes [93-95].

HYPOTHESES

The objective of *Chapter 2* was to test the hypothesis that Cav-3 co-localizes with G protein-coupled receptor (GPCR) signaling components in both sarcolemmal and intracellular membranes in mature cardiac myocytes. We thus used adult CM to determine if Cav-3 distributes differently in adult CM versus other cardiac cell types, if GPCRs (e.g., β-adrenergic, muscarinic, and μ-opioid receptors) and key post-receptor signaling components, including heterotrimeric G proteins and adenylyl cyclase co-localize with Cav-3 in intracellular domains (i.e., T-tubules) in addition to the sarcolemma, and whether Cav-3 scaffolds GPCR signaling components capable of stimulating and inhibiting cAMP synthesis.

The objective of *Chapter 3* was to test the hypothesis that adult CM express all three caveolin isoforms and that they localize with gaseous signaling components involved in free radical generation (e.g, HO and NOS) in sarcolemmal caveolin-associated

microdomains. In addition this aim tested the hypothesis that sub-sarcolemmal mitochondria are closely apposed to sarcolemmal caveolar microdomains.

The objective of *Chapter 4* was to test the hypothesis that disruption of cytoskeletal components (i.e., microtubule and microfilament) affects the distribution and phosphorylation of caveolin isoforms, the distribution of GPCR signaling components, and alters GPCR-mediated cAMP production in adult CM.

Chapter 2

G-protein coupled receptor signaling components localize in both sarcolemmal and intracellular caveolin-3-associated microdomains in adult cardiac myocytes

ABSTRACT

The present study tests the hypothesis that G protein-coupled receptor (GPCR) signaling components involved in the regulation of adenylyl cyclase localize with caveolin, a protein marker for caveolae, in both cell surface and intracellular membrane regions. Using sucrose density fractionation of adult cardiac myocytes, we detected caveolin-3 (Cav-3) in both buoyant membrane fractions (BF) and heavy/non-buoyant fractions (HF), β_2-adrenergic receptors (β_2-AR) in BF, adenylyl cyclase 5/6 ($AC_{5/6}$), β_1-AR, M_4-muscarinic receptors (M_4-mAChR), μ-opioid receptors (μ-OR), and $G\alpha_s$ in both BF and HF, while M_2-mAChR, $G\alpha_{i-3}$, and $G\alpha_{i-2}$ were only found in the HF. Immunofluorescence microscopy showed co-localization of Cav-3 and $AC_{5/6}$, $G\alpha_s$, β_2-AR, and μ-OR on both sarcolemmal and intracellular membranes, while M_2-mAChR were only detected intracellularly. Immunofluorescence of adult heart revealed a distribution of Cav-3 identical to that of isolated adult cardiac myocytes. By immunoelectron microscopy Cav-3 co-localized with $AC_{5/6}$ and $G\alpha_s$ on sarcolemmal and intracellular vesicles, the latter closely allied with transverse tubules (T-tubules). Cav-3 immunoprecipitates possessed components that were necessary and sufficient for GPCR agonist-promoted stimulation and inhibition of cAMP formation. The distribution of GPCRs, G-proteins and AC with Cav-3 on both sarcolemmal and intracellular, T-tubule-associated regions indicates the existence of multiple Cav-3-localized cellular microdomains for signaling by hormones and drugs in the heart.

INTRODUCTION

Caveolar microdomains have been proposed as sites that concentrate G protein-coupled receptors (GPCR), heterotrimeric G-proteins, and GPCR/G-protein-regulated effector molecules in a confined region so as to facilitate coordinated and kinetically favorable generation of second messengers [22, 23]. Caveolae, "little caves", cholesterol- and sphingolipid-enriched 50-100 nm invaginations of the plasma membrane [3, 4], are considered a subset of lipid rafts [5]. Caveolin (Cav), a protein marker for caveolae, is

present in three isoforms (Cav-1$_{\alpha, \beta}$, -2, and –3); Cav-3 is preferentially expressed in skeletal and cardiac muscle. Caveolae help regulate a variety of cellular functions, including endocytosis, calcium homeostasis, skeletal muscle transverse tubule (T-tubule) formation and GPCR compartmentation [11, 12]. Components involved in GPCR signaling, i.e., certain receptors, G-proteins and G-protein regulated effectors, localize with Cav in the plasma membrane [5, 14, 28, 30-32, 34, 96].

The caveolin/lipid raft signaling hypothesis proposed that compartmentation of signaling molecules in caveolae provides a mechanism for temporal and spatial signal transduction and cross talk among signaling pathways [15]. In spite of substantial data supporting this notion [16, 33], little is known regarding the expression of caveolae in the plasma membrane versus non-plasma membrane locations. One cell type in which GPCR compartmentation has been studied is the cardiac myocyte (CM) but virtually all previous studies related to caveolae have involved the use of neonatal CM [28, 97]. Adult CM differ from neonatal CM in numerous ways, including being more extensively differentiated, multi-nucleated, larger in volume and possessing a more developed T-tubule network. In the current study, we hypothesized that Cav-3 co-localizes with GPCR signaling components in both sarcolemmal and intracellular membranes and used adult CM to determine if: a) Cav distributes differently in adult CM versus other cardiac cell types, b) GPCRs (e.g., β-adrenergic, muscarinic, and μ-opioid receptors) and key post-receptor signaling components, including heterotrimeric G proteins and adenylyl

cyclase co-localize with Cav-3 in intracellular domains (i.e., T-tubules) in addition to the

sarcolemma, and c) Cav-3 scaffolds GPCR signaling components capable of stimulating

and inhibiting cAMP synthesis

RESULTS

Caveolin (Cav) distributes differently in adult CM compared to other

cardiovascular cells. The distribution of Cav was investigated in human coronary artery

smooth muscle cells (hCASMC), and adult rat cardiac fibroblasts (ACF) and CM

following sucrose density fractionation. We detected the majority of Cav-1 in buoyant

fractions (4 and 5) from ACF and hCASMC (Fig. 2-1*A*). In adult CM Cav-3 was

detected in both buoyant fractions (4 and 5, termed buoyant fractions, BF) and non-

buoyant fractions (9-12, which we called heavy fractions, HF) (Fig. 2-1*A*). Following

equal protein loading of sucrose density fractions of adult CM (Fig. 2-1*B*), BF were

enriched in Cav-3; HF had a lower proportion of Cav-3 (Fig. 2-1*A*, bottom two panels).

BF contained < 5% of total cellular protein (Fig. 2-1*B*). Adult CM fractions in Fig. 2-1*A*

(from equal volume-loaded gels) that were immunoblotted for the transverse (T-) tubule

markers vinculin and DHPR, a marker for voltage-sensitive calcium channels, showed a

distribution pattern similar to that of Cav-3 (Fig. 2-1*C*). The sarcoplasmic reticulum

marker, ryanodine receptor (RyR), and β-adaptin, a marker of clathrin-coated pits, were

detected only in HF (Fig. 2-1*C*). To test whether the Cav-3 distribution pattern observed

with Na_2CO_3-sucrose density fractionation of adult CM was unique to this method of

cellular disruption and fractionation, we fractionated adult CM in alternative lyses

buffers, one with Triton X-100 (1%) and the other in a high salt buffer to extract

contractile myofibrils. Immunoblot of equal volume loaded fractions from the Triton X-

100 fractionation revealed a broad distribution of Cav-3 (Fig. 2-1*D*). Following extraction

of the contractile myofibrils using a high salt buffer, we detected buoyant and heavy

pools of Cav-3, albeit with a substantially greater amount of Cav-3 in the heavier

fractions (Fig. 2-1*D*). Overall, these results show that Cav-3 is present in both BF and

HF following sucrose density fractionation, indicating a different cellular distribution

when compared to Cav-1 in two other cardiovascular cell types, hCASMC and ACF.

GPCR signaling components distribute nonuniformly with Cav-3 in adult CM.

Using immunoblot analyses, we investigated co-localization of G_s- and G_i protein-coupled

receptor signaling components with Cav-3 in adult CM. $AC_{5/6}$, β_1-AR and β_2-AR were

detected in BF while a portion of β_1-AR was also detected in the HF (Fig. 2-2*A*). $G\alpha_s$

was detected as two bands, which represent the short and long splice variants of $G\alpha_s$, in

BF and HF (Fig. 2-2A). Because the β-AR and mAChR pathways act antagonistically in

the regulation of cardiac rate and force of contraction, we investigated if M_2- and M_4-

mAChR localize to BF. We found that M_2-mAChR are excluded from BF, as are $G\alpha_{i-3}$

and $G\alpha_{i-2}$, G-proteins through which both M_2- and M_4-mAChR signal, whereas we

detected M_4-mAChR in both the BF and HF (Fig. 2-2*B*,*C*). We also detected μ-opioid

receptor (μ-OR), another G_i-coupled receptor, in adult CM by polymerase chain reaction

(data not shown) and by immunoblot, in both BF and HF (Fig. 2-2*B*).

As an alternative means to test for interaction of the signaling components with

Cav-3, we assessed BF and HF following immunoprecipitation with a Cav-3 antibody

(Fig. 2-2*D*). $AC_{5/6}$, β_1-, β_2-AR, $G\alpha_s$, M_4-mAChR, μ-OR, and Cav-3 were all detected in

Cav-3 immunoprecipitates from both BF and HF. By contrast, M_2-mAChR and $G\alpha_{i-3}$

(Fig. 2-2*D*) were detected only in Cav-3 immunoprecipitates from HF, while $G\alpha_{i-2}$ and β-

adaptin were not detected in immunoprecipitates from either BF or HF.   Thus, the

results with the Cav-3 immunoprecipitates from BF and HF confirm the immunoblot

findings with sucrose density fractions and demonstrate that GPCR signaling components

vary in their cellular distribution with Cav-3.

Immunofluorescence microscopy shows co-localization between Cav-3 and $AC_{5/6}$,

$G\alpha_s$-protein, β_2-AR, μ-OR, and M_4-mAChR in the sarcolemmal and intracellular regions

in adult CM. We used immunofluorescence microscopy as a further means to assess

GPCR co-localization with Cav-3 in CM. Cav-3 was detected in the sarcolemma as a

punctate pattern and in striations running transversely across the interior of the cell (Figs.

2 3-8). To assess co-localization of Cav-3 with AC_6, a key post GPCR/G-protein

effector in CM, we used an adenoviral vector to over-express AC_6 because available

antibodies do not readily detect endogenous AC_6 in adult CM. Individual components

showed different extents of co-localization with Cav-3 in sarcolemmal and intracellular

regions, respectively (Figs. 2-3, 2-4, and 2-5, data expressed relative to Cav-3 expression):

$AC_{5/6}$, 27% and 11%; $G\alpha_s$, 32% and 7%; β_2-AR, 43% and 59%; μ-OR, 39% and 32%;

M_4-mAChR, 21% and 34%; and M_2-mAChR, 12% and 45% (Fig. 2 3-5). As a negative

control, incubation with secondary antibodies revealed minimal background staining (Fig.

2-4, *bottom panel*). AC_6, $G\alpha_s$, β_2-AR, M_4-mAChR, and μ-OR displayed greater co-

localization with Cav-3 in the sarcolemma than did M_2-mAChR. The distribution of

intracellular β_2-AR was predominantly in sub-sarcolemmal locations (Fig. 2-3) while M_2-

mAChR displayed a more transverse intracellular distribution (Fig. 2-5*A, top panels*).

Treatment with the agonist carbachol (100 μM; 10 min) disrupted the transverse staining

pattern of M_2-mAChR, with redistribution to the sarcolemma and nucleus (Fig. 2-5*A,

bottom panels*). Quantitation of Cav-3 immunofluorescence revealed that ~ 25% of total

cellular Cav-3 was sarcolemmal (Fig. 2-5*B, left panel*), a value similar to that for Cav-3

detected in BF (Fig. 2-5*B, right panel*) from sucrose density fractionation (Fig. 2-1*C, third

panel*). Thus, Cav-3 appears to be present in both intracellular and sarcolemmal regions

and different GPCRs differ in their co-localization with Cav-3.

*Immunofluorescence microscopy of adult heart shows co-localization of Cav-3 and

$G\alpha_s$-protein in both the sarcolemmal and intracellular regions.* Immunofluorescence

microscopy revealed that the cellular distribution of Cav-3 in adult heart is similar to that

in adult CM (Fig. 2-3, 2-4): with Cav-3 in a punctate pattern in the sarcolemma and in

striations that run transversely across the cell interior (Fig. 2-6, *top panel*). In tissue

sections $G\alpha_s$ co-localized with Cav-3 in intracellular regions, most predominantly in

intercalated discs (arrow), which demarcate junctions between adjacent myocytes (Fig. 2-

6, *bottom panel*, *arrow*).

Immunofluorescence microscopy shows co-localization between Cav-3 and T-

tubule (DHPR and vinculin) and sarcoplasmic reticulum (RyR) markers in both adult CM

and heart. Immunostaining of adult CM revealed that Cav-3 co-localizes with two

different T-tubule markers (vinculin and DHPR) in a transverse pattern and along the

sarcolemma (Fig. 2-7*A*). Tissue sections of heart assessed with antibodies for Cav-3 and

DHPR revealed a similar pattern to that found in isolated CM with Cav-3 and DHPR co-

localizing in intracellular regions running transversely across the cell, along the

sarcolemma, and in intercalated discs (Fig. 2-7*B, arrow*). Staining for Cav-3 and RyR, a

sarcoplasmic reticulum (SR) marker, revealed co-localization predominantly in

intracellular regions running transversely across the cell in both isolated CM and heart

(Fig. 2-8*A*) and in intercalated discs (*arrows*) in sections of heart. We detected minimal

co-localization of Cav-3 and α-actinin, a Z-disc marker (data not shown). As an

alternative means to test for Cav-3-RyR interaction, we assessed lysates from CM

immunoprecipitated with Cav-3 and RyR antibodies (Fig. 2-8*C*) and observed Cav-3 and

RyR in both Cav-3 and RyR immunoprecipitates, thus confirming results from

immunofluorescence microscopy showing the co-localization between Cav-3 and the SR

marker. Thus Cav-3 not only localizes along the sarcolemma but also in T-tubule/SR

regions in both adult CM and heart.

Immunoelectron microscopy (immunoEM) detects Caveolin-3 in sarcolemmal

invaginations and in intracellular domains in the adult CM. We used immunogold labeling

as a further means to assess the distribution of Cav-3 in adult CM. ImmunoEM

demonstrated abundant sarcolemmal caveolae, present as invaginations that labeled with

antibodies directed against Cav-3 (Figs. 2-9*A,* 2-9*B*). We also detected Cav-3 in

membranes flanked by Z-discs, which correspond to the T-tubule network within the cell

interior (Fig. 2-9*C*). These immunoEM data confirmed and extended results from

immunofluorescence microscopy, demonstrating Cav-3 on both sarcolemmal and

intracellular regions, and are consistent with the detection of Cav-3 in the HF following

sucrose density fractionation (Fig. 2-1).

Immunoelectron microscopy shows co-localization of Cav-3 with AC_6 and $G\alpha_s$.

Using immunogold labeling we detected Cav-3 (10 nm gold) with AC_6 (5 nm gold) in

invaginations of the sarcolemma (Fig. 2-9*D*) and on intracellular membranes (Fig. 2-9*E*)

located between adjacent Z-discs. We also detected Cav-3 (10 nm gold) with $G\alpha_s$ (5 nm

gold) on vesicles near myofibrils (Fig. 2-9*F,G*). These immunoEM findings are consistent

with results of Cav-3 immunoprecipitation studies, which showed multi-protein

interaction between Cav-3 and AC_6 and $G\alpha_s$ in adult CM (Fig. 2-2*C*).

AC_6 overexpression enhances GPCR-stimulated cAMP production in adult CM.

To confirm that the overexpressed AC_6 that we analyzed microscopically (Fig. 2-3, 2-9)

was functional, we assessed cAMP production in adult CM. Overexpression of AC_6 increased levels of cAMP produced in response to isoproterenol, a β-AR agonist, without an increase in agonist potency (Fig. 2-10*A*). Thus, the overexpressed AC_6 that co-localized with Cav-3 in adult CM (as shown by both immunofluorescence and imunoEM) is enzymatically active. Moreover, by assaying forskolin-stimulated cAMP accumulation, we obtained functional evidence for the presence of μ-OR in adult CM: the μ-OR agonist DAMGO significantly reduced forskolin-stimulated cAMP production ($p<0.05$, n=5; Fig. 2-10*B*).

Cav-3 immunoprecipitates multi-protein complexes capable of producing and inhibiting cAMP. To demonstrate that Cav-3 interacts with and organizes components that mediate stimulation and inhibition of cAMP formation we assessed AC activity in Cav-3 immunoprecipitates of adult CM lysates. Forskolin increased cAMP production (Fig. 2-10*C*); this stimulation was significantly ($p<0.01$) inhibited by DAMGO, a response that was inhibited by the opioid receptor antagonist, naloxone. Immunoblot analysis detected μ-OR and, $G\alpha_{i-3}$ in the Cav-3 immunoprecipitates used in the AC activity experiments (data not shown). These data show functional evidence for the existence of μ-OR and support the conclusion that Cav-3 interacts with multi-protein complexes that can both stimulate and inhibit cAMP production in adult CM.

DISCUSSION

Caveolae-localized signaling microdomains have been proposed as sites that concentrate GPCR, heterotrimeric G-proteins and G-protein regulated effector molecules, so as to facilitate coordinated, precise and rapid regulation of cell function [5, 14, 28, 30-32, 34, 96]. Cav-rich domains thus may serve as spatial organizers of GPCR signaling, although not all data have supported this conclusion [96, 98]. Using multiple experimental approaches - subcellular fractionation, immunoprecipitation, immunofluorescence, immunoEM, as well as functional assays of cAMP formation - we provide here new evidence that extend the notion of Cav-rich domains as organizers of GPCR-signaling components and in support of the novel conclusion that Cav-3 organizes GPCR signaling components in both sarcolemmal and intracellular regions (e.g., T-tubules in cardiac myocytes) in the adult heart.

Most previous studies [13, 34, 97, 99] on compartmentation of GPCR signaling components in CM have utilized embryonic and neonatal cells. However, it is preferable to study adult CM, which are more akin to the *in vivo* setting than are neonatal CM and other non-striated cardiovascular cells [100]. Because of development-related changes in ion channels and contractile proteins, it can be difficult to extrapolate results from the neonatal to the adult heart. The present results regarding Cav-3 distribution in adult CM differ from findings reported for neonatal CM and certain non-cardiac cell types in which cav distributes only to buoyant fractions [13, 34, 97, 99, 101]. Demonstration that M_2-mAChR

are excluded from BF and expressed in intracellular sites confirms and extends previous

results for adult CM [102] and contrasts with findings from neonatal CM where M_2-

mAChR were detected in both bouyant and heavy fractions [34]. Such differences imply

developmental changes related to caveolar compartmentation of the β-AR and mAChR

signaling cascades, which perhaps contribute to differences during development in

response to physiologic stimuli. Compartmentation of GPCR signaling components in

adult CM also contrasts with findings from adult rat aortic smooth muscle cells in which

$β_1$- and $β_2$-AR are found only in heavy fractions, implying that localization of particular

GPCR to Cav-rich fractions is cell-type dependent [14, 23].

Previous workers have observed intracellular Cav-3 in skeletal myocytes [11, 47, 103].

A possible role for intracellular Cav in adult CM may be as a regulator of calcium

homeostasis [104]: T-tubules in adult CM are continuous with the sarcolemma and are

essential for the influx of calcium via L-type Ca^{2+} channels, or DHPRs, and regulation of

myocyte contractility [105-108]. DHPRs are located primarily at the T-tubule/SR junction

proximal to where the SR Ca^{2+} release channels, or RyRs, are found [36, 109]. The present

study shows Cav-3 co-localizing with DHPRs and RyRs in adult CM and whole tissue

(Fig. 2-7, 2-8), and Cav-3 in regions between adjacent Z-discs morphologically

corresponding to T-tubules (Fig. 2-9), results which complement evidence for Cav-3 in T-

tubules in striated myocytes [11, 47]. In addition, our detection of $AC_{5/6}$ in intracellular

membranes that correspond to T-tubules agrees with results that suggest a T-tubule

localization of the $AC_{5/6}$ protein [37]. The biochemical and immunofluorescent data indicate that the inhibition of AC by G_i-coupled receptors occurs in Cav-3 rich microdomains in the T-tubular system. Intracellular Cav may provide a scaffold that helps organize GPCR-signaling components and proteins that regulate calcium homeostasis at the T-tubule/SR junction. We attempted to assess for differences in AC activity between sarcolemmal and intracellular Cav-rich regions, but due to the lengthy preparation required to isolate fractions and conduct activity assays, we were unable to detect stable AC enzyme activity (data not shown).

Although caveolae are morphologic entities, virtually all previous work has utilized subcellular fractionation or immunoprecipitation to infer co-localization of GPCR-signaling components with caveolins. Plating of adult CM on laminin-coated surfaces allowed us to utilize microscopic techniques, both light and electron, to show Cav-3 in a punctate pattern along the sarcolemma and in intracellular transverse striations. The present study thus provides the first microscopic evidence of Cav-3 co-localization with GPCRs and GPCR signaling components in both sarcolemma and intracellular membranes, in particular T-tubule-associated membrane regions, in adult CM (Fig. 2-9*D-G*). The results from immunofluorescence microscopy of adult myocardium showing a similar Cav-3 distribution to that seen in isolated adult CM (Fig. 2-6, 2-7*B*, 2-8*B*), supports the use of isolated adult CM as an *in vitro* model [100].

Opioid receptors have been shown to play an important role in protecting the

heart from ischemic injury [110, 111] and arrhythmias [112]. However, ambiguity exists regarding the receptor subtypes expressed and activated by agonists in the myocardium [113]; in particular, the presence of μ-OR has been disputed [114]. Past studies that utilized radioligand-binding experiments were performed on membranes prepared from whole hearts, making it difficult to distinguish sarcolemma from intracellular CM membranes and membranes contributed by other cell types. Our results obtained using four different techniques (PCR, Western blotting, immunofluorescent microscopy, and assay of cAMP generation) provide evidence consistent with the idea that functional μ-OR are expressed in CM of adult heart.

In conclusion, in this study we used multiple complementary techniques - subcellular fractionation, immunochemistry, morphology and functional assays - to documents a role for cardiac Cav-3 as an organizer of signaling components that regulate cAMP production for multiple classes of GPCRs (i.e., β-AR, mAChR and μ-OR). The results imply that spatial organization of GPCR signaling components occurs in microdomains in both sarcolemmal and intracellular membrane regions in the hear.

The text of Chapter Two is a reprint of the material as it appears in Journal of Biological Chemistry: Head BP, Patel HH, Lai NC, Niesman IR, Roth DM, Farquhar MG, and Insel PA. 2005. G-protein coupled receptor signaling components localize in both sarcolemmal and intracellular Caveolin-3-associated microdomains in adult rat cardiac

myocytes. *J Biol Chem.* 280: 31036-31044, 2005. I was the primary author and the co-authors listed in this publication directed and supervised the research which forms the basis for this chapter.
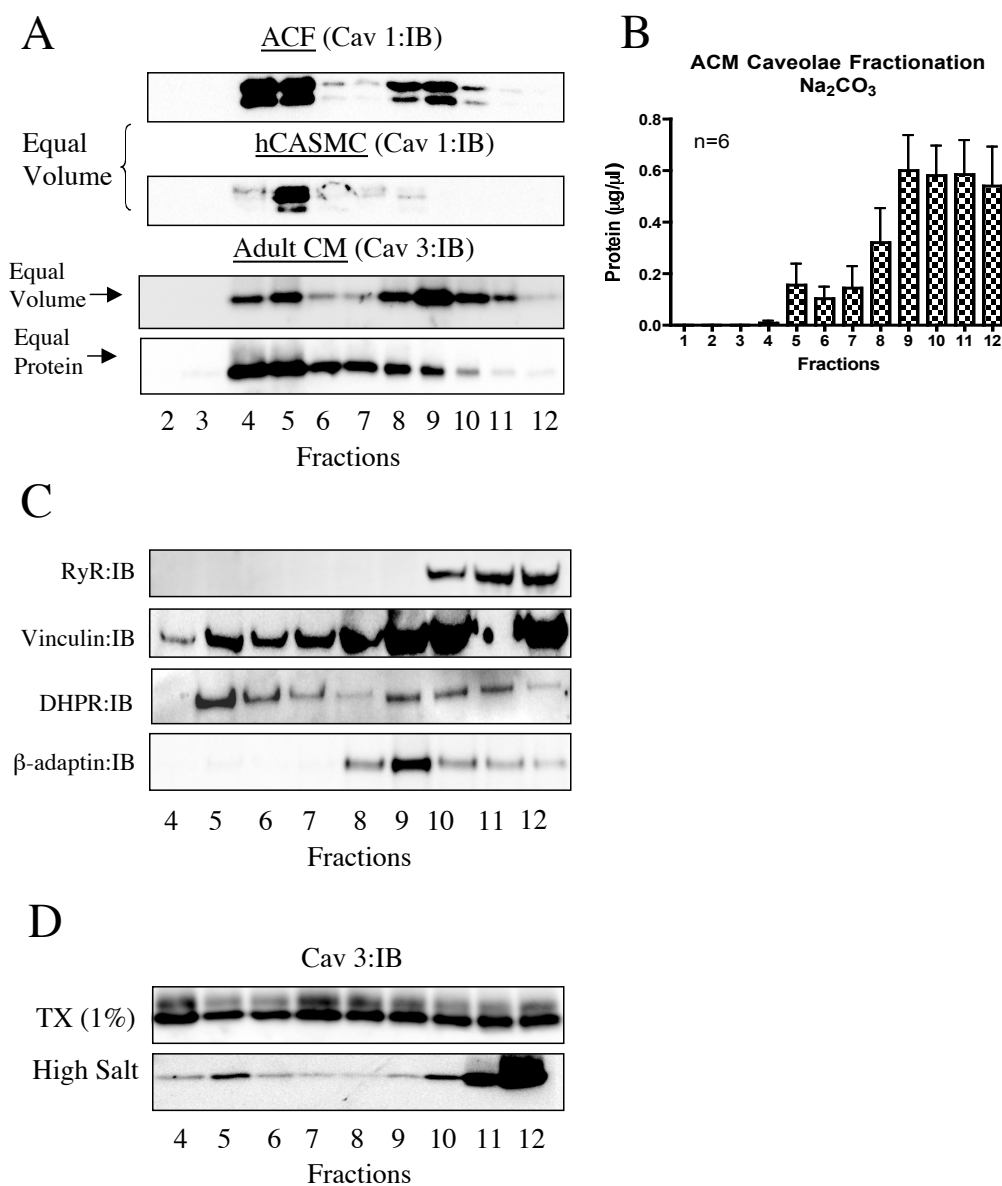
Fig. 2-1. Distribution of Cav-3 protein and markers in cardiac myocytes (CM) and fibroblasts (ACF), and coronary artery smooth muscle cells (hCASMC). *A,* Na_2CO_3 extraction followed by sucrose density fractionation as described in Experimental Procedures was undertaken with adult CM, ACF, and CASMC. *B,* Protein concentrations ($\mu g/\mu l$) are shown for fractions 4-12 and are representative of caveolar fractionation experiments from adult CM (n=6). *C,* Equal volume loaded samples following sucrose density fractionation were assessed for localization of ryanodine receptor (RyR, sarcoplasmic reticulum marker), vinculin (T-tubule marker), dihydropyridine receptor (DHPR, voltage sensitive Ca^{2+} channel; T-tubule marker), and localization of β-adaptin (clathrin-coated pit marker) in adult CM. *D,* Equal-volume loading of adult CM subjected to Triton X-100 and high salt extraction followed by subcellular fractionation.
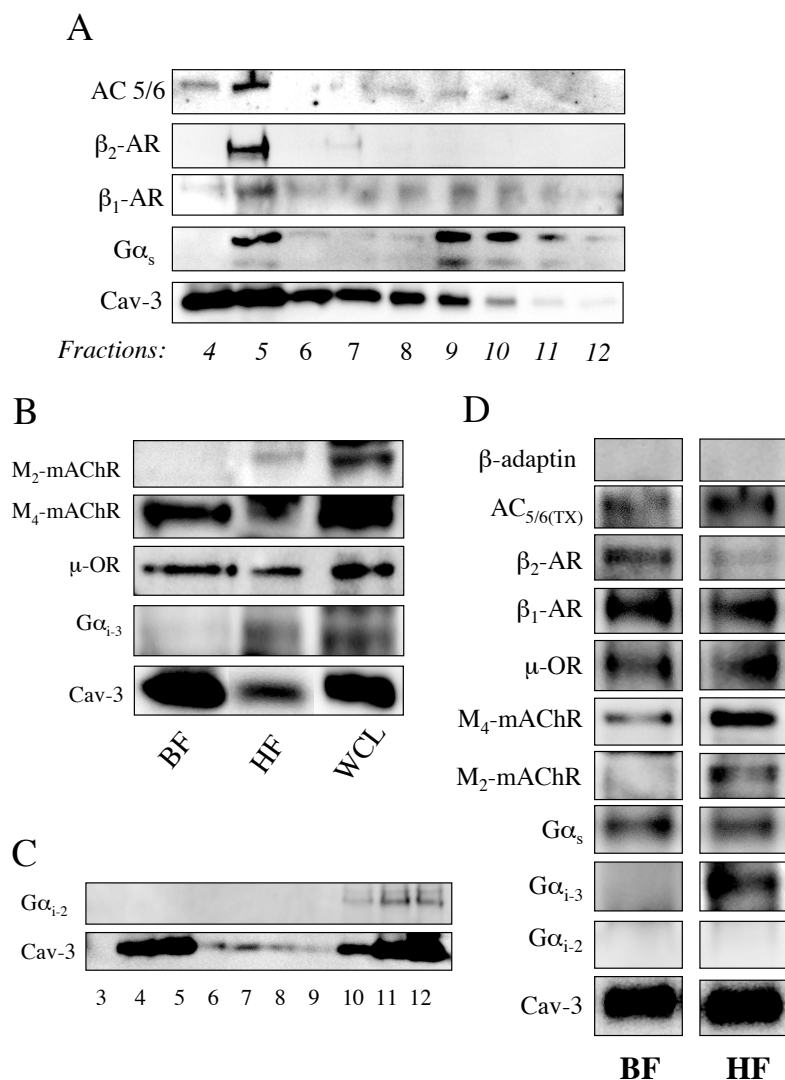
Fig. 2-2 Expression and localization of β-adrenergic, muscarinic, and opioid receptor signaling components in sucrose density fractionations of Na_2CO_3 extracts and Cav-3 immunoprecipitates of BF and HF generated from Na_2CO_3 extracts from adult CM. *A,* $AC_{5/6}$, $β_2$-AR, $β_1$-AR, and $Gα_S$ localization in sucrose density fractionation of Na_2CO_3 extracts. *B,* Fractions 4 and 5 (BF) and 9-12 (HF) were pooled and compared to whole cell lysates (WCL) from adult CM for expression of mAChR subtypes (M_2 and M_4), μ-OR, $Gα_{i-3}$, and Cav-3 by immunoblot analysis. Approximately 4 μg of protein from each fraction were loaded into each lane. *C,* $Gα_{i-2}$ and Cav-3 localization in sucrose density fractionation of Na_2CO_3 extracts (equal volume). *D,* BF and HF generated from adult CM sucrose density fractionations were pH neutralized with HCl, immunoprecipitated with Cav-3 antibodies and immunoprecipitates were then probed with antibodies for β-adaptin, $AC_{5/6}$, β-AR, μ-OR, mAChR, $Gα_s$, $Gα_{i-3}$, $Gα_{i-2}$, and Cav-3.
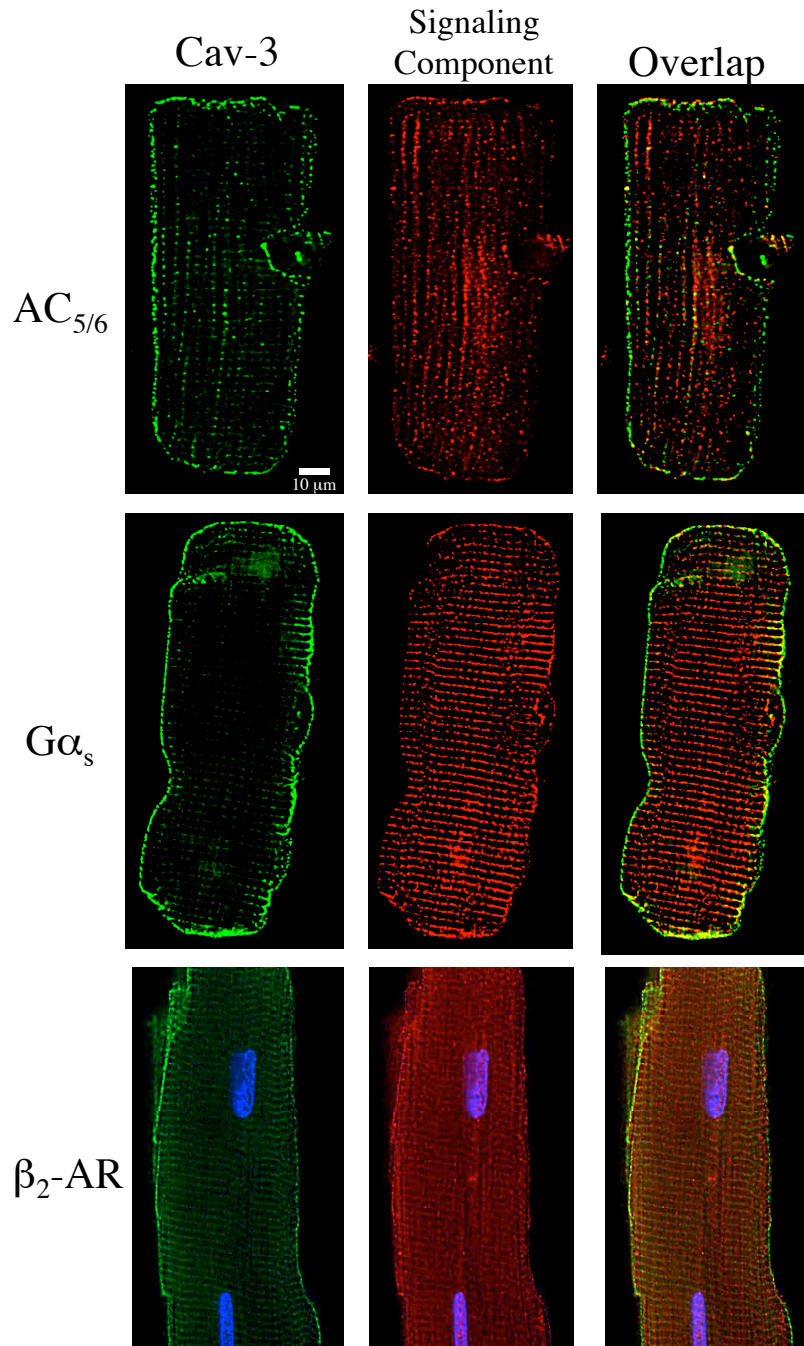
Fig. 2-3. Immunofluorescence and de-convolution analysis of the co-localization between Cav-3, $AC_{5/6}$, $G\alpha_s$ and β_2-AR in adult CM. Cells were co-stained with antibodies for Cav-3 and $AC_{5/6}$, $G\alpha_s$ or β_2-AR. Images were deconvolved and shown as single stained or overlaid to show co-localization. Scale bar, 10 μm.
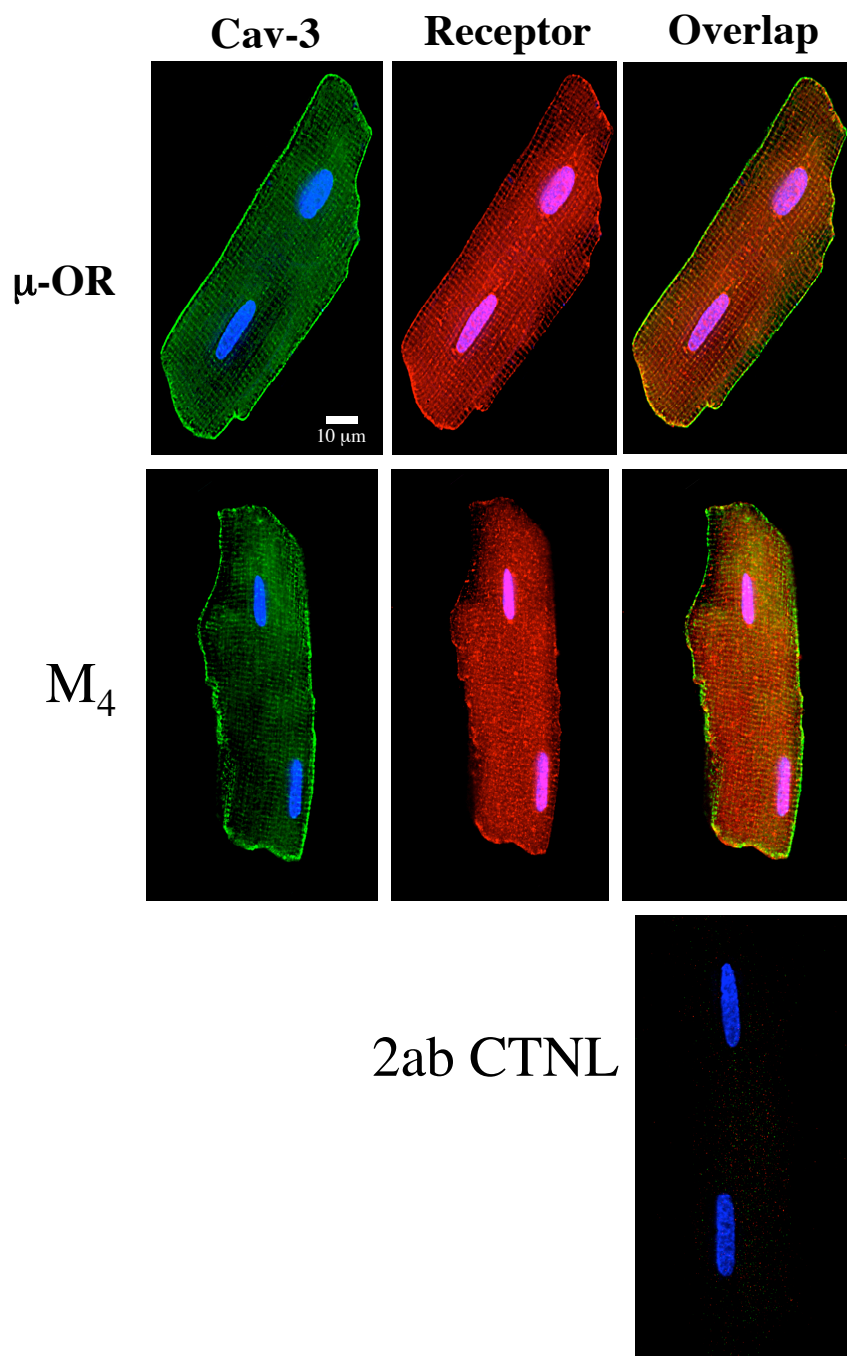
Fig. 2-4. Immunofluorescence and de-convolution analysis of the co-localization between Cav-3 and μ-OR, and M₄-mAChR in adult CM. Cells were stained with antibodies for Cav-3, μ-OR and M₄-mAChR. Images were deconvolved and shown as single stained or overlaid to show co-localization. As a negative control, incubation with secondary antibodies revealed minimal background staining (*bottom panel*). Scale bar, 10 μm.

A)

B)
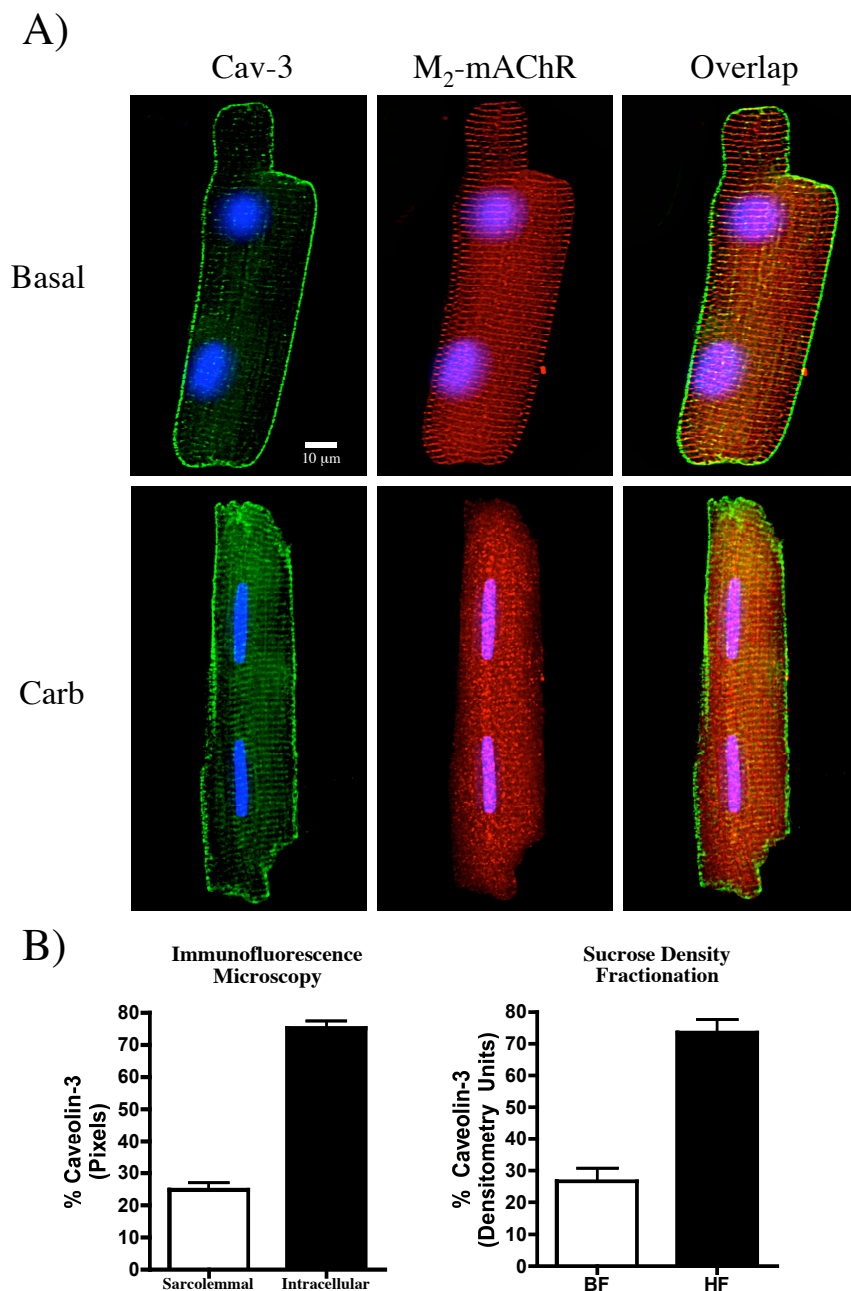
Fig. 2-5. Immunofluorescence and de-convolution analysis of the co-localization between Cav-3 and M$_2$-mAChR following treatment with carbachol in adult CM. Cells were co-stained with antibodies for Cav-3 and M$_2$-mAChR under basal conditions and following treatment with carbachol (Carb, 100 µM; 10 min). Under basal conditions M$_2$-mAChR were found predominantly in a discrete transverse pattern across the interior of the cell. After treatment with carbachol, M$_2$-mAChR was more sparsely distributed within the interior of the cell and redistributed to sarcolemmal and nuclear regions of the cell. Scale bar, 10 µm.

Cav-3

Gα_s

Overlap
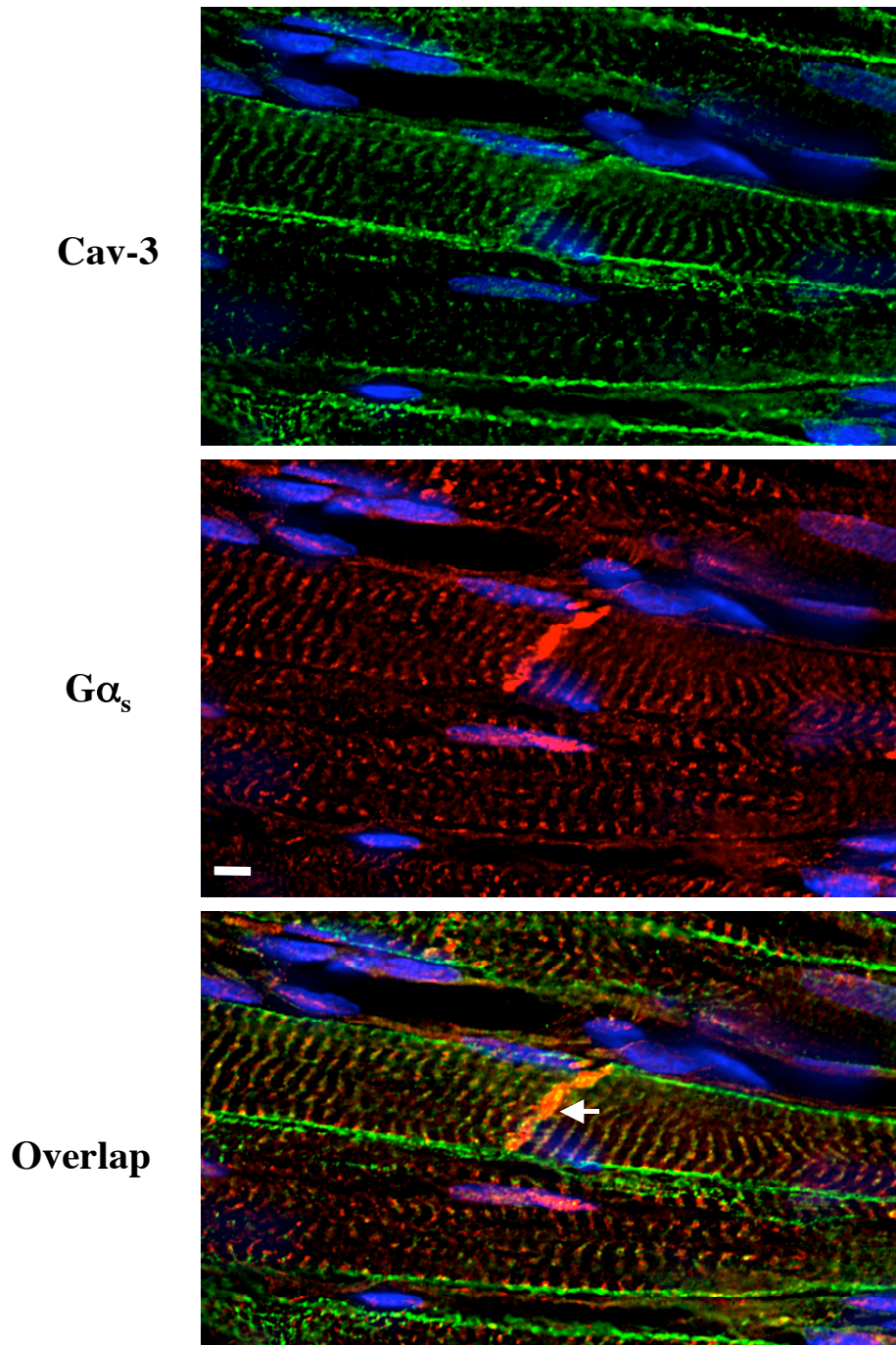
Fig. 2-6. Immunofluorescence and de-convolution analysis of the co-localization between Cav-3 and Gα$_s$ in adult heart. Semithin sections (5 μm) of adult heart were co-stained with antibodies for Cav-3 and Gα$_s$. Cav-3 co-localized with Gα$_s$ in transverse striations within the cell and in intercalated discs between two cardiac myocytes. Images were deconvolved and shown as single-stained or overlaid to show colocalization. Scale bar, 10 μm.

A)

Cav-3   DHPR   Overlap

Cav-3   Vinculin   Overlap

B)

Cav-3   DHPR   Overlap
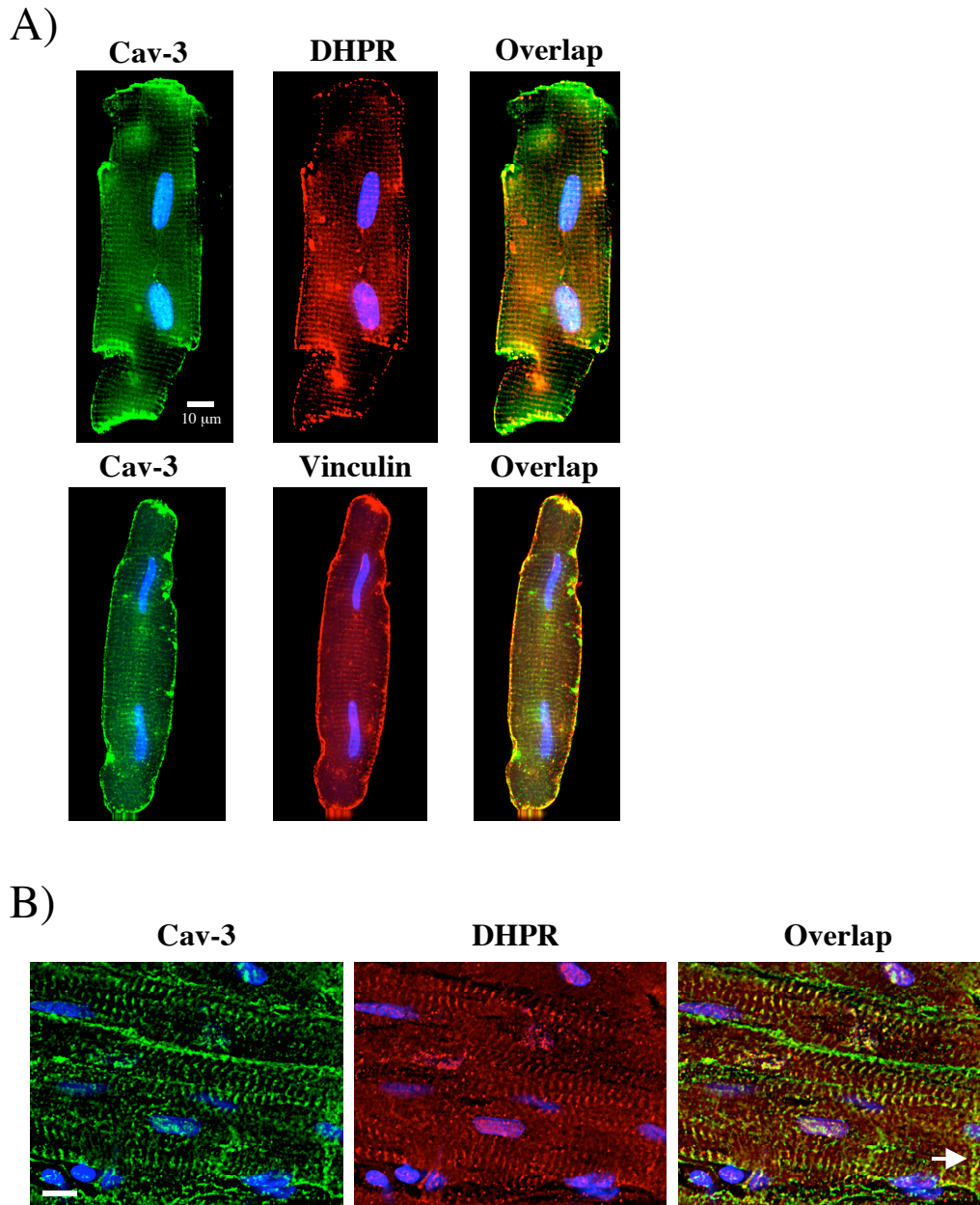
Fig. 2-7. Immunofluorescence and de-convolution analysis of the co-localization between Cav-3 and T-tubule markers, dihydropyridine receptor (DHPR) and vinculin, in adult CM and heart. *A*, Cells stained with antibodies for Cav-3, DHPR and vinculin revealed co-localization between Cav-3 and T-tubule markers on the sarcolemma and in a transverse intracellular pattern *B*, Semithin sections (5 μm) of heart stained with antibodies for Cav-3 and DHPR displayed co-localization along the sarcolemma, in transverse intracellular striations and intercalated discs (arrow) between adjacent CM. Images were deconvolved and shown as single-stained or overlaid to show co-localization. Scale bar, *A*, 10 μm; *B*, 30 μm.
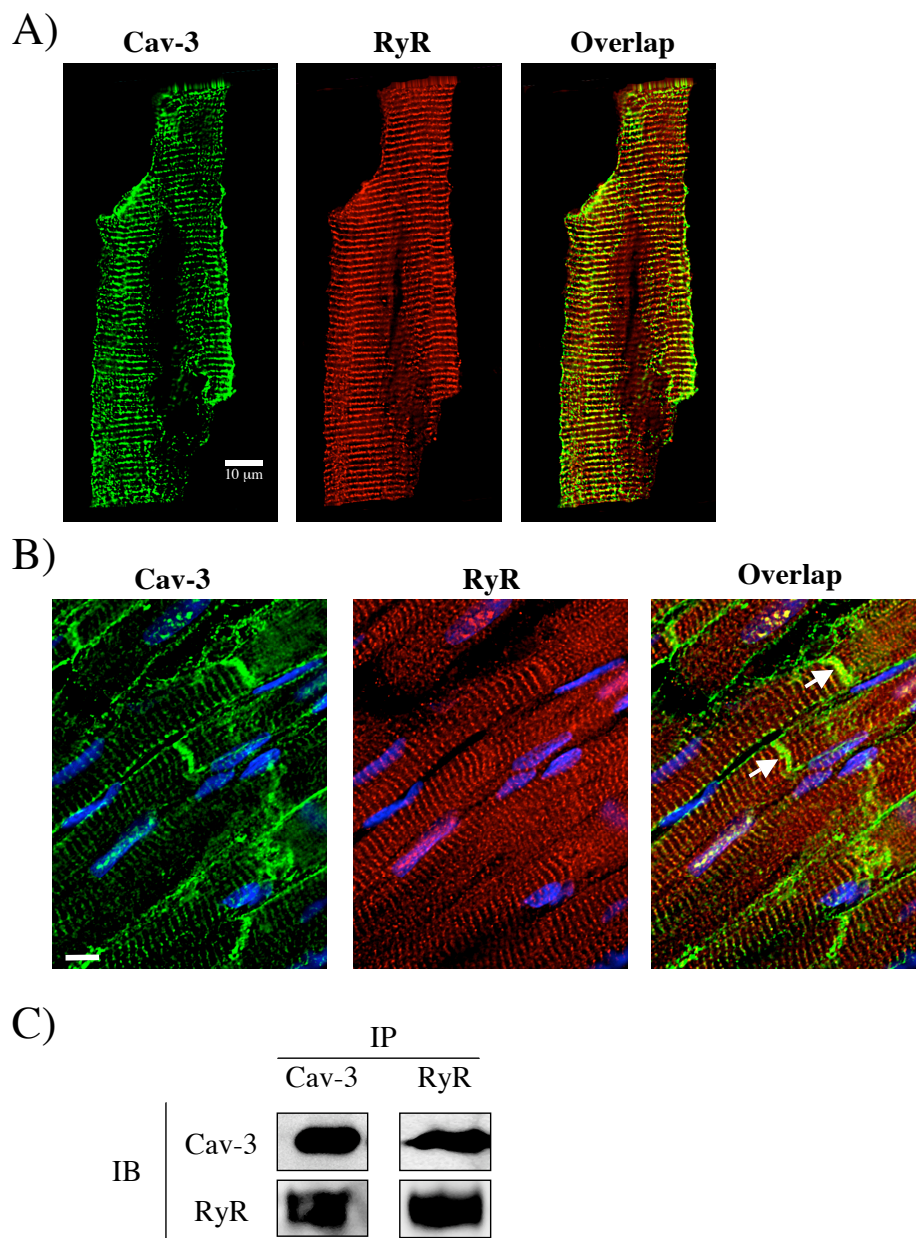
Fig. 2-8. Immunofluorescence and de-convolution analysis of the co-localization between Cav-3 and the SR marker, ryanodine receptor (RyR), in CM and adult heart. *A*, Cells co-stained with antibodies for Cav-3 and RyR revealed co-localization between Cav-3 and the SR marker in a transverse pattern within the cell interior. *B*, Semithin sections (5 μm) of adult heart co-stained with antibodies for Cav-3 and RyR displayed co-localization in transverse striations within the cell and in intercalated discs (arrows) between adjacent CM. Images were deconvolved and shown as single stained or overlaid to show co-localization. Scale bar, *A*, 10 μm; *B*, 30 μm. *C,* RyR and Cav-3 immunoprecipitates were probed for RyR and Cav-3.
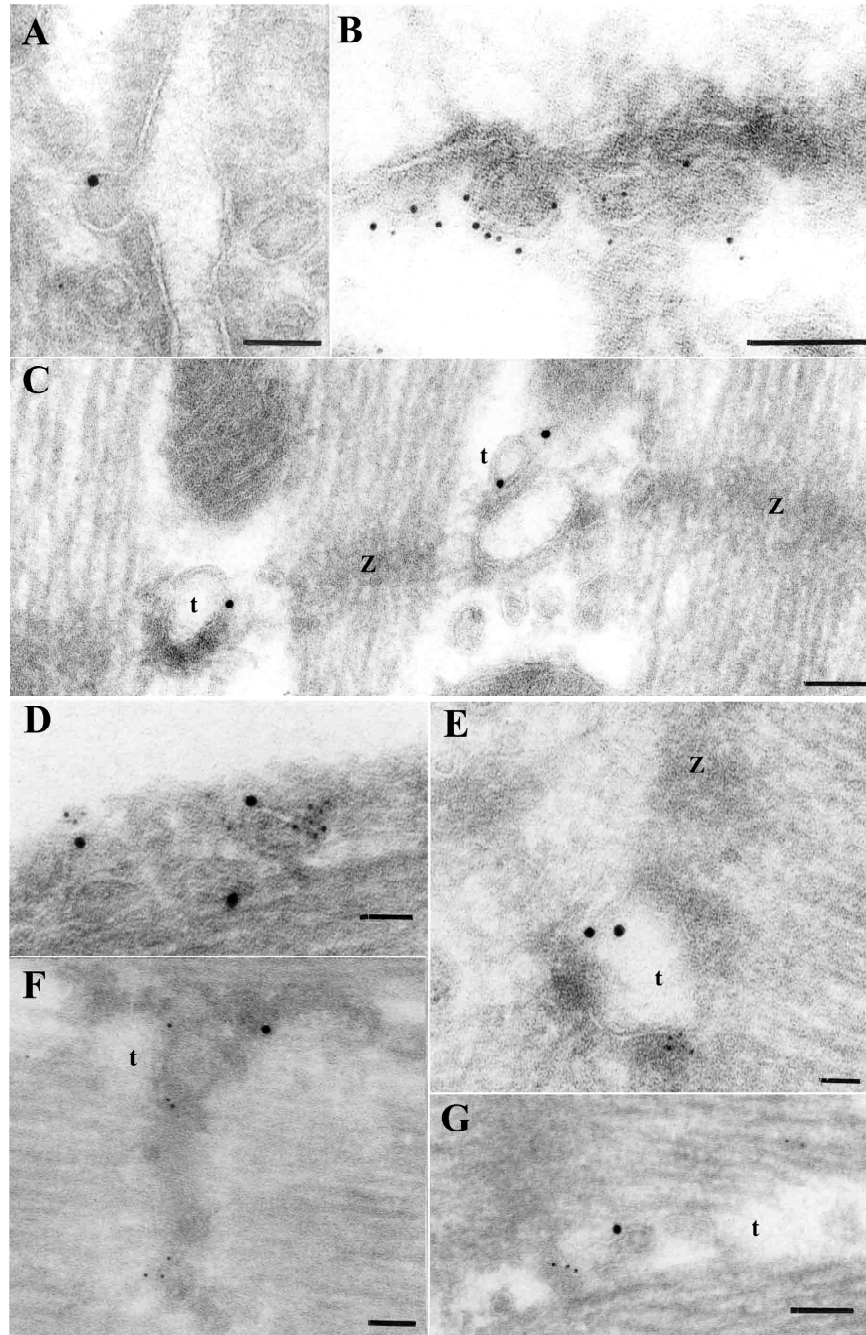
Fig. 2-9. Immunoelectron microscopic localization of Cav-3 with AC_6 and $G\alpha_s$ on the sarcolemma and on intracellular membranes morphologically corresponding to T-tubules in adult CM. Immunogold labeling detected Cav-3 (10 nm) on the sarcolemmal membrane (*A* and *B*) and on intracellular membranes anchored to Z-discs (*C*). Additional immunogold labeling detected Cav-3 (10 nm) with AC_6 (5 nm) on sarcolemmal invaginations (*D*) and on intracellular membranes near Z-discs (*E*). Similarly Cav-3 (10 nm) with $G\alpha_s$ (5 nm) is detected on intracellular membranes corresponding to T-tubules (*F, G*). *Z denotes Z-discs; t denotes T-tubules*. Scale bar, 0.05 μm.
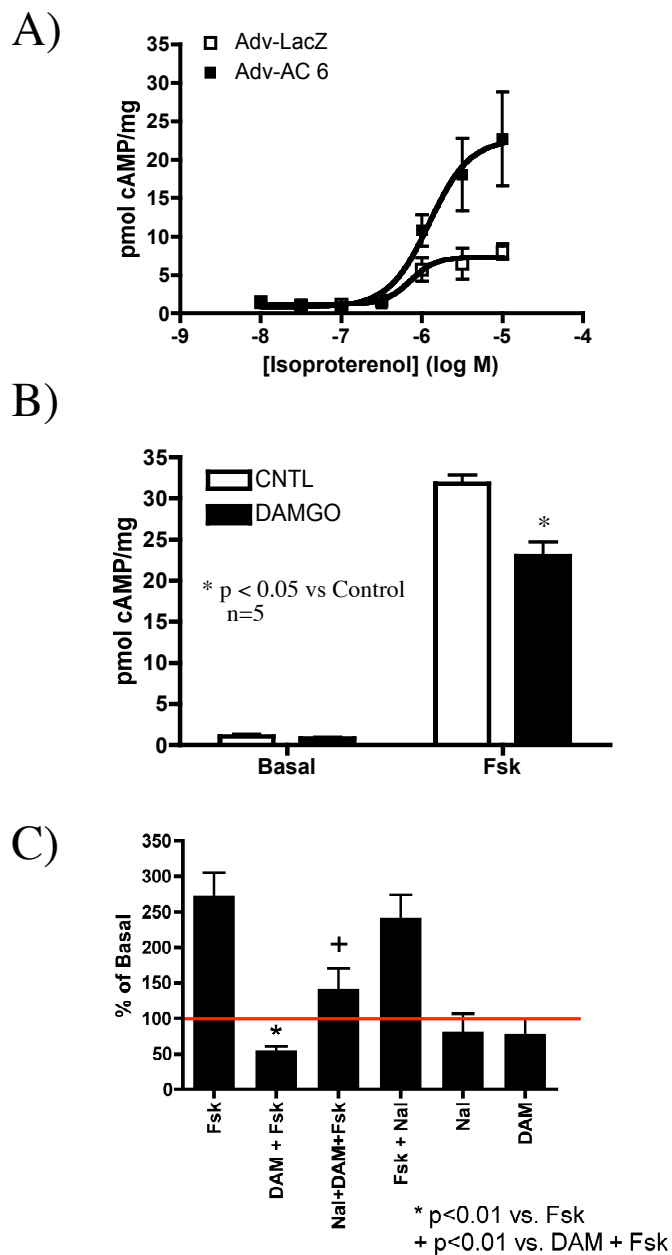
Fig. 2-10. cAMP formation (measured over 10 min) in adult CM and Cav-3 immunoprecipitates. *A*, cAMP accumulation in response to isoproterenol in adult CM incubated with either adenoviral LacZ (control, *open squares*) or AC_6 (closed *squares*). Data are expressed as total pmol cAMP/mg ± SEM, n=3. *B*, Effect of forskolin (10 μM) and the μ-OR agonist DAMGO (1 μM) on cAMP formation was measured in adult CM. Data are expressed as total pmol cAMP/mg ± SEM, n=5. *C*, Effect of forskolin (10 μM), the μ-OR agonist DAMGO (1 μM), and the opioid antagonist naloxone (0.1 μM) on AC activity was measured in Cav-3 immunoprecipitates (Cav-3 IP) of adult CM lysates. Data are expressed as fold over basal and each bar represents average ± SEM, n=6.

Chapter 3

Expression of caveolin-1, -2, and -3 in adult ventricular cardiac myocytes and interaction with heme oxygenase-1 and endothelial nitric oxide synthase

ABSTRACT

Caveolae, membrane structures involved in multiple cellular events, including transport and signal transduction, are composed of lipids and the structural protein caveolin. Recently, heme oxygenase (HO), the rate-limiting enzyme involved in the oxidative degradation of heme into carbon monoxide (CO), biliverdin, and free iron, was detected in caveolae in endothelial cells. Here, we used cardiac myocytes (CM) isolated from adult rats and mice and sought to determine whether HO-1 and endothelial nitric oxide synthase (eNOS), two enzymes involved in free radical generation, localize to buoyant Cav fractions and co-immunoprecipitate with caveolin isoforms. Immunoblotting of sucrose density gradient fractions detected both HO-1 and eNOS in buoyant Cav fractions (BF) and non-buoyant, heavy fractions (HF) from adult CM. Additional experiments revealed that all three Cav isoforms and HO-1 co-immunoprecipitated. Immunohistochemistry showed ~67% co-localization between Cav-3 and cytochrome C, a mitochondrial marker, along the sarcolemma. Additional, electron microscopy revealed closed apposition between sub-sarcolemmal mitochrondria (within 200 nm of sarcolemma) and sarcolemmal caveolae. This presence of caveolae near sub-sarcolemmal mitochondria was completely disrupted with methyl-β-cyclodextrin (MβCD, 2 mM). The localization of HO-1 and eNOS with caveolin, and the close apposition between caveolae and mitochondria suggests that caveolae in addition to being sites that generate gaseous signaling components (i.e. CO and NO) may also be sites for generation of antioxidants (biliverdin), and thus "sinks" for free radicals in adult CM.

INTRODUCTION

Caveolae ("little caves"), cholesterol- and sphingolipid-enriched 50-100 nm invaginations of the plasma membrane,[3, 4] are a subset of lipid rafts [5]. Caveolae, as membrane microdomains, help regulate a number of cellular functions, including endocytosis, calcium homeostasis, transverse tubule (T-tubule) formation in skeletal muscle and G protein-coupled receptors (GPCR) compartmentation [11, 12]. Caveolar microdomains have been proposed as sites that concentrate GPCR, heterotrimeric G-proteins and GPCR/G-protein-regulated effector molecules [23, 99]. Other work has indicated that caveolae are sites that concentrate the expression of endothelial nitric oxide

synthase (eNOS, NOS3), which synthesizes NO in numerous cell types, including cardiac

myocytes [27, 32]. It was recently reported that heme oxygenase-1 (HO-1), the rate-limiting

enzyme in the degradation of heme that generates biliverdin, iron and carbon monoxide

(CO), also localizes to caveolae in pulmonary arterial endothelial cells and renal mesangial

cells [26, 115]. Together, such findings suggest that GPCR-derived second messengers, as well

as NO and CO, can be generated in localized membrane regions so as to facilitate

coordinated and kinetically favorable signaling, perhaps together with regulation of

reactive oxygen species [22, 26, 35, 116-120]. Whether caveolae from cardiac cells, in particular

adult cardiac myocytes (CM), also localize such signaling components has not been

demonstrated although recent work indicated co-localization of eNOS and certain GPCR

signaling components in neonatal CM [35].

The precise determinants of localization of components in caveolae are not fully

understood [24]. One key contributor is caveolin (Cav), a structural and scaffolding protein

essential for the formation of caveolae, that exists in three isoforms (Cav-1, -2, and -3);

Cav-1 is highly expressed in adipocytes, endothelial cells, fibroblasts, smooth muscle

cells, and epithelial cells [43, 121] while Cav-3 is preferentially expressed in striated muscle

[45, 122]. Cav-1 co-localizes with Cav-2 and forms hetero-oligomeric complexes of 14-16

monomers in caveolae, while Cav-3 typically forms larger homo-oligomers *in vitro* [45].

Arterial smooth muscle cells are the only adult cell type known to express all three

caveolin isoforms [122, 123].

The use of Cav-1-deficient mice has facilitated the study of the functional role of

caveolae *in vivo* [10]. The absence of caveolae, observed in multiple tissues in these mice,

blunts NO and calcium signaling in the cardiovascular system, resulting in impaired endothelium-dependent relaxation, contractility and maintenance of myogenic tone [59]. Cav-1-null mice express Cav-3 in cardiac and other striated muscle but the animals have abnormal cardiac function, including an enlarged right ventricular cavity, decreased systolic function, myocyte hypertrophy, and hyperactivation of the p44/42 MAPK (Erk 1/2) cascade [59, 61]. Although no detailed studies have characterized the localization of Cav-1 in adult CM, the findings from Cav-1-deficient mice provide circumstantial evidence that Cav-1 may be present and functionally active in the heart. Other studies have detected co-fractionation and co-immunoprecipitation of Cav-2 and Cav-3 in cardiac preparations [124]. Capozza *et al* [125] recently reported the co-immunoprecipitation of all three caveolin isoforms in transfected L6 myoblast cells but not in mouse embryonic fibroblasts, indicating that this interaction is cell type-specific.

In the present study, we used primary cultures of adult rat and mouse CM and utilized sucrose density centrifugation, co-immunoprecipitation, immunofluorescence and electron microscopy to determine if adult CM express all three caveolin isoforms together with enzymes involved in free radical generation (e.g, HO-1 and eNOS). Our findings support this hypothesis and suggest an important role for caveolin family members in cardiac physiology and pathophysiology, in particular in regulation mediated by the activation of eNOS and HO-1, perhaps, at least in part, as the consequence of close association of caveolae and mitochondria.

RESULTS

Caveolin mRNA and protein expression in adult rat and mouse CM. We initially

investigated the expression of mRNA and protein for Cav-1, Cav-2, and Cav-3 in

ventricular CM isolated from adult rats and mice. Analysis by real-time PCR showed the

expression of all three Cav isoforms, with higher levels of mRNA expressed in rat versus

mouse ($P<0.05$, Fig. 3-1*A*). The relative expression of the different Cavs was different in

rat (Cav-1>Cav-3>Cav-2) vs. mouse (Cav-3>Cav-1>Cav-2). To assess for expression of

Cav proteins, we used sucrose density centrifugation of CM disrupted using a non-

detergent method and probed with antibodies specific for each of the Cav isoforms. All 3

forms of Cav were detected in buoyant fractions (BF, 4-5) and heavy fractions (HF, 9-12)

in adult rat CM, albeit with more Cav-3 than Cavs-1 and –2 in HF (Fig. 3-1*B*). Adult

mouse CM subjected to sucrose density fractionation revealed a distribution of Cavs

similar to that in rat CM: Cav's-1, -2, and –3 were present in BF but much less Cav-1

was detected in HF compared to Cav-2 and Cav–3 (Fig. 3-1*C*). Taken together, these

findings demonstrate expression of mRNA and protein for all three Cav isoforms in adult

rat and mouse CM with all three isoforms present in BF following sucrose density

fractionation.

Co-immunoprecipitation reveals Cav-1 and Cav-3 in multi-protein complexes in

CM. Assessment of rat CM lysates by co-immunoprecipitation revealed Cav-1, Cav-2

and Cav-3 in Cav-1, Cav-2, and Cav-3 immunoprecipitates (Fig. 3-2*A*). Because filamin is

an F-actin cross-linking protein and known ligand for Cav-1 [73], we assessed whether Cav-

1 and Cav-3 are present in filamin immunoprecipitates. Comparing CM of wild-type mice

for Cav expression with CM of Cav-1-null mice, we detected Cav-1 in both Cav-3 and

filamin immunoprecipitates but only in lysates of control, not those from Cav-1-null mice

(Fig. 3-2*B*). Cav-1, Cav-2 and Cav-3 were also detected in Cav's-1, -2, and -3

immunoprecipitates of mouse CM lysates (Fig. 3-2*B*). Thus, all three Cav isoforms are

expressed and form multi-protein complexes in adult rat and mouse CM lysates.

Immunofluorescence microscopy demonstrates expression of Cav's-1, -2, and –3

and co-localization between Cav-3 and Cytochrome C in CM. We used

immunofluorescence and deconvolution microscopy as a further means to assess whether

adult CM express all three caveolin isoforms and to determine if Cav-3 localizes near

other cellular organelles. We detected Cav-1 and Cav-3 in a punctate pattern along the

sarcolemmal membrane and in transverse striations within the interior of the cell while

Cav-2 stained predominantly along the sarcolemmal membrane with diffuse intracellular

staining (Fig. 3-3*A*). Cav-3 co-localized with cytochrome C, a mitochondrial marker, along

the sarcolemmal membrane and in sub-sarcolemmal regions (Fig. 3-3*B*, ~70% co-

localization within 2 mm of the surface). By contrast with the co-localization in those

regions, Cav-3 and cytochrome C stained in parallel, transverse patterns with minimal co-

localization within the interior of the cells. Electron microscopy revealed that rat CM

have abundant caveolae closely apposed to sub-sarcolemmal mitochondria (arrows, Fig. 3-

4*A*,*B*). Quantitation revealed that more sub-sarcolemmal mitochondria are associated with

regions of the membrane that contain caveolae (~10 fold more, Fig. 3-4*C*) and that ~50%

of total caveolae/mm of sarcolemma associates with sub-sarcolemmal mitochondria (Fig.

3-4*D*). These data indicate that adult CM express all three Cav isoforms and that Cav-3 is

found along the sarcolemmal membrane and in sub-sarcolemmal regions, in some sites closely juxtaposed to sub-sarcolemmal mitochondria.

HO-1 and eNOS are present in BF following sucrose density fractionation of rat CM. To assess whether HO-1 and eNOS co-localize with caveolin in adult CM, we tested whether these enzymes distribute to BF and immunoprecipitate together with Cav isoforms. Both eNOS and HO-1 were detected in BF of adult rat CM following sucrose density fractionation (Fig. 3-5*A*). In addition, Cav-1, Cav-3, and HO-1 were detected in HO-1 and eNOS immunoprecipitates of rat and mouse CM lysates (Fig. 3-5*B*). HO-1 was also detected in Cav's-1, -2, -3 immunoprecipitates from mouse and rat lysates. Thus, enzymes involved in the generation of CO and NO distribute to buoyant caveolin fractions and are present in multi-protein complexes with caveolin in adult CM.

DISCUSSION

The current studies provide new information regarding several aspects of caveolae and caveolins in the heart: 1) using multiple techniques, we show that in addition to the well-known expression of Cav-3, Cav-1 and Cav-2 are also expressed in adult CM; 2) we found that caveolins in adult CM localize with two key enzymes, eNOS and HO-1, that are involved in regulation of reactive species; 3) we show the close apposition of caveolae and mitochondria, thus identifying an aspect of cardiac caveolae expression that has not been previously emphasized.

The repetitive movement of the heart requires an ongoing supply of energy and oxygen consumption, which likely is reflected in the high mitochondrial content. Preservation of mitochondrial function [126, 127] and stimulation of mitochondrial ATP-dependent potassium channels (K_{ATP}) [110, 128, 129] have been linked to protection of the ischemic myocardium; however, little is know regarding mechanisms by which extracellular stimuli "communicate" with intracellular organelles, such as mitochondria, to produce these effects. Our finding that caveolae are in close proximity to sub-sarcolemmal mitochondria define potential microenvironments in adult CM that may contribute to the regulation of cardiac function, a result akin to findings observed in certain smooth muscles [130]. Of note, pathophysiologic conditions, such as ischemia, that deprive the heart of oxygen or that result in a mismatch between energy production and energy utilization (e.g., congestive heart failure) have been linked to altered expression of caveolae and/or redistribution of caveolin [48, 49, 131, 132].

The contribution of mitochondria in cardiovascular disease suggests that there may be a close link between generation of reactive species and mitochondrial signaling, however, the precise mechanisms involved in regulating cardiac energetics during conditions of increased demand and reduced supply are unknown. Several studies have demonstrated the phosphorylation of Cav on Tyr^{14} by Src family kinase members following oxidative stress, thus implicating such modifications of Cav in signaling by reactive species [50, 52, 53, 133, 134]. These reactive species may serve as a bridge between surface sarcolemmal caveolae and mitochondria that are in close proximity and thereby may contribute to intracellular regulation by extracellular signals. Increased free radicals can produce damage via reactivity with biologically important molecules such as lipids [135, 136], proteins [137-139], and DNA [140, 141], while CO and NO are signaling molecules that help modulate the negative impact of reactive species [142-144].

Our finding that expression of eNOS and HO-1, which generate NO and CO, respectively, co-fractionate and co-immunoprecipitate with caveolins suggests that caveolae are sites that regulate production of these reactive species. Of note, biliverdin, the other product of catalysis of heme by HO besides CO, also provides protection from oxidative damage [145-147]. Other data link mitochondrial K_{ATP} channel activity to actions of NO in ventricular myocytes [148] and to generation of reactive species in an atrial-derived cell line [149]. HO-1 expression is enhanced with ischemia [150] while over-expression of HO-1 protects rat hearts from ischemia/reperfusion injury via an anti-apoptotic mechanism [151] and improves post-ischemic dysfunction [152]. Such studies, which suggest potential links

between the generation of reactive species and protection of the heart from oxidative

damage, are consistent with the current results that emphasize caveolae and mitochondria

and the association with caveolin of HO and eNOS in adult CM.

Unlike the well-known expression of Cav-3, the existence of Cav-1 and -2 in adult

CM has not previously been reported, although others have noted a relationship between

Cav-2 and Cav-3 with increasing expression of Cav-2 in neonatal CM placed in culture [124]

as well as muscle-type-specific expression and interactions of caveolins [125]. Our recent

data suggest that caveolin-3 acts as a scaffolding molecule in adult CM at sites in addition

to surface sarcolemmal caveolae [40]. Observations akin to ours have been made by Li *et al*

[153] who have suggested that localization of Cav-1 is not restricted to plasma membrane

caveolae but can occur in other cellular regions, including mitochondria in airway epithelial

cells. Such findings and others indicate that not only caveolin isoform distribution but also

protein composition of caveolae varies among cell types, although the precise

determinants for the latter differences have not-yet been defined [24].

In conclusion, our findings show that all three caveolin isoforms are expressed in

adult CM and that they interact with both eNOS and HO-1, enzymes that form gases

that regulate cells. The interaction of caveolin isoforms with enzymes involved in

generating reactive species and the enrichment of these enzymes in caveolar microdomains

provides a novel mechanism for regulation of CM by external stimuli. The close

proximity of caveolae with mitochondria may provide a means to regulate mitochondrial

function and impact of mitochondrial products on other organelles in CM. We speculate

that studies designed to explore this association between mitochondria and caveolae have the potential to yield information that will further our understanding of cardiac myocyte energetics and pathophysiology.

A)

B)

Rat ACM

Cav-1
Cav-2
Cav-3

4 5 6 7 8 9 10 11 12
BF   HF

C)

Mouse ACM

Cav-1
Cav-2
Cav-3

4 5 6 7 8 9 10 11 12
BF   HF
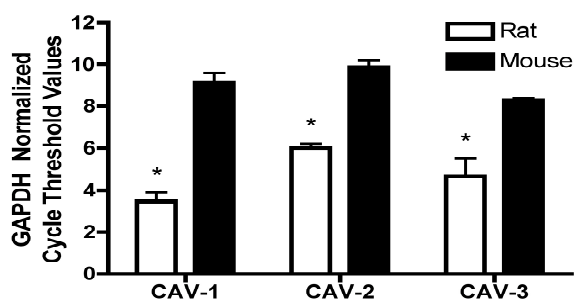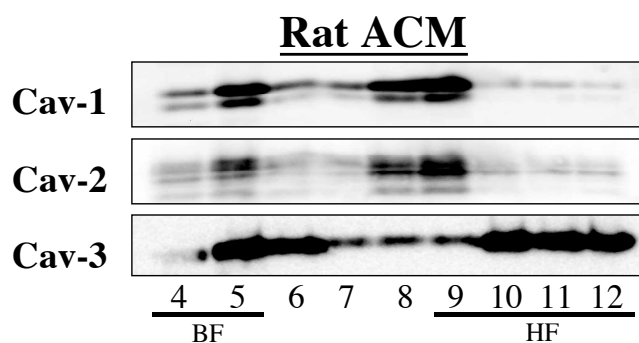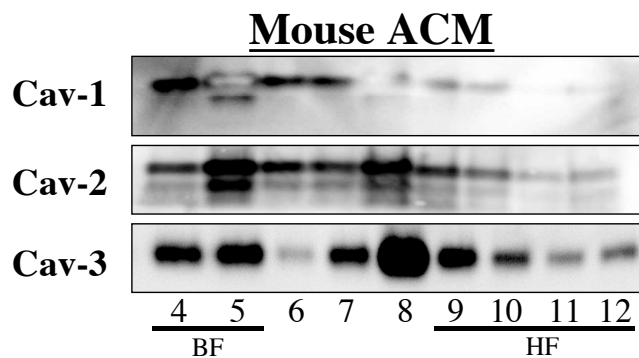
Fig. 3-1. Real-time -PCR and immunoblot analysis shows expression of Cav's-1, -2, and -3 in adult rat and mouse CM. *A,* Real-time PCR analysis of Cav-1, Cav-2, and Cav-3 in adult rat and mouse CM. *B and C,* Adult rat (B) and mouse(C) CM were subjected to Na_2CO_3 extraction followed by sucrose density fractionation, as described in Methods and demonstrate Cav's-1, -2, and –3 are distributed in buoyant (BF, 4-5) and heavy fractions (HF, 9-12).

A)
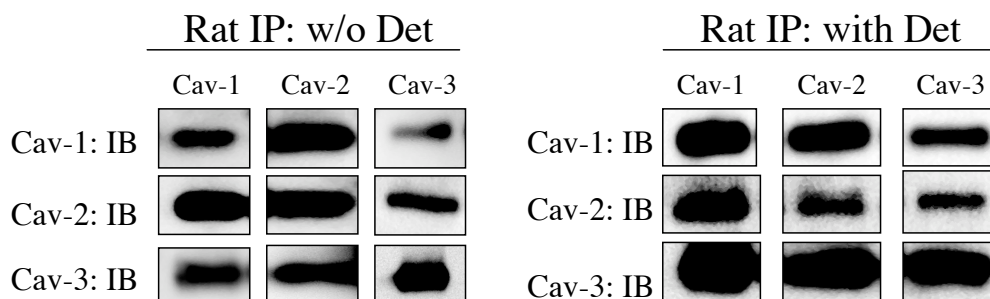
B)
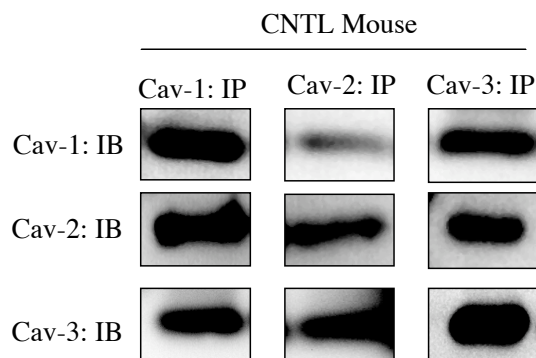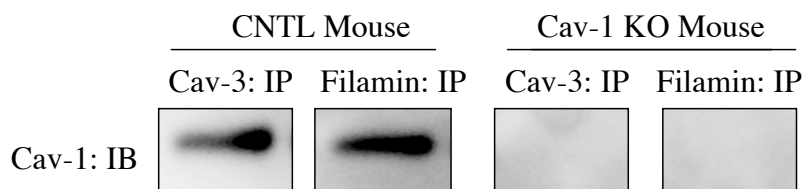
Fig. 3-2. Caveolin isoforms co-immunoprecipitate in adult rat and mouse CM lysates. *A,*
Immunoblot analysis shows Cav's-1, -2 and -3 in Cav's-1, -2, and -3 immunoprecipitates
(without and with detergent [Igepal 1%]) of rat (*A*) and mouse (*B*) adult CM. *B,* Cav-1
was detected in Cav-3 and filamin immunoprecipitates of wild-type adult CM, but not in
Cav-3 and filamin immunoprecipitates from Cav-1 null adult CM.

A)

Cav-1 **Cav-2** **Cav-3**

B)

Cav-3   Cyto-C   Overlap
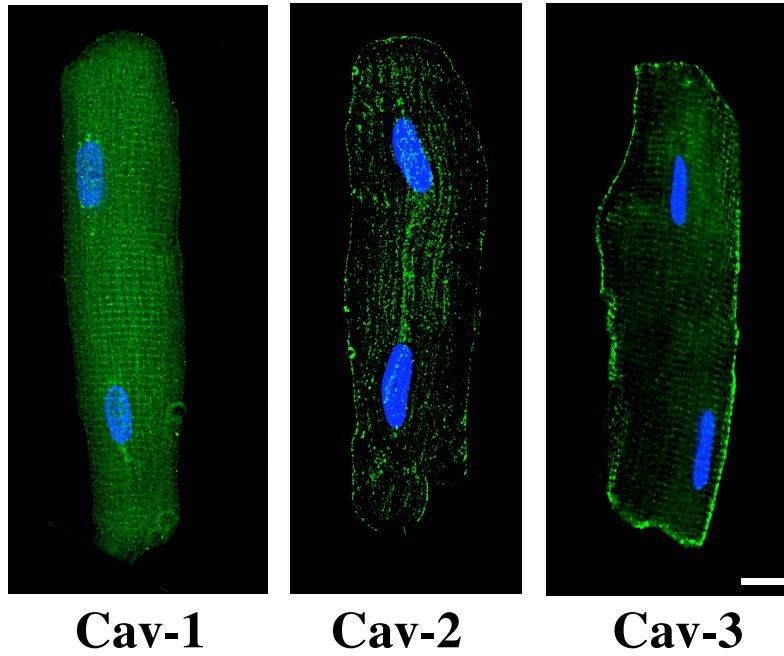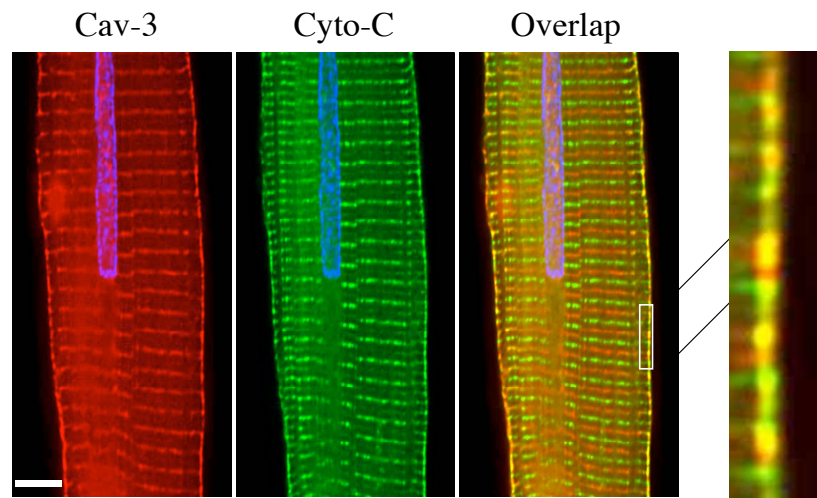
Fig. 3-3. Immunofluorescence and de-convolution microscopy demonstrates expression of Cav's-1, -2, and −3 and co-localization between Cav-3 with cytochrome C in rat CM. Adult rat CM were stained with antibodies for Cav-1, Cav-2, and Cav-3 (A) or with antibodies for Cav-3 and cytochrome C, a mitochondrial marker (B). Inset represents quantitated regions within 2 μm of image surface that reveal ~70% co-localization between Cav-3 and Cyto C. Images were de-convolved and shown as single stained myocytes or overlaid to show co-localization. Scale bar, 10 μm.
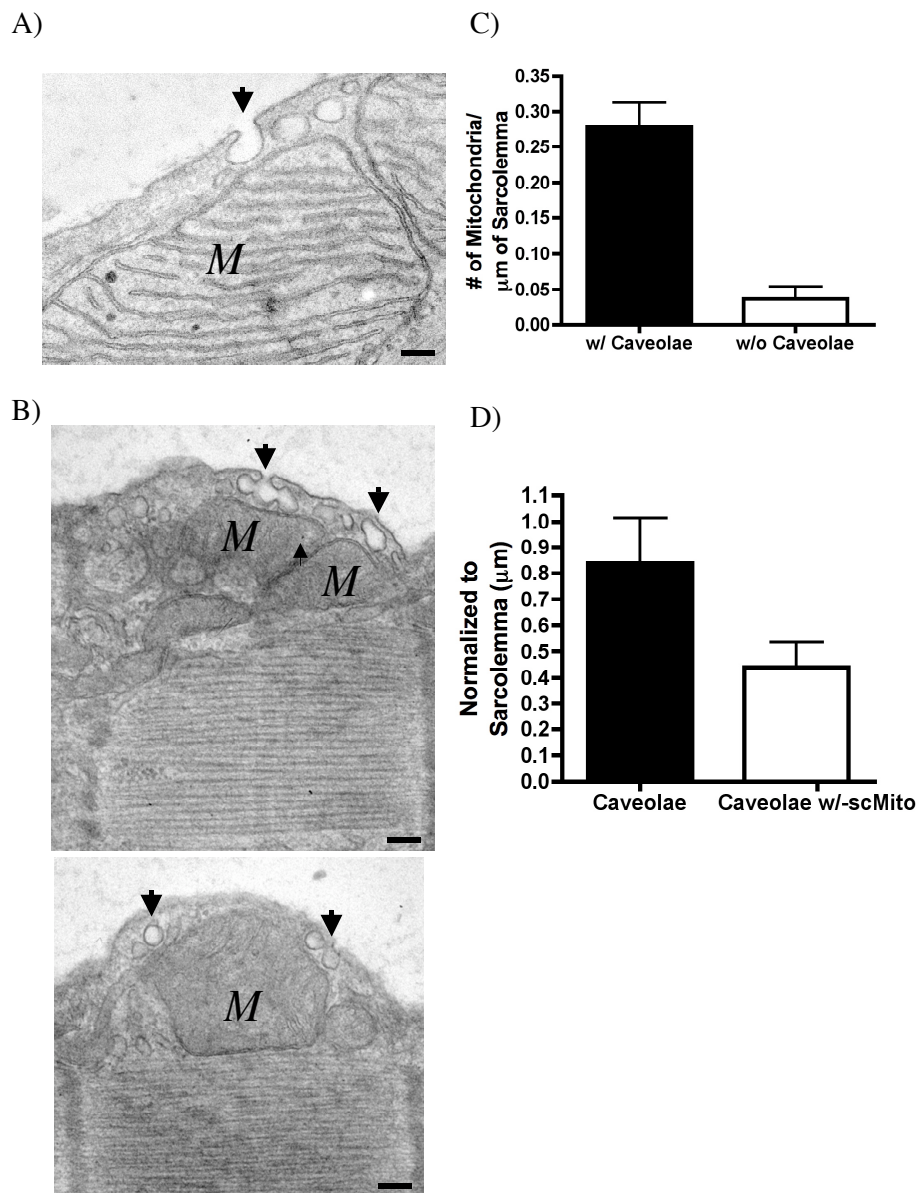
Fig. 3-4. Electron microscopy reveals abundant caveolae clustering near sub-sarcolemmal caveolae in adult rat CM. *A,* Electron microscopy, performed as described in Methods, shows that sarcolemmal caveolae are adjacent to sub-sarcolemmal mitochondria. Scale bar, 0.1 μm. *B,* A lower magnification image reveals clusters of sarcolemmal caveolae adjacent to sub-sarcolemmal mitochondrial membrane (arrow). *C,* Data were quantitated as total subsarcolemmal-mitochondria/mm of sarcolemma that are and are not associated with caveolae. Association was defined as less than the diameter of 2 caveolae, i.e., ~200 nm. *D*, Data were quantitated as total caveolae/mm of sarcolemma and total caveolae associated with subsarcolemmal-mitochondria (sc-Mito) with 2 μm. of the cell surface. Each mitochondrion is represented by *M* and arrows indicate caveolae. Scale bar, 0.2 μm.
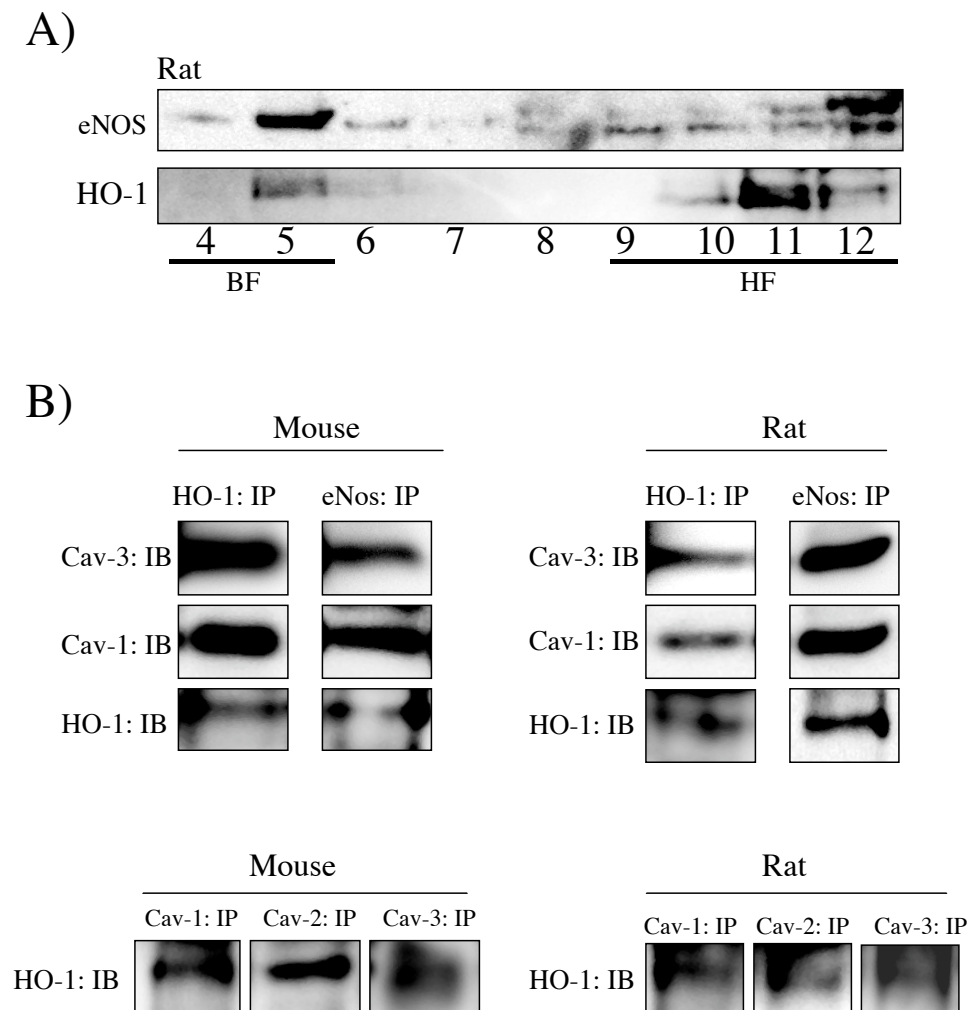
Fig. 3-5. HO-1 and eNOS distribute to buoyant Cav fractions and are detected in immunoprecipitates for Cav's-1, -2, and −3 in adult CM. *A,* HO-1 and eNOS localized in both buoyant (BF, 4-5) and heavy fractions (HF, 9-12) following sucrose density centrifugation of Na_2CO_3 extracts of rat CM. *B,* Cav-3 and Cav-1, and HO-1 were detected in HO-1 and eNOS immunoprecipitates of mouse and rat CM. HO-1 was also detected in all Cav's-1, -2, and −3 immunoprecipitates from rat and mouse lysates. Due to the close proximity of the agarose band with the predicted molecular weight of HO-1 (37 kDa), short exposure times (10 s) were used to detect HO-1, thus generating a relatively faint band.

Chapter 4

Cytoskeletal components regulate expression of caveolae, caveolin phosphorylation and cAMP production

ABSTRACT

Microtubules and microfilaments regulate plasma membrane topography but their role in compartmentation of caveolar-resident signaling components, in particular those that regulate cAMP production, has not been defined. The present study tests the hypothesis that the microtubular and actin cytoskeleton influences localization of caveolin (Cav) and presence of caveolae, thereby altering the distribution of G protein-coupled receptor (GPCR) signaling components involved in regulating cAMP production in adult cardiac myocytes. Depolymerization of microtubules with colchicine (Colch) for 60 min or of microfilaments with cytochalasin D (CD) for 90 min dramatically reduced the percent of cellular Cav-3 in buoyant membrane fractions following sucrose density gradient fractionation: Colch, 4.0 ± 1.9 %, n=4, CD, 2.1 ± 0.9 %, n=4, vs. Control, 26.2 ± 2.3 % (n=11, p<0.0001), increased the expression of Cav-3 in "heavy" fractions. Colch or CD treatment caused Cav-1, Cav-2, β_1-adrenergic receptors (β_1-AR), β_2-AR, $G\alpha_s$ and adenylyl cyclase (AC)$_{5/6}$ to be excluded from buoyant fractions but increased, isoproterenol (β-AR agonist)-stimulated cAMP production ($P<0.05$ vs. Control). Immunofluorescence microscopy showed that Colch decreased co-localization of Cav-3 and α-tubulin and that both Colch and CD decreased co-localization between Cav-3 and filamin, an F-actin cross-linking protein. Colch and CD decreased phosphorylation of Cav-1, Src, and p38 MAP kinase and reduced the number of caveolae/μm sarcolemma, as measured by electron microscopy. Taken together, the findings implicate a role for microtubules and microfilaments in the presence of morphologic caveolae and indicate that phosphorylation of caveolin appears to be required for its ability to blunt GPCR-AC signal transduction.

INTRODUCTION

The three components of the cytoskeleton - intermediate filaments, microtubules, and microfilaments - contribute to the structural organization of the cytoplasm and help regulate the topography of the plasma membrane in eukaryotic cells [62-64]. Microtubules and microfilaments have nucleotide-binding and hydrolyzing activity, while intermediate filaments, which serve as cytoskeletal 'identity cards' to distinguish among different cell types, have no known enzymatic activity. The actin-associated cytoskeleton,

microfilaments, are involved in cell motility, adhesion, and endocytosis; disassembly of the actin cytoskeleton leads to fusion of intracellular vesicular membranes with the plasma membrane [75]. The polymerized tubulin cytoskeleton, microtubules, are involved in cell locomotion, movement of organelles and mitosis. Both microfilaments and microtubules are implicated in membrane trafficking, including that of caveolae-containing membranes, in mitotic cells [74].

A growing body of evidence suggests a connection between cytoskeletal components and caveolar-regulated cellular events [73-75]. Caveolae, 50-100 nm invaginations of the plasma membrane that contain cholesterol, sphingolipids, and the structural protein caveolin (Cav-1, -2, and –3) [3, 5], have been shown to serve as sites for actin "tail" formation [75] and can be anchored to the cell surface by cortical actin filaments [77]. Caveolae participate in a variety of cellular functions, including endocytosis [154], calcium homeostasis [155], skeletal muscle transverse tubule (T-tubule) formation [11] and compartmentation of receptor-mediated signaling components [22, 40]. Among the latter are G protein-coupled receptors (GPCR), heterotrimeric G-proteins, and GPCR/G-protein-regulated effector molecules, a population of which localize in caveolae, thereby facilitating coordinated and rapid generation of second messengers and regulation of cell function [22, 40]. However, the contribution of microtubules and microfilaments to caveolar-regulated signal transduction, in particular GPCR-G-protein signaling, remains relatively unknown. In this regard, it is of interest that treatment of cells with cytoskeletal

disrupting agents can influence GPCR-mediated signal transduction and GPCR desensitization/resensitization, as will be described subsequently.

An example of a physiologically important GPCR is the β-adrenergic receptor (β-AR), whose activation by the sympathetic nervous system or circulating catecholamines is a key mechanism for production of the second messenger cAMP in numerous tissues, including the mammalian heart [156]. The synthesis of cAMP is regulated by GPCR that activate (via G_s) or inhibit (via G_i) the activation of adenylyl cyclase (AC). Substantial data over the past three decades have indicated that β-AR-stimulated cAMP formation can be enhanced by agents that disrupt microtubules or microfilaments but the precise mechanisms have not been defined [157-159]. Other data have indicated co-localization with and regulation by caveolins of β-AR and other GPCR, G_s, and ACs [14, 40]. Since the effectiveness of this signaling cascade is dependent upon the organization and location of signaling proteins within the plasma membrane, in the present study we sought to determine if there was a mechanistic link between the localization of GPCR signaling components in caveolae and the ability of cytoskeletal agents to alter β-AR signal transduction. We thus undertook experiments to assess the impact of disruption of microtubules and microfilaments in adult cardiac myocytes on the distribution of caveolae, caveolins and GPCR signaling components, in particular as related to GPCR-G_s mediated-cAMP production. The results indicate that intact microtubules and microfilaments contribute to the presence of caveolae and the phosphorylation state of

caveolin, which appears to be required for tonic inhibition of GPCR-G_s-AC signal transduction.

RESULTS

Caveolin (Cav) isoforms, β-AR, $G\alpha_s$, and $AC_{5/6}$ are excluded from buoyant fractions following cytoskeletal disruption. To test the impact of cytoskeletal disrupting agents on expression and co-localization of caveolins and GPCR-G_s-AC, we investigated the distribution of Cav-3 and signaling components in fractions prepared by sucrose density gradient fractionation of adult CM treated with colchicine (Colch) or cytochalasin D (CD), using conditions previously validated to lead to inhibition of microtubule and microfilament assembly, respectively [67, 160, 161]. Cav-3 was detected in both buoyant fractions (fractions 4 and 5, termed buoyant caveolin-rich fractions, BF) and heavy/non-buoyant fractions (fractions 9-12, HF) in non-treated cardiac cells (Fig. 1*A, top panel*). Treatment with Colch and CD prominently decreased the percent of total cellular Cav-3 detected in BF: Colch, 4.0 ± 1.9, n=4, CD, 2.1 ± 0.9, n=4, vs. control, 26.2 ± 2.3, n=11 (*P*<0.0001) with compensatory increases in Cav-3 in HF (Fig. 4-1*A,B*). Treatment with Colch or CD also redistributed Cav-1 and Cav-2 from BF to HF and produced a similar redistribution of β_1-AR, β_2-AR, $AC_{5/6}$, and $G\alpha_s$ (Fig. 4-2*A-C*). In parallel with this redistribution of signaling components, the β-AR agonist isoproterenol produced a greater amount of cAMP in Colch-, nocodazole- (Nocod; another microtubule disrupter), and CD-treated CM (Fig. 4-2*D*; *P*<0.05 vs. Control). These results show that agents that

depolymerize microtubules and microfilaments of adult CM redistribute caveolin isoforms and β-AR signaling components (i.e., β-ARs, $AC_{5/6}$, $G\alpha_s$) from BF to HF and enhance β-AR-stimulated cAMP production, suggesting disruption of caveolae, which we corroborated by electron microscopy, to be shown subsequently (Fig. 4-8).

   Treatment with Colch and CD decreases Cav-1, p38 MAP kinase, and Src phosphorylation in adult CM. In addition to redistributing caveolins, β-AR, $AC_{5/6}$, and $G\alpha_s$, treatment with Colch or CD altered the phosphorylation of Cav, which has been shown to be mediated by Src tyrosine kinase family members [50]. Colch treatment decreased the amount of phospho-Cav-1 (P-Cav-1), phospho-Cav-2 (P-Cav-2), P-p38, and P-Src, albeit the latter exhibited a somewhat slower time course (Fig. 4-3*A*). CD treatment decreased P-Cav-1, P-p38, and P-Src, but not P-Cav-2 (Fig. 4-3*B*). In contrast to P-p38, P-Erk 1/2 expression was not altered following treatment with Colch or CD (data not shown). Sucrose density centrifugation revealed that in control cells, the majority of P-Cav-1 and P-Src (but not Src [T-Src in Fig. 4-3C]) distribute in BF, with some P-Src in HF, and Colch or CD treatment decreases and redistributes P-Cav-1, P-Src and T Src (Fig. 4-3*C*). The antibody for P-Src may cross-react with other Src family members in equivalent phosphorylation states (according to the antibody manufacturer), thus potentially explaining the different bands detected in BF and HF. These results demonstrate that disruption of microtubules and microfilaments in adult CM alters caveolin phosphorylation without changing total caveolin expression and also alters phosphorylation of p38 and Src.

Treatment with methyl-β-cyclodextrin (MβCD) decreases P-Cav-1 and -2, P-p38 MAP kinase, P-Src P-Erk 1/2 and expression of total Cav-3 and increases basal, but not isoproterenol-stimulated, cAMP production in adult CM. We used MβCD, a cholesterol-depleting agent [9, 35], as an alternative approach to assess the impact of caveolae/caveolin structure on expression of signaling components and cAMP production. Treatment of CM with MβCD (2 mM; 90 min) yielded certain findings similar to those observed after cytoskeletal disruption: P-Cav-1 and -2, P-p38, P-Src decreased with MβCD treatment while expression of Cav-1 and 2 was maintained (Fig. 4-4). However, unlike what occurred with Colch or CD (Fig. 4-3), total Cav-3 expression and P-Erk 1/2 decreased in CM treated with MβCD (Fig. 4-4*A*). In addition, by contrast with results obtained in cells treated with Colch and CD (Fig. 4-2*D*), MβCD treatment increased basal cAMP content and forskolin-stimulated, but not isoproterenol-stimulated cAMP accumulation (Fig. 4-4*B*). Effects of MβCD on cAMP accumulation were not observed if cholesterol was added together with MβCD (Fig. 4-4*B*). Thus, cholesterol depletion of adult CM lowers caveolin phophorylation and has different effects on cAMP formation than does cytoskeletal disruption.

Immunofluorescence microscopy of adult CM after treatment with Colch and CD reveals irregular Cav-3 clusters in sub-sarcolemmal regions. We used immunofluorescence microscopy as a more direct means to assess the intracellular distribution of Cav-3 following cytoskeletal disruption. In untreated adult CM, Cav-3 was detected in a punctate pattern on the sarcolemmal membrane and in transverse

striations across the cells (Fig. 4-5*A, left image*). In comparison with untreated cells, treatment with Colch (*middle image*) and CD (*right image*) resulted in more prominent irregular Cav-3 clusters and aggregates in regions proximal to the sarcolemmal membrane (Fig. 4-5*A*). In untreated cells, Cav-3 co-localized with α-tubulin on both the sarcolemma and intracellular transverse striations (Fig. 4-5*B*, *left image*). Colch treatment decreased co-localization between Cav-3 and α-tubulin in both the whole cell (*P*<0.05 vs control) and sarcolemma (*P*<0.05 vs control) (Fig. 4-5*B,C*). Treatment with CD resulted in irregular Cav-3 clusters in sub-sarcolemmal regions; quantitation revealed no reduction in co-localization between Cav-3 and α-tubulin, in particular in the sarcolemma. Thus, cytoskeletal disruption causes irregular Cav-3 clustering in sub-sarcolemmal and intracellular regions and co-localization between Cav-3 and α-tubulin is dependent upon proper microtubule assembly.

Localization between Cav-3 and filamin is decreased following cytoskeletal disruption. To determine whether filamin, an F-actin cross-linking protein and known ligand of Cav-1 in non-striated cells [73], is detected in multi-protein complexes with Cav-3, we performed immunoprecipitation experiments with a filamin antibody. Cav-3 was detected in immunoprecipitates of adult CM lysates using such an antibody (Fig. 4-6*A*). Treatment with Colch, Nocod, and CD decreased the amount of Cav-3 in filamin immunoprecipitates. Immunofluorescence microscopy demonstrated that Cav-3 and filamin co-localize on the sarcolemmal membrane and in sub-sarcolemmal regions but this co-localization was decreased in both regions following disruption of microtubules or

microfilaments (Fig. 4-6*B* and 4-6*C*). Thus, Cav-3 localizes in multi-protein complexes with filamin and this complex is disrupted following depolymerization of microtubules or microfilaments.

Immunofluorescence microscopy of cytoskeletal-disrupted and cholesterol-depleted adult CM reveals a significant reduction in phosphorylation of Cav-1. We used immunofluorescence microscopy to assess phosphorylation of Cav-1 (P-Cav) following treatment of cells with Colch, CD, and MβCD in adult CM. Control CM incubated with antibodies for P-Cav-1 (red pixels) and Cav-3 (green pixels) revealed discrete regions of co-localization on the sarcolemmal membrane as well as in sparse regions within the interior of the cell (Fig. 4-7*A*, *far left image*). Treatment with Colch, CD and MβCD, but not cholesterol + MβCD, reduced Cav-1 phosphorylation ($P<0.0001$ vs control, Fig. 4-7*A,B*). Thus, both by immunoblotting (Fig. 4-3 and 4-4) and microscopy (Fig. 4-7) cytoskeletal disruption and cholesterol depletion decrease P-Cav-1 in adult CM.

Cytoskeletal disruption decreases the number of caveolae. We used EM as a direct means to assess the presence of caveolae (50-100 nm sarcolemmal membrane invaginations or vesicles within close proximity (~5-10 nm) to sarcolemma) and observed a loss of caveolae following either Colch or CD treatment (Fig. 4-8). Fig. 4-8*A* reveals abundant caveolae along the sarcolemma and closely apposed to sub-sarcolemmal mitochondria (within 0.5 μm of sarcolemma). Treatment with Colch (4-8*B*) and CD (4-8*C*) did not appear to alter the number of sub-sarcolemmal mitochondria but resulted in the loss of adjacent caveolae both on the sarcolemma (4-8*Bi,Ci*) and near sub-sarcolemmal

mitochondria (4-8*Bii,Cii*). In addition, Colch treatment resulted in vacuoles associated with omega shaped membranes resembling caveolae (4-8*Biii*), while CD treatment yielded structures adjacent to the sarcolemma that resemble fused caveolae (4-8*Ciii*) and ranged between 50-100 nm in diameter. Quantitation of total caveolae per μm of sarcolemmal membrane revealed ~ 60% reduction of caveolae (Fig. 4-8*D*) with Colch and CD treatment. These data demonstrate that cytoskeletal disruption by Colch or CD decreases the number of caveolae along the sarcolemma, near sub-sarcolemmal mitochondria and results in vacuoles (Colch) or fused omega shaped vesicles (CD) that resemble caveolae in both morphology and size.

MβCD treatment decreases sarcolemmal caveolae in adult CM. EM analysis (Fig. 4-9*A*) demonstrated that MβCD (*ii*) treatment decreases the number of sarcolemmal caveolae compared to control (*i*) or cholesterol-MβCD-treated cells (*iii*). Pooled data show that MβCD treatment produced a striking decrease in number of caveolae per μm of membrane (Fig. 4-9B). Sucrose density fractionation (data not shown) confirmed that MβCD treatment decreases the amount of Cav-3 in BF compared to untreated and cholesterol-MβCD controls.

DISCUSSION

Microtubules and the actin-associated cytoskeleton (i.e., microfilaments) are two key components for establishing membrane topography, dynamics, trafficking, and organelle movement. Proper biological function of cellular membranes (e.g., signal

transduction) can be regulated by dynamics of microtubules and the actin cytoskeleton [157-159, 162]; moreover, the role of those cytoskeletal components changes during aging and disease [79]. Here we combined the use of biochemical, functional, and microscopic techniques to investigate the role of microtubules and the actin-associated cytoskeleton in caveolae expression and β-AR-G$_s$-AC signaling compartmentation. The role of those cytoskeletal components in organizing caveolar-related GPCR signal transduction has not been previously examined. We chose to focus our efforts on adult cardiac myocytes because: 1) previous work from our lab has shown localization of β-AR-G$_s$-AC signaling components in buoyant caveolin-associated microdomains in these cells [40]; 2) past studies have demonstrated alterations in microtubule content [79, 81] (in spite of the relatively low abundance of cardiomyocyte tubulin [~0.01% of total myocyte protein]) and changes in number and morphology of caveolae during cardiac hypertrophy [163]; and 3) evidence that caveolin is redistributed in both aging and failing hearts [48].

Tissue remodeling involves alterations of both cellular and sub-cellular structures. For example, pressure-overload cardiac hypertrophy is associated with increased content of microtubules while microtubular disruption increases contraction and alters Ca^{2+} currents, β-AR responsiveness, and heart rate in normal and failing myocytes [82]. Microtubular stabilization decreases cardiac calcium transients, thus implying a role for microtubules as regulators of calcium handling [164]. In smooth muscle cells, increases in contractile tone due to mechanical stress results in cytoskeletal stiffening, actin accumulation at stress sites, and cell remodeling [165]. Treatment of smooth muscle cells

with cAMP or cytochalasin B causes disintegration of actin filaments [166] while treatment of endothelial cells with cAMP or agents that disrupt microtubules (i.e. Colch) inhibits cell migration and partial dissolution of microtubules leads to endothelial cell barrier dysfunction [167, 168]. These and other data implicate microtubules and microfilaments in cell migration, barrier dysfunction, and cellular remodeling.

Our results show co-localization of Cav-3 with α-tubulin and filamin, an F-actin cross-linking protein, interactions that were altered following cytoskeletal disruption. In spite of this disruption, we observed an enhancement in β-AR-stimulated cAMP production following treatment with Colch, Nocod and CD (Fig. 4-2*B*), implying that caveolar-related GPCR-G$_s$-AC signal transduction is restrained by normal cytoskeletal assembly and dynamics. These results are consistent with and provide a mechanism to explain prior findings pertaining to cytoskeletal-associated alterations in cAMP and [Ca]$_i$ in a variety of cells types [157-159, 169] and may relate to the ability of microtubular depolymerization to increase [Ca^{2+}]$_i$ transients [86, 87, 89].

Disruption of caveolar microdomains through the use of cholesterol-depleting agents results in exclusion of caveolin and GPCR signaling components from buoyant membrane fractions [35] and morphologic disruption of caveolae [9]. A difference between the current results and previous data is the increase in basal cAMP levels that we observed in MβCD-treated CM (Fig. 4-4*B*) that is not seen in other cell types [35]. The loss in isoproterenol-stimulated cAMP production following MβCD treatment indicates that the β-AR-Gα$_s$ or Gα$_s$-AC signaling cascade is disrupted in cholesterol-depleted adult

CM. An explanation for the increase in basal cAMP levels is loss in cyclic nucleotide phosphodiesterase (PDE) activity following caveolar disruption of adult CM, an idea consistent with recent results that indicate compartmentation of AC, PDEs and cAMP signaling components in caveolae [40, 170, 171]. Clustering of these signaling components by the cytoskeletal infrastructure may form microdomains for cAMP formation, degradation and action. Depletion of cholesterol leads to loss of sarcolemmal caveolae and may imbalance the opposing effects of resident ACs and PDEs, offsetting cAMP gradients [172-174] and disrupting cellular homeostasis [171]. The loss of Cav-3 expression following MβCD treatment (Fig. 4-4*A*), which did not occur in Colch- or CD-treated cells (Fig. 4-3), may result from degradation of components. We immunoprecipitated the cell culture media with Cav-3 antibodies but failed to find shedding of Cav-3 into the media following cholesterol depletion (data not shown), implying that intracellular degradation likely mediates the decrease in Cav-3 expression following MβCD treatment.

Previous studies have linked caveolin phosphorylation to internalization of caveolae [75, 175]. Work in mitotic cells has shown that cell detachment produces a shift in localization of phospho-caveolin-1 from focal adhesion sites to caveolae, resulting in the internalization of cholesterol-enriched membrane microdomains [175]. In the present study we detected P-Cav-1 and P-Src in buoyant fractions prior to loss of caveolae due to cytoskeletal disruption and cholesterol depletion, indicating that caveolae may be sites for activated caveolin and Src family kinases. In addition, the decrease in phosphorylated caveolin and Src tyrosine kinase in conjunction with the clearance of caveolae extends the

notion that caveolar microdomains maintain the fidelity of multiple signaling pathways and in addition, may serve as sites of attachment to the extracellular matrix in non-mitotic cells.

We also found constitutive phosphorylation of Cav-1, Cav-2, p38 MAP kinase, and Src but that this phosphorylation is reduced following treatment with agents that alter the presence of sarcolemmal caveolae (Figs. 4-3, 4-4, 4-7). Although the role of P-Cav in signal transduction is not fully understood, we hypothesize that phosphorylation of caveolin isoforms is important for maintaining caveolin hetero- and homo-oligomers [54] and forming a scaffold for signaling components, perhaps by stabilizing multi-protein complexes between caveolar resident and cytoskeletal proteins (i.e., tubulin and filamin), thereby optimizing cell signaling. In hypertrophied hearts, one finds a transient increase in the number of caveolae and abnormal caveolae associated with filamentous structures [48]. In addition, hypertrophied myocardium has an increase in phosphorylated Src tyrosine kinase at Tyr-416 [176], the active state required for caveolin phosphorylation, suggesting that cytoskeleton-membrane junctions contain binding domains for Src family kinases and that phosphorylation by these kinases is important for signal transduction [177]. Because low M_r phosphotyrosine-protein phosphatase localizes to caveolae, co-immunoprecipitates with caveolin, and dephosphorylates P-Cav [178], it will be of interest to assess the impact of cytoskeletal disruption and MβCD on this enzyme's distribution and activity.

In conclusion, cytoskeletal disruption produces loss of morphologic caveolae and redistribution of caveolar-resident proteins from sarcolemmal locales, increases cAMP production and decreases phosphorylation of caveolin isoforms, results that help explain previous observations related to the ability of cytoskeletal inhibitors to increase cellular cAMP levels. The ability of cytoskeletal components to influence the phosphorylation state of caveolins and caveolar-resident protein interactions have implications for signal transduction processes as well as for age- and pathophysiological-related changes in the heart and possibly other tissues [48].

The text of Chapter Four has been submitted for publication of the material as it appears: Head BP, Patel HH, Niesman IR, Roth DM, Farquhar MG, and Insel PA. Cytoskeletal components regulate expression of caveolae, caveolin phosphorylation and cAMP production. Submitted to *J Biol Chem*. I was the primary author and the co-authors listed in this publication directed and supervised the research which forms the basis for this chapter.

A)

Cav-3 Western

CNTL

Colch

CD

3　4　5　6　7　8　9　10　11　12

Fractions

B)

Sucrose Density Centrifugation

% Caveolin (Densitometry Units)

100

75

50

25

0

#

##

*

**

□BF
■HF

Control　　Colchicine　Cytochalasin D

* p < 0.001 vs CNTL BF　　** p < 0.01 vs CNTL BF
\# p < 0.001 vs CNTL HF　　\#\# p < 0.01 vs CNTL HF
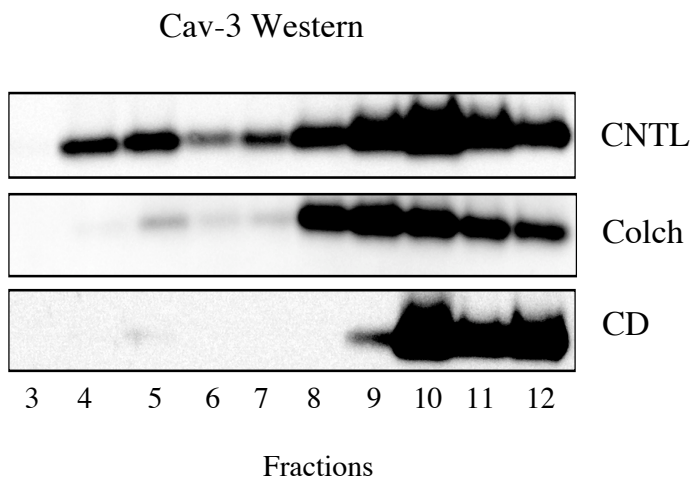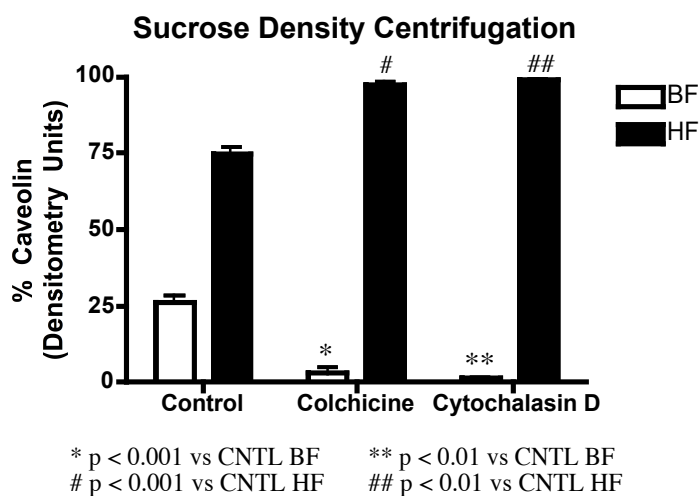
Fig. 4-1. Distribution of Cav-3 protein in adult cardiac myocytes (CM) following cytoskeletal disruption. *A,* Na_2CO_3 extraction followed by sucrose density fractionation, as described in Experimental Procedures, was undertaken with adult CM following treatment with colchicine (Colch, 30 μM; 1 h) and cytochalasin D (CD, 20 μM; 1.5 h). Cav-3 immunoblot analysis shows a decrease in the amount of Cav-3 in buoyant fractions (BF) after treatment with Colch and CD. *B,* Densitometric analysis of the Cav-3 immunoblots from Fig. 1*A* show a significant decrease in Cav-3 detected in buoyant fractions after Colchicine and Cytochalasin D.
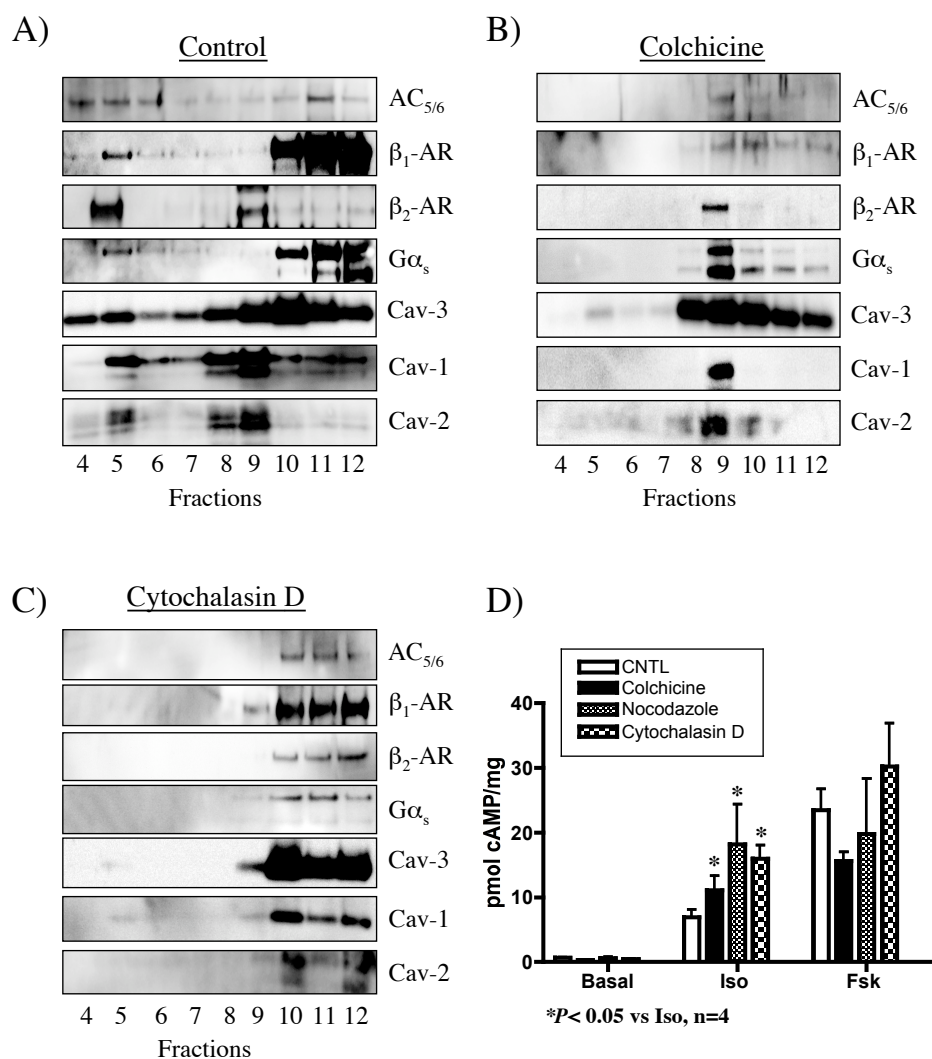
Fig. 4-2. Distribution of $AC_{5/6}$, β_1-AR, β_2-AR, $G\alpha_s$ and Cav isoforms and effects on isoproterenol-stimulated cAMP accumulation following cytoskeletal disruption of adult cardiac myocytes (CM). *A,* $AC_{5/6}$, β_1-AR, β_2-AR, $G\alpha_s$, Cav-1, -2, and –3 were detected in bouyant fractions (4,5; BF) and heavy fractions (10-12; HF) from sucrose density fractionation of Na_2CO_3 extracts. *B,* Colch (30 μM; 1 h) and *C,* CD (20 μM; 1.5 h) treatment of adult CM resulted in the total exclusion of $AC_{5/6}$, β_1-AR, β_2-AR, $G\alpha_s$, Cav-1, -2, and –3 from BF. *D,* Isoproterenol-, but not forskolin-,stimulated cAMP accumulation significantly increased ($P<0.05$) in adult CM treated with Colch, nocodazole (Nocod, 33 μM; 1 h), and CD compared to non-treated adult CM. Data are expressed as total pmol cAMP/mg ± SEM, n=4.
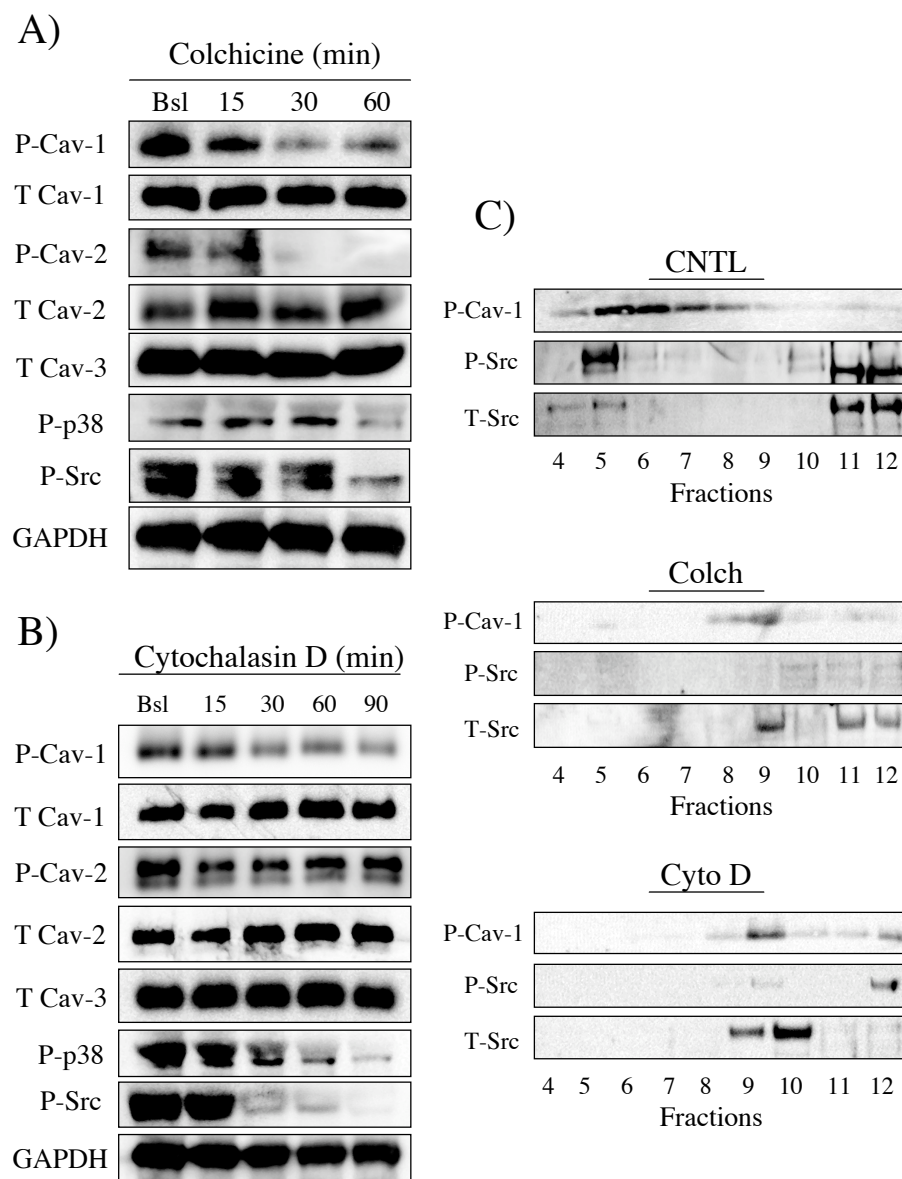
Fig. 4-3. Cytoskeletal disruption of adult cardiac myocytes decreases phosphorylation of Cav, p38 MAP kinase, and Src tyrosine kinase. Adult CM were treated with Colch (30 μM; 1 h) for 15, 30, and 60 min and CD (20 μM; 1.5 h) for 15, 30, 60, and 90 min followed by immunoblot analysis. *A,* Colch treatment decreased the amount of P-Cav-1, P-Cav-2, P-p38 MAP kinase, and P-Src tyrosine kinase after 60 min, while total Cav-1, Cav-2, and Cav-3 protein expression did not change. *B,* CD treatment decreased P-Cav-1, P-p38, and P-Src after 90 min without altering protein expression of total Cav-1, Cav-2, and Cav-3. *C,* P-Cav-1, P-Src, and total Src tyrosine kinase redistributed to HF from sucrose density fractionation of Na_2CO_3 extracts following Colch and CD treatment of adult CM.
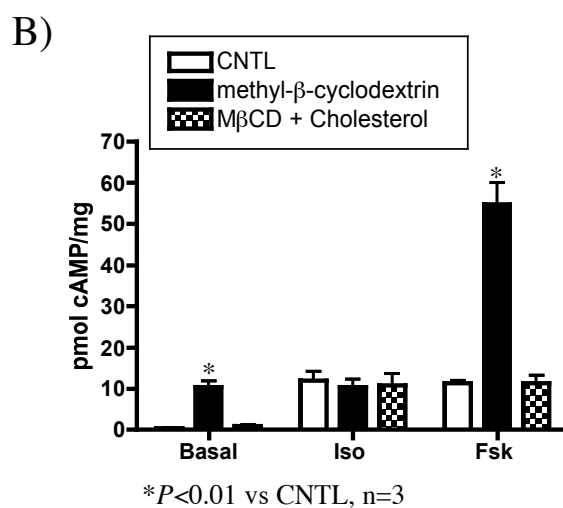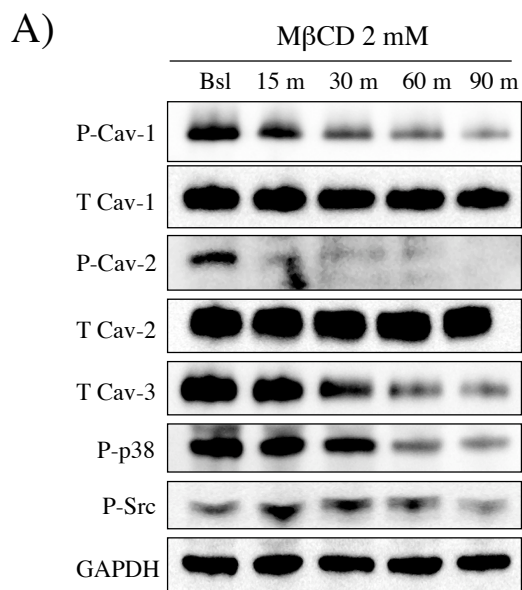
Fig. 4-4. Methyl-β-cyclodextrin (MβCD) treatment decreases phosphorylation of Cav-1 and -2, p38 MAP kinase, Src, and total Cav-3 and alters cAMP accumulation in adult CM. *A,* Cells treated with MβCD (2 µM) for 15, 30, 60, and 90 min followed by immunoblot analysis revealed a decrease in the expression of P-Cav-1, P-Cav-2, P-p38, P-Src, and total Cav-3 after 90 min. *B,* Treatment with MβCD significantly increased ($P<0.01$) basal cAMP levels. Incubation with forskolin (10 µM; 10 min), but not isoproterenol (1 µM; 10 min), following treatment with MβCD (2 µM; 1.5 h) significantly increased ($P<0.01$) cAMP accumulation compared to controls (no MβCD and cholesterol-loaded MβCD). Data are expressed as total pmol cAMP/mg ± SEM, n=3.

A) Cav-3 (**green**)

Control   Colch   CD

B) Cav-3 (**green**) and α-tubulin (**red**)

Control   Colch   CD

C)

Whole Cell
Sarcolemma

Percent of Cav-3 and α-tubulin co-localization

100

75

50

25

0

Control   Colchicine   Cytochalasin D

*
#

*p<0.05 vs control whole cell
#p<0.05 vs control sarcolemma
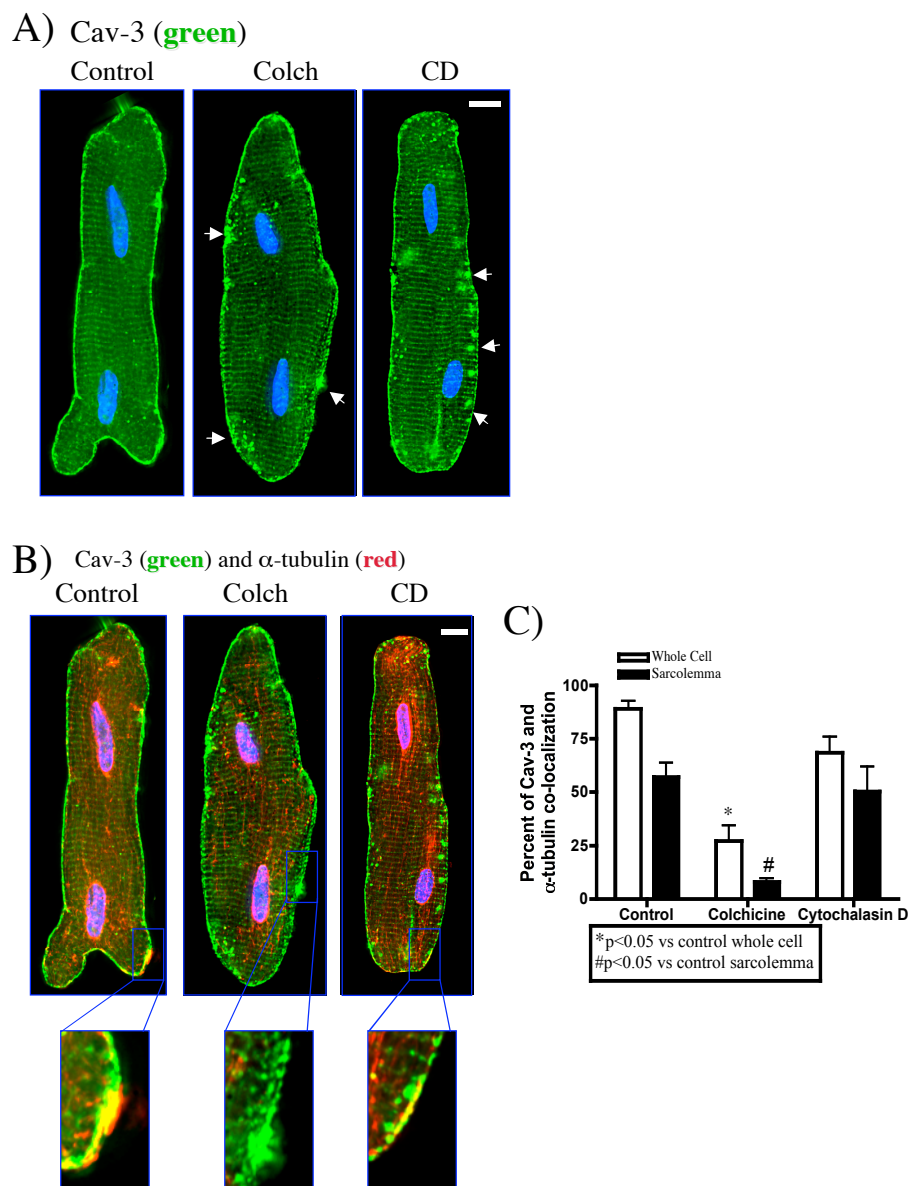
Fig. 4-5. Immunofluorescence and de-convolution analysis of the co-localization between Cav-3 and the microtubule marker (α-tubulin) following cytoskeletal disruption of adult cardiac myocytes. *A,* Treatment with Colch and CD revealed irregular Cav-3 aggregates (arrows) in sub-sarcolemmal membrane regions and in intracellular regions compared to non-treated cells. *B,* Immunofluorescence microscopy reveals that co-localization between Cav-3 and α-tubulin is significantly decreased (*P<0.5 vs* whole cell and membrane, n=3) following Colch (30 µM) treatment. *C,* Data from panel *B* is expressed as percent co-localization between Cav-3 and α-tubulin in whole cell and sarcolemmal membrane. Images were de-convolved and shown as single stained or overlaid to show co-localization. Scale bar, 10 µm.
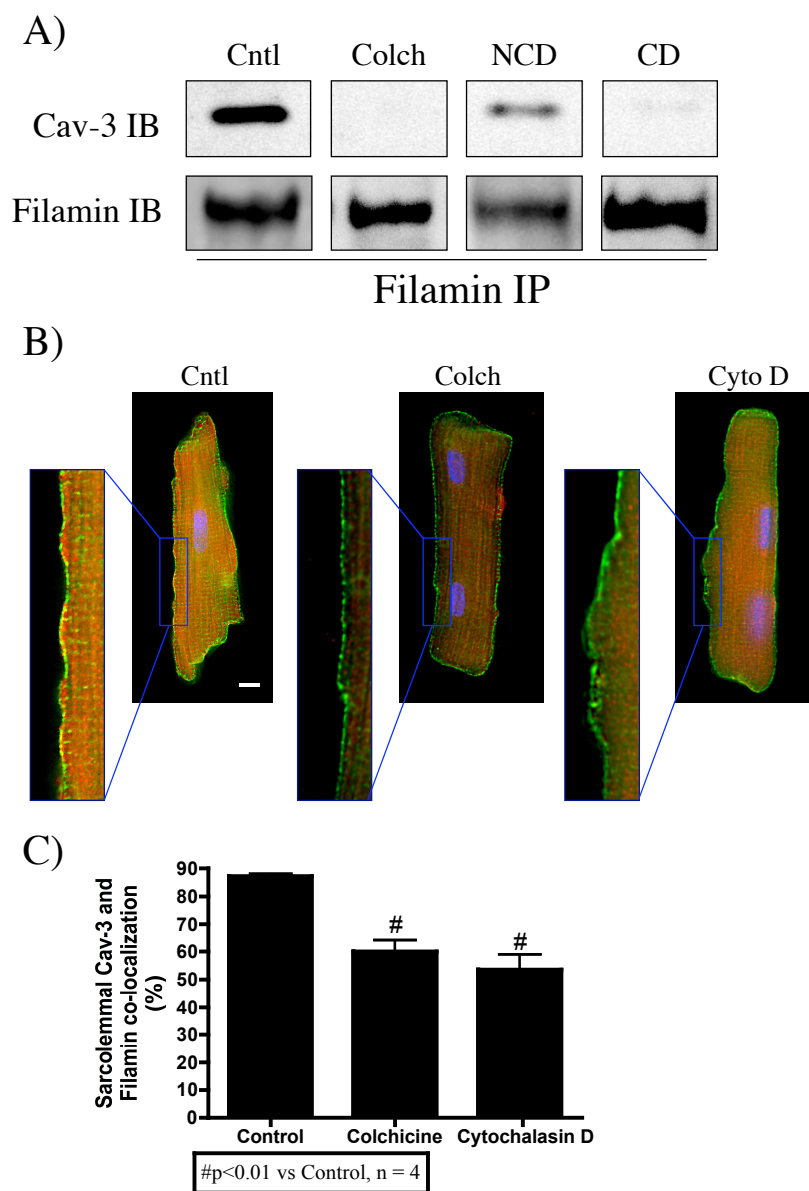
Fig. 4-6. Cytoskeletal disruption decreases co-localization between Cav-3 and filamin in adult CM. *A*, Cav-3 was detected in filamin immunoprecipitates of adult CM lysates. Treatment with Colch (30 μM; 1 h), CD (20 μM; 1.5 h) and Nocod, (33 μM; 1 h) decreased the amount of Cav-3 detected in filamin immunoprecipitates. *B*, Co-localization of Cav-3 with filamin on the sarcolemmal membrane was significantly reduced ($P<0.01$, n=4) in the presence of Colch and CD, as indicated by a reduction in yellow fluorescence (overlapping pixels). *C,* Data from Fig. 6*B* are expressed as percent sarcolemma co-localization between Cav-3 and filamin. Images were de-convolved and shown as single-stained or overlaid to show co-localization. Scale bar, 10 μm.

A)

B)
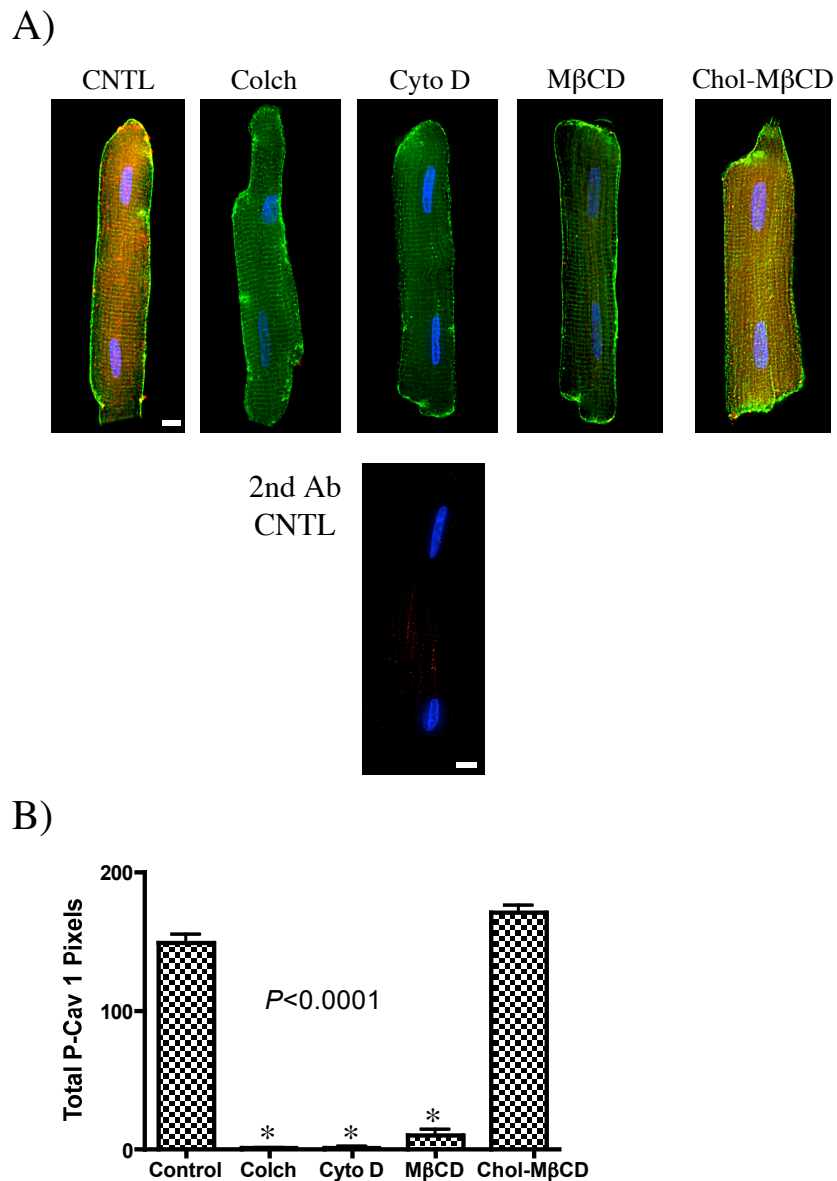
Fig. 4-7. Cytoskeletal disruption and cholesterol depletion significantly decreases P-Cav-1 expression in adult CM. *A,* Immunofluorescence and deconvolution microscopy shows partial co-localization between P-Cav-1 (red pixels) and Cav-3 (green pixels) on the sarcolemmal membrane and in sparse, intracellular locations. P-Cav-1 expression was significantly reduced ($P<0.0001$, n=3) following treatment with Colch (30 μM; 1 h), CD (20 μM; 1.5 h), and MβCD (2 mM; 1.5 h). Incubation with secondary antibodies only shows minimal background staining. *B,* Quantitation of data is expressed as P-Cav-1 pixels. Scale bar, 10 μm.

A) Control

B) Colchicine

C) Cyochalasin D

D)

EM Routine Morphology
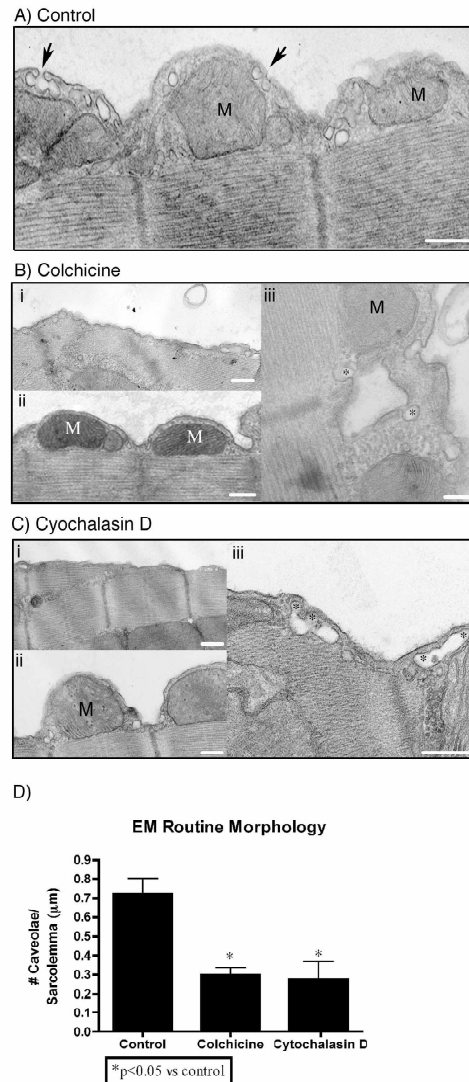
Fig. 4-8. Cytoskeletal disruption of adult cardiac myocytes decreases the number of sarcolemmal caveolae as determined by electron microscopy *A*, EM demonstrates the presence of several caveolae (arrows) on the sarcolemmal membrane near sub-sarcolemmal mitochondria (scale bar, 1 μm). Colchicine (*B*) treatment significantly decreased (*P<0.05*, n=3) the number of total sarcolemmal caveolae. *Bi* and *Bii* (scale bar 1 μm) show a decrease in the presence of caveolae while maintaining sub-sarcolemmal mitochondria and demonstrate the existence of vacuoles associated with omega shaped membranes (asterisks) (*Biii,* scale bar 0.2 μm) resembling caveolae. *Ci* and *Cii* demonstrate that cells treated with CD results in the loss of caveolae on the sarcolemma without displacing sub-sarcolemmal mitochondria (scale bar 1 μm). *Ciii* (scale bar 0.5 μm) shows CD treatment results in clustering of structures resembling caveolae adjacent to the sarcolemma (asterisks). *D*, Quantitation of data is expressed as number of caveolae per micrometer of sarcolemma. M, mitochondrion.

A)
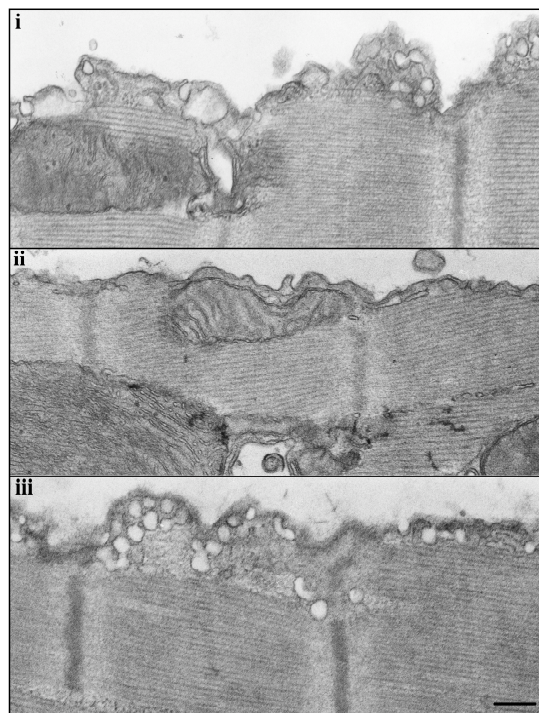
B)
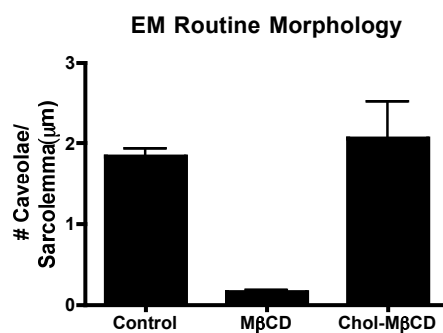
Fig. 4-9. MβCD treatment decreases sarcolemmal caveolae as determined by electron microscopy and buoyant Cav-3 as determined by sucrose density fractionation. *A*, MβCD (*i*) treatment decreases the amount of sarcolemmal caveolae in adult CM compared to control (*ii*) and cholesterol-MβCD control (*iii*), scale bar 0.2 μm. *B*, Quantitation of data is expressed as # caveolae per micrometer of sarcolemma.

Chapter 5

Caveolin-associated G protein-coupled receptors (GPCR), δ- and μ-opioid receptors (OR), inhibit β-adrenergic receptor promoted apoptosis in adult ventricular cardiac myocytes

ABSTRACT

Previous studies conducted with isolated adult cardiac myoctes (CM) demonstrate that stimulation of β_1-adrenergic receptors (β_1-AR) promotes apoptosis in a cAMP-dependent manner. Agonists of opioid receptors (OR) act via $G\alpha_i$ to inhibit adenylyl cyclase (AC) activity and protect the heart from ischemic injury but whether this protection represents blockade of apoptosis is not known. In the present study, we used CM isolated from adult rat hearts to test the hypothesis that activation of multiple OR block β-AR/AC/cAMP-induced apoptosis. CM were treated with agonists or antagonists for 24 h prior to assessing apoptosis by TUNEL staining. Pre-treatment with SNC 121 (1 μM), a δ-OR agonist, significantly ($P<0.05$) inhibited isoproterenol (1 μM)-promoted apoptosis. SNC 121 significantly ($P<0.01$) inhibited cAMP production stimulated by isoproterenol and isoproterenol plus forskolin. Treatment with DAMGO (1 μM), a μ-OR agonist, also inhibited apoptosis promoted by isoproterenol or by the AC activator forskolin. The anti-apoptotic effects of both δ-OR and μ-OR stimulation were blocked by the non-selective opioid antagonist, naloxone (0.1 μM). These data provide evidence that two different OR subtypes (δ and μ) block β-AR induced apoptosis in cardiac myocytes, at least in part by regulating activation (i.e. phosphorylation) of MAPK family members. The results thereby define a mechanism by which OR activation may protect the heart following ischemic injury or other states that lead to β-AR activation.

INTRODUCTION

Apoptosis of cardiac myocytes (CM) during fetal and early postnatal development determines the number of myocytes in the adult heart [179]. The inability of adult CM to regenerate suggests that the continued decline in the number of CM to apoptosis may contribute to loss of function in the "aging heart" and perhaps to progressive myocardial failure. Studies have shown that activation of β_1-AR-promotes apoptosis in adult cardiac myocytes, while stimulation of the β_2-AR subtype inhibits

apoptosis, primarily by coupling to $G\alpha_i$ [180]. Treatment with pertussis toxin (PTX),

which inactivates $G\alpha_i$ increases β-AR stimulated apoptosis [181]. In addition stimulation of

the M_2 muscarinic receptor, a $G\alpha_i$-coupled GPCR, with carbachol, inhibits β-AR

mediated apoptosis [181]. Similar to β_2-AR and M_2-AChR, other GPCRs that couple to

$G\alpha_i$, such as opioid receptors (δ-, μ-, and κ-OR), can protect the heart from ischemic

injury, and this protection was accomplished through the $G\alpha_i$ pathway [182]. Agonist

activation of opioid receptors has also been demonstrated to protect CM from apoptosis

[183]; however, it is not known whether OR activation protects CM from β-AR-promoted

apoptosis.

Several pathological states of the heart are associated with myocyte apoptosis

include heart failure [184, 185], myocarditis [186], and myocardial infarction [187]. Apoptotic cells

have been detected along the border zone of an ischemic region and are also present

following acute myocardial infarction in humans [188, 189]. Studies involving ischemic injury

have demonstrated cardioprotective effects through activation of δ-opioid receptor (δ-

OR)-$G\alpha_i$-protein signaling pathway [190]. Opioid receptor subtypes (δ-, μ-, and κ-OR) are

members of seven-transmembrane domain GPCRs and are present on numerous cell

types, including the central nervous system and on cardiac myocytes [191]. Radioligand

binding studies in cardiac myocytes have identified the presence of the delta (δ) and

kappa (κ) subtype of opioid receptors on ventricular rat myocytes [192, 193]. Recent work

in our lab has demonstrated the μ-OR are expressed, attenuate β-AR promoted cAMP

production, and localize with β-AR to caveolin-associated microdomains in adult CM [40].

OR may exert anti-apoptotic effects and therefore be of therapeutic significance for patients suffering from increased sympathetic nerve activity and excessive β-adrenergic stimulation, which is suggested to play a role in progressive heart failure [194]. Previous studies have shown that stimulation of δ-OR attenuates ischemic-induced apoptosis in cultured ventricular CM, suggesting a protective role of opioid receptors against cardiac myocyte apoptosis [29, 183]. With the apparent regulation of myocardial apoptosis through opposing effects from $G\alpha_s$ and $G\alpha_i$, we hypothesized and tested whether activation of opioid receptor subtypes block β-AR-promoted apoptosis in adult CM.

RESULTS

Stimulation of OR subtypes inhibit β-AR promoted apoptosis in adult CM. To test whether stimulation of OR subtypes inhibit β-AR-promoted apoptosis, we pretreated adult CM with SNC 121 (1 μM; 15 min), a δ-OR agonist, or with DAMGO (1 μM; 15 min), a μ-OR agonist, followed by treatment with isoproterenol (ISO) (1 μM; 15 min), forskolin (FSK) (10 μM; 15 min), and ISO plus FSK for 24 h (Fig. 5-1). Adult CM treated with ISO, FSK, and ISO plus FSK significantly increased the percent of TUNEL positive cells (Figs. 5-1, 5-2*A,B*; ISO, 49±6%, FSK, 50±4%, ISO + FSK, 45±1% versus control, 21±3%, *P*=0.008, 0.004, 0.001, respectively; n=4). SNC 121 significantly decreased ISO-promoted apoptosis (SNC 121, 21±4%, *P*=0.03), but had no effect on FSK or ISO plus FSK. The inhibitory effect by SNC 121 was significantly blocked by

the non-selective OR antagonist, naloxone (0.1 μM; 38±2%, versus SNC 121 + ISO, P=0.02). Pre-treatment with DAMGO (1 μM; 15 min) significantly decreased ISO, FSK, and ISO plus FSK promoted apoptosis (Fig. 5-1C). This inhibition by DAMGO was blocked by pre-treatment with naloxone (15 min). These data demonstrate that stimulation of OR subtypes attenuate β-AR-promoted apoptosis in adult CM.

SNC 121 and DAMGO lower the potency of increasing doses of ISO-stimulated apoptosis in adult CM. Because OR stimulation attenuated ISO-promoted cardiac apoptosis, we next assessed the pharmacodynamics by using SNC 121 and DAMGO in the presence of increasing concentrations of ISO (Fig. 5-3). Increasing concentrations of ISO (10^{-8} to 10^{-5} M; 24 h) augmented adult CM apoptosis, while pre-treatment with SNC 121 (1 μM; 15 min) or DAMGO attenuated ISO-stimulated apoptosis (P<0.05; Fig. 5-3A). Increasing concentrations of SNC 121 (P<0.05; 10^{-8} to 10^{-5} M) or DAMGO (10^{-8} to 10^{-5} M) prior to treatment with ISO (1 μM; 24 h) lowered ISO-promoted apoptosis (Fig. 5-3B). These data show that treatment with SNC 121 or DAMGO attenuates increasing concentrations of ISO-promoted apoptosis in adult CM.

Stimulation of OR decreases β-AR-promoted cAMP production and increases phosphorylated-p38 MAPK expression. Because stimulation of μ-OR has been shown to decrease β-AR-promoted cAMP production in adult CM [40], we tested the hypothesis that stimulation of δ-OR, a $G\alpha_i$-coupled receptor, will decrease β-AR stimulated cAMP production in these cells. Pre-treatment with SNC 121 significantly reduced ISO-stimulated (P<0.05; SNC 121, 2.5±0.6 versus control, 9.2±1, control; n=7; Fig. 5-4A) and

ISO plus FSK stimulated ($P<0.05$; SNC 121, 38.6±3.8 versus control, 51.9±7.6) cAMP production. These data show that stimulation of δ-OR significantly attenuates ISO-stimulated cAMP production in adult CM.

Because p38 MAPK activation has been shown to be anti-apoptotic in adult CM [190], we stimulated OR subtypes prior to β-AR stimulation and assayed for phosphorylation of p38 MAPK (P-p38). ISO (1 μM; 15 min) - or FSK (10 μM; 15 min) - treated adult CM showed no increase in p38 phosphorylation compared to basal (Fig. 5-4*B*). Treatment with DAMGO (15 min; 1 μM) or SNC 121 (15 min; 1 μM) increased phosphorylation of p38 without changing total p38 expression. This increase in P-p38 was blocked by the non-selective opioid antagonist, naloxone (0.1 μM). Thus, both δ-OR and μ-OR stimulation increase the phosphorylation of p38, an anti-apoptotic MAPK, and this increased phosphorylation is blocked by an opioid receptor antagonist, naloxone, in adult CM.

Agonist stimulation of β-AR and μ-OR increases Cav-1, Cav-2, and Src tyrosine kinase phosphorylation in adult CM. Because β-AR subtypes and μ-OR distribute to buoyant fractions on a sucrose density gradient and localize with caveolin on surface sarcolemma [40], we thus tested if simulation of β-AR or μ-OR increases phosphorylation of caveolin in adult CM. Treatment with ISO (1 μM) or DAMGO (1 μM) increased Cav-1, Cav-2, and Src tyrosine kinase phosphorylation with a maximal effect at 30 min (Fig. 5-5*A, B, C*). PP2, a Src tyrosine kinase inhibitor, blocked both β-AR and μ-OR stimulated induction of Cav-1 and Cav-2 phosphorylation (Fig. 5-5*D*).

DISCUSSION

Previous work from our lab has shown that β-AR and ORs localize to caveolin membrane fractions and stimulate or inhibit cardiac myocyte cAMP production, respectively [40]. Regulation of intracellular cAMP levels through stimulation of the β-AR-$G\alpha_s$-AC pathway increases the rate (chronotropy) and force of contraction (inotropy) and force of relaxation (lusitropy). This signaling pathway is considered the principal physiological mechanism for production of the second messenger cAMP in the mammalian heart, in particular by cardiac myocytes. The effectiveness of this signaling cascade is dependent upon the location and compartmentation of key signaling proteins within sarcolemmal caveolin-associated microdomains [9, 34, 35]. The findings that increased myocyte apoptosis in patients with heart failure is accompanied by increased sympathetic adrenergic activity suggests that β-AR hyper-stimulation contributes to the pathophysiology of myocardial failure [195, 196]. The present study utilized biochemical and functional techniques to test whether OR stimulation blocks β-AR-promoted apoptosis in mature cardiac myocytes.

Studies involving cardiac ischemic injury have demonstrated cardioprotective effects through activation of the δ-opioid receptor (δ-OR)-$G\alpha_i$-protein signaling pathway [190]. In addition, apoptosis has been implicated in ischemic injury in the heart [188, 197, 198] and OR stimulation has been shown to have anti-apoptotic affects in cardiac myocytes [183]. The mechanism through which OR protect the heart from ischemic injury is not well

understood. We have recently shown that μ-OR are expressed and localize with caveolin on the sarcolemmal membrane in adult cardiac myocytes, as well as attenuating β-AR-stimulated cAMP production [40]. Our findings that μ-OR stimulation blocks β-AR-promoted cardiac myocyte apoptosis independent of intact caveolae (Fig. 5*E*), and that agonist stimulation of both OR and β-AR increases phosphorylation of Cav-1, Cav-2, and Src tyrosine kinase extends the notion that μ-OR are expressed and functionally active and suggest that caveolin phosphorylation is upstream of β-AR and OR signal transmission and regulation of cardiac myocyte apoptosis.

Mitogen-activated protein kinases (MAPK) play a variety of different roles in regulating cardiac myocyte apoptosis [199]. Several studies have demonstrated p38 (four isoforms α, β, γ, and δ) can have both pro- and anti-apoptotic actions [200, 201]. Since p38 activation has been associated with $G\alpha_i$-protein coupled receptors [202], we hypothesize that the inhibitory effects from δ- and μ-OR are via activation of p38. Consistent with this hypothesis we found that treatment with SNC 121 and DAMGO, δ-OR and μ-OR increased phosphorylated-p38 expression in the presence of ISO and FSK suggesting that OR induced phosphorylation of p38 MAPK may be involved in attenuating β-AR-promoted apoptosis in adult CM.

The literature suggests that lipid caveolin-associated complexes serve as platforms to recruit and concentrate signaling molecules in order to create preformed signaling complexes [16, 22, 23]. Several lines of evidence have shown that numerous receptor tyrosine kinases (RTKs), non-receptor tyrosine kinases (NRTKs; Src-family kinases), G protein-

coupled receptors (GPCR), and heterotrimeric G-proteins localize to caveolin-associated microdomains in numerous cell types [9, 34, 35, 40]. Caveolin (Cav-1) can be tyrosine phosphorylated (Tyr^{14}) by Src family tyrosine kinases via activation of p38 MAPK in response to extracellular signaling events such as osmotic and oxidative stress, integrin ligation, epidermal growth factor, and insulin [50, 203, 204]. Cav-2 can also be phosphorylated on tyrosine 19 (Tyr^{19}) in addition to serine phosphorylated on serines 23 and 36 by casein kinase 2 [54, 55]. Src induced phosphorylation of Cav-2 localizes near focal adhesions and remains associated with caveolae suggesting that phosphorylation of Cav-2 may signal the cellular machinery to induce dissociation of Cav-2 from Cav-1 oligomers [54]. Although GPCR family members have been shown to co-localize with caveolin and distribute to buoyant Cav-membrane fractions in sucrose density gradients, our findings that stimulation of β-AR and OR induces the phosphorylation of caveolin isoforms and Src tyrosine kinase is the first to demonstrate that GPCR family members coupled to both Gα$_s$ and Gα$_i$ are involved in caveolin phosphorylation, in particular in cardiac myocytes.

In summary, the present findings demonstrate that OR stimulation attenuates β-AR promoted apoptosis in fully differentiated cardiac myocytes. Our evidence that OR and β-AR stimulation induces caveolin phosphorylation further suggests that caveolin may be upstream of GPCR-mediated cardiac myocyte apoptosis during development and aging. Pathophysiologic states, such as ischemia, which deprive the heart of oxygen or that result in an imbalance between energy production and energy utilization (e.g.,

congestive heart failure) have been linked to altered expression of caveolae and/or redistribution of caveolin [48, 49, 131, 132], and therefore point to these distinct microdomains as potential therapeutic targets for patients with increased β-AR stimulation and heart failure.

TUNEL (24 h)

Basal

Isoproterenol
(1 µM)

Forskolin
(10 µM)

Isoproterenol
+ Forskolin
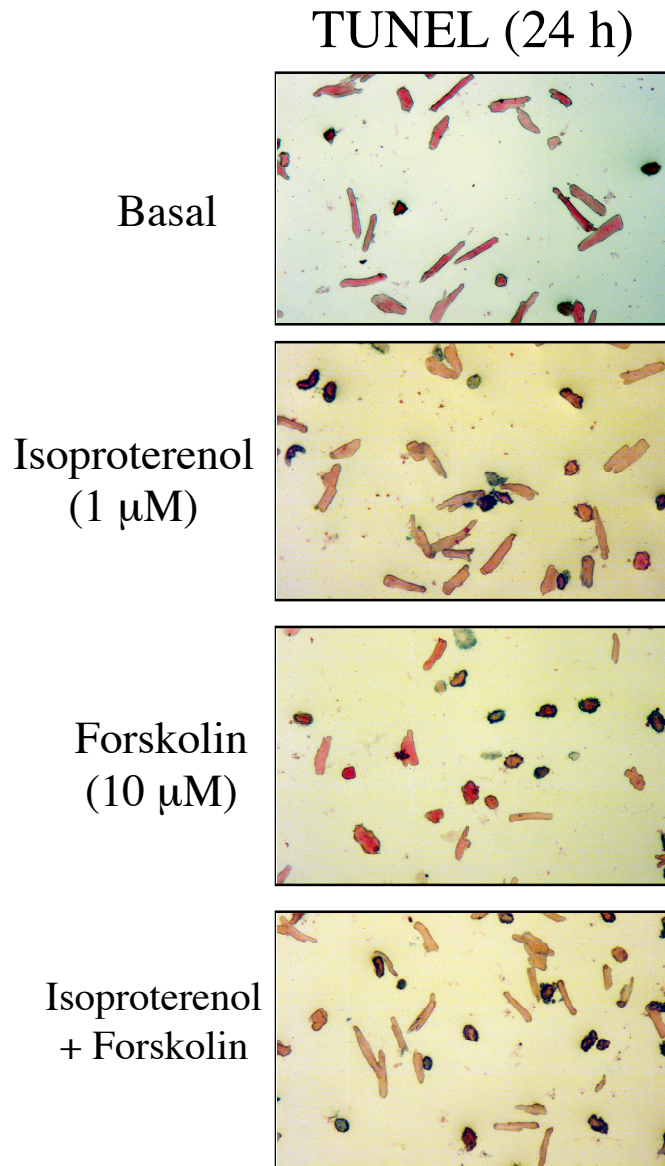
Fig. 5-1. Stimulation with isoproterenol and/or forskolin induces apoptosis in adult CM. Adult CM cultured on laminin coated wells were exposed to isoproterenol (1 µM; ISO), forskolin (10 µM; FSK), and ISO plus FSK for 24 hours and apoptosis was assessed with TUNEL staining.

A)

B)
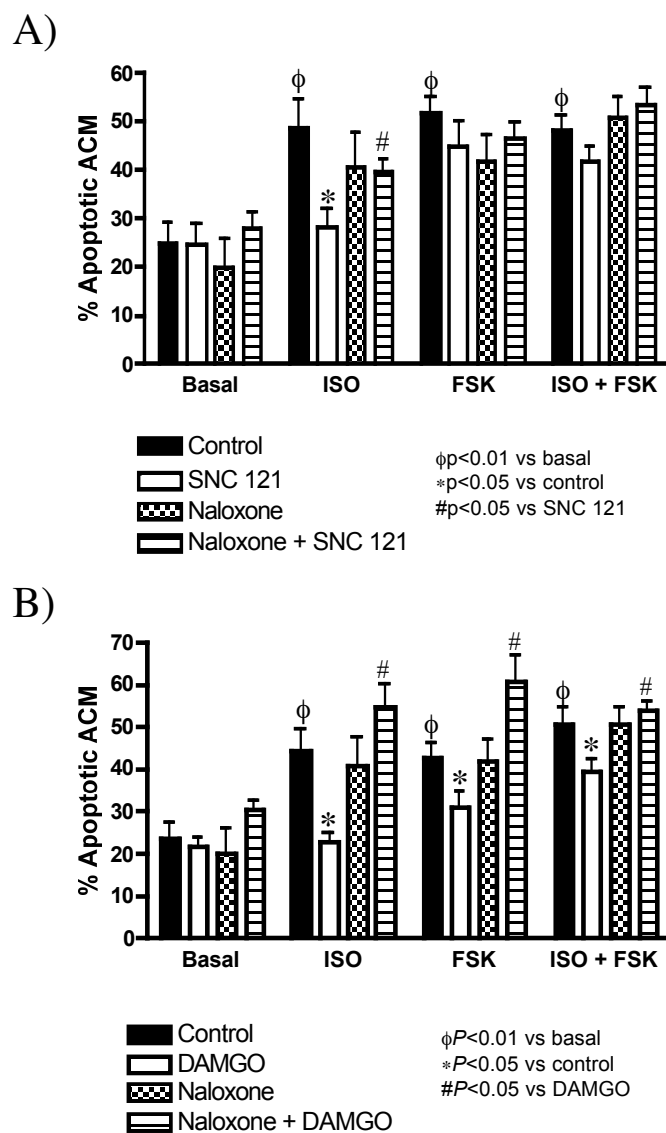
Fig. 5-2. Stimulation of δ-OR or μ-OR inhibits β-AR-promoted apoptosis in adult CM. Adult CM were pre-treated with the δ-OR (*A*) agonist SNC 121 (1 μM; 15 min) or the μ-OR (*B*) agonist, DAMGO (1 μM; 15 min) followed by exposure to isoproterenol (ISO), forskolin (FSK), and ISO plus FSK for 24 hr. The opioid receptor antagonist, naloxone (0.1 mM; 15 min), blocked OR inhibition of cardiac myocyte apoptosis. Data are mean ± SEM from 4 animals, each performed in triplicate. ϕ*P*<0.01 vs basal; *P*<0.05 vs control; #*P*<0.05 vs either SNC or DAMGO.

A)

B)
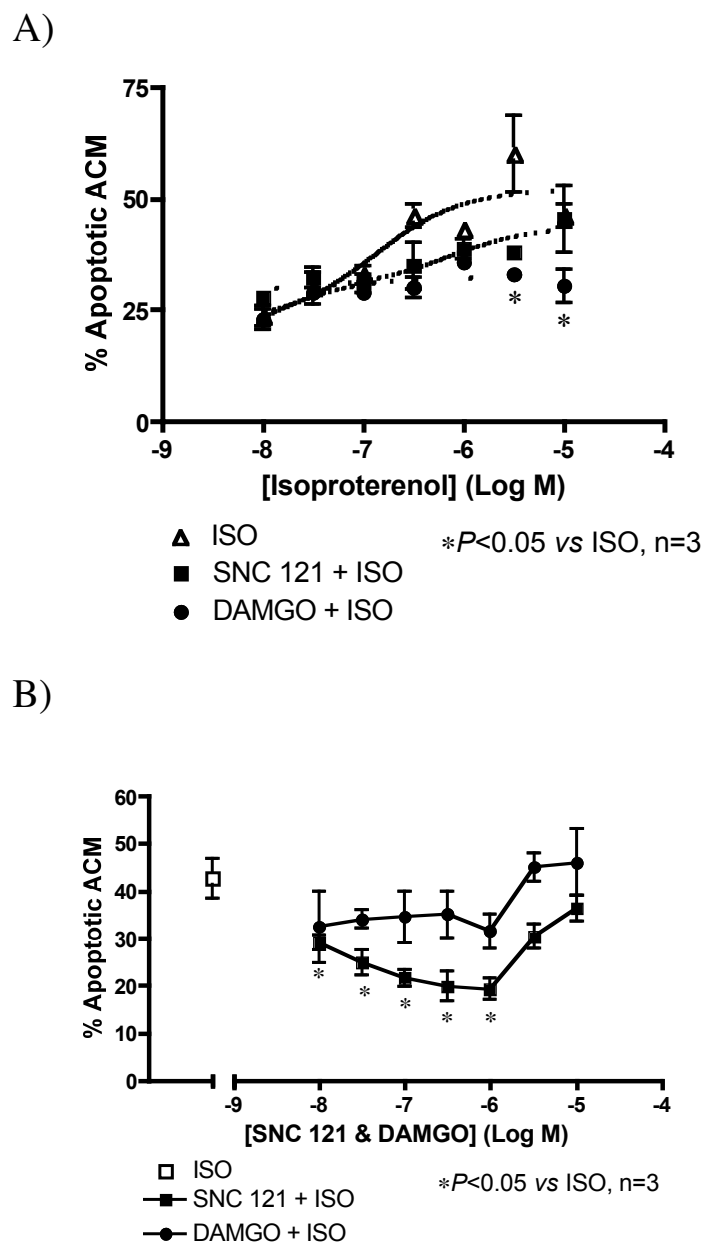
Fig. 5-3. SNC 121 and DAMGO lowers the potency of ISO-induced apoptosis in adult CM. (*A*) Increasing concentrations of ISO (10^{-8} to 10^{-5} M; 24 h; open triangles) augmented adult CM apoptosis (EC_{50} of 1.3 nM), while pre-treatment with SNC 121 (1 μM; 15 min; closed squares) or DAMGO (1 μM; 15 min; closed circles) decreased increasing concentrations of ISO-stimulated apoptosis. (*B*) Increasing concentrations of SNC 121 (10^{-8} to 10^{-5} M) or DAMGO (10^{-8} to 10^{-5} M) prior to treatment with ISO (1 μM; 24 h) lowered ISO-promoted apoptosis. Data are expressed as mean $\pm$ SEM from 3 animals, each performed in triplicate.

A)

B)
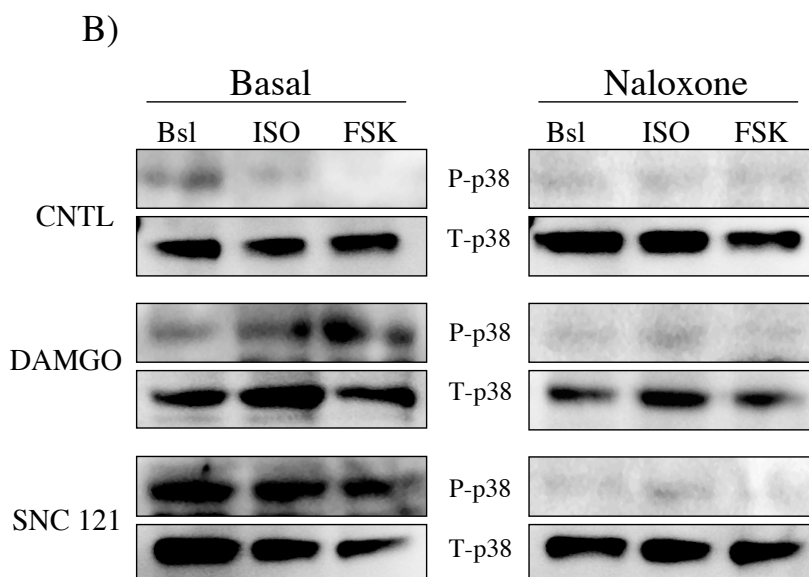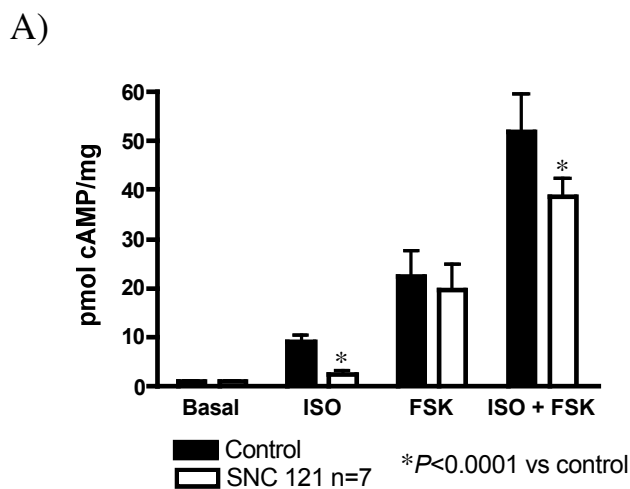
Fig. 5-4. Stimulation of OR decreases β-AR-promoted cAMP production and increases phosphorylated-p38 MAPK expression. (*A*) Pre-treatment with SNC 121 significantly reduced ISO-stimulated (SNC 121, 2.5±0.6 *vs* control, 9.2±1, control; n=7; Fig. 4*A*) and ISO plus FSK stimulated (SNC 121, 38.6±3.8 *vs* control, 51.9±7.6) cAMP production. Data are expressed as mean ± SEM from 7 animals, each performed in triplicate. *$P<0.0001$ vs control. (*B*) Treatment with DAMGO (15 min; 1 μM) or SNC 121 (15 min; 1 μM) increased phosphorylation of p38 without changing total p38 expression. This increase in P-p38 was blocked by the non-selective opioid antagonist, naloxone (0.1 μM).
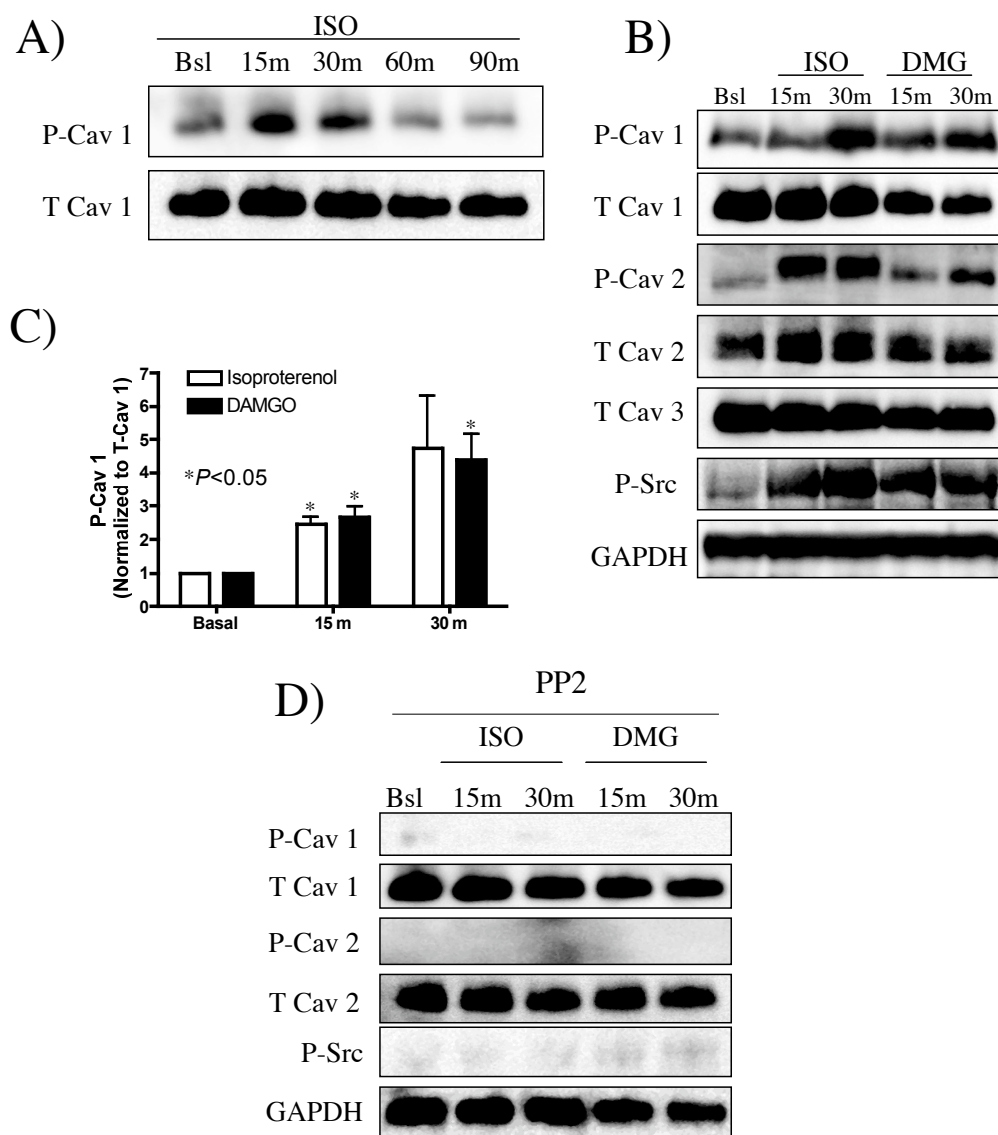
Fig. 5-5. Agonist stimulation of β-AR and μ-OR increases Cav-1, Cav-2, and Src tyrosine kinase phosphorylation in adult CM. Treatment with ISO (1 mM) or DAMGO (1 μM) increased Cav-1, Cav-2, and Src tyrosine kinase phosphorylation with a maximal effect at 30 min (*A, B, C*). PP2, a Src tyrosine kinase inhibitor, blocked both β-AR and μ-OR stimulated induction of Cav phosphorylation (*D*). Data are expressed as mean ± SEM, from 3 animals. *P<0.05 vs basal.

Chapter 6

Conclusion and Perspective

THE ROLE OF CAVEOLIN/TRANVERSE TUBULES IN ADULT VENTRICULAR CARDIAC MYOCYTES

Adult versus neonatal cardiac myocytes

The present thesis investigated the role that caveolin-associated microdomains play in scaffolding GPCR components involved in regulating cAMP formation and how the cytoskeleton affects this signaling organization in adult ventricular cardiac myocytes. Although considerable amounts of research have been conducted on cardiac myocytes regarding caveolae and GPCR compartmention, most studies have utilized neonatal or embryonic rather than adult cells, likely due to the difficulty in obtaining healthy, viable cells following enzymatic isolation. However, with respect to cardiac physiology and the *in vivo* myocadium it is more advantageous to use mature cardiac myocytes because of changes in expression of ion channels and contractile proteins, and development of the transverse tubule system, a system absent in neonatal cells [205, 206] as well as adult atrial myocytes [104]. Adult CM are multi-nucleated, contain abundant mitochondria and are 20 by 100 μm in size [207], several times larger in volume than non-striated cells such as endothelial, epithelial, fibroblasts, smooth muscle cells, etc. I established a model for isolating adult ventricular cardiac myocytes and used these cell to ask a variety of questions regarding GPCR compartmentation in caveolin-associated microdomains.

Caveolae and surface area

Caveolae, omega (Ω) shaped 50-100 nm regions of the plasma membrane, are expressed by many cell types, and are believed to increase the surface area of cells. However, previous studies have shown that non-striated cells have much greater amounts of plasmalemmal caveolae than striated myocytes [208, 209]. Findings from these studies demonstrate that the packing density of caveolae is $6/\mu m^2$ of the cell surface and increases the cell membrane surface area by approximately 27% in rat myocardium, while caveolae of endothelial and smooth muscle cells possess a greater packing density of $75/\mu m^2$ and $35/\mu m^2$, respectively, increasing the surface in smooth muscle cells by 75% [209, 210]. Yet, if caveolae do serve to increase the surface area of cells, then why would a cell, such as the adult CM, which is much larger in volume and contains more nuclei and organelles, express fewer caveolae? I speculate that CM have adapted to this situation by having a transverse (T-) tubule network. The T-tubule system originate from invaginations of the sarcolemmal membrane and eventually runs in both transverse and longitudinal directions [104]. Striated myocytes, instead of expressing more caveolae to accommodate the increased cell volume, have replaced these flask like invaginations of the plasmalemma (i.e. sarcolemma in myocytes) with T-tubules, a more efficient system to expose intracellular proteins and organelles to the extracellular environment.

Caveolae, Transverse Tubules, and Mitochondria

This idea is supported by evidence that caveolae and T-tubules are not distinct entities, but rather are components of the cell that are similar to one another in that they localize Cav-3 and are continuous with the plasma membrane [211, 212]. Parton et al. 1997 [11] elegantly showed that the caveolar protein marker, caveolin (Cav), in particular Cav-3, transiently associates with T-tubules in developing skeletal muscle as a part of interconnected caveolae but predominantly associates with the sarcolemma following myocyte maturation. In contrast, my work [40] shown in this thesis indicates that in mature cardiac muscle (both isolated adult CM and heart) Cav-3 distributes to the saroclemmal membrane and co-localizes with the T-tubule markers, dihydropyridine receptor (DHPR) and vinculin, suggesting that caveolin's association with T-tubules is not transient in mature cardiac muscle, a conclusion that extends previous findings in mature skeletal muscle [47].

Cell surface caveolae and other caveolin-associated microdomains have been demonstrated to be in close proximity with certain organelles, in particular mitochondria and sarcoplasmic reticulum [130, 208, 213]. Data shown in this thesis lead to the hypothesis that caveolin-associated microdomains localize components involved in antioxidant generation (i.e., heme oxygenase, NOS, biliverdin, NO) thus serving as "sinks" for free radicals generated by mitochondria (Chpt. 4). In addition, work shown by co-immunoprecipitation and co-localization between Cav-3 and the sarcoplasmic reticulum (SR) marker, ryanodine receptor (RyR), and co-localization of Cav-3 with DHPR indicate

that Cav-associated microdomains localize protein complexes involved in intracellular calcium flux and excitation-contraction coupling [40, 41]. Close proximity between caveolin-associated protein complexes in T-tubules with both the SR and mitochondria is consistent with the idea that there is preferential coupling of Ca^{2+} transport form SR to mitochondria in cardiac myocytes [214]. Several types of G protein coupled receptors, G proteins, and effector enzymes localize to caveolin-associated microdomains both on the surface sarcolemma and in T-tubules, extending the notion that surface caveolae and caveolin-associated microdomains in T-tubules serve the same overall objective, which is to localize signaling components in proximity to subcellular organelles [37-39]. The findings thus suggest that T-tubules take on a key task that surface caveolae accomplish in non-striated cells, which is to 1) increase the surface area, 2) transduce extracellular signals from outside to inside the cell, 3) regulate intracellular calcium homeostasis, and 4) compartmentalize and localize caveolin-associated signaling complexes within close proximity to subcellular organelles [104]. It is intriguing that T-tubules are found in cardiac tissue of mammals, yet are absent from avian, reptile, and amphibian cardiac tissue, an observation suggesting that T-tubules may serve to provide ions, nutrients, and metabolites to the interior of myocytes in hearts with increased metabolic demand [104, 215, 216]. It thus would be of interest to assess caveolin-3 expression in cardiac tissue of lower vertebrates (i.e., birds, fish, reptiles, and amphibians).

In conclusion, the combined use of multiple experimental approaches such as Q-PCR, immunoblot analysis of subcellular fractions, immunoprecipitation,

immunofluorescence and de-convolution microscopy, and immunoelectron microscopy demonstrate that Cav-3 is present and co-localizes with certain GPCRs (i.e. β-AR, mAChR, and opioid receptors) and their signaling components in both surface sarcolemmal and non-surface sarcolemmal membranes, and Cav-3 interacts with protein complexes capable of producing and inhibiting cAMP production in adult CM. The localization of HO-1 and eNOS with caveolin, and the close apposition between caveolae and mitochondria suggests that caveolae may not only be sites that generate gaseous signaling components (i.e. CO and NO) but may also serve as discrete cellular regions for antioxidant production, and thus "sinks" for free radicals in adult CM. Finally, the results demonstrating that disruption of microtubules and microfilaments prevents localization of Cav isoforms and GPCR signaling components to buoyant membranes, and decreases phosphorylation of caveolin isoforms while enhancing cellular cAMP formation implicate a role for microtubules and microfilaments in the formation and/or maintenance of caveolar-mediated GPCR signal transduction, in particular in adult CM.

Appendix

EXPERIMENTAL PROCEDURES

Materials. Antibodies for $AC_{5/6}$, β_1-, β_2-AR, $G\alpha_s$, $G\alpha_{i-3}$, $G\alpha_{i-2}$, M_2-, M_4-mAChR, μ-OR, and β-adaptin were obtained from Santa Cruz Biotechnology (Santa Cruz, CA), for eNOS, Cav-3, Cav-1, Cav-2 (monoclonal). phosphorylated caveolin (P-Cav) were obtained from BD Biosciences (San Jose, CA), for DHPR, vinculin, and RyR from Sigma-Aldrich, and for Cav-3 (polyclonal) and HO-1 from Abcam (Cambridge, MA). Antibodies for Src, P-Src, p38, and P-p38 kinase were obtained from Cell Signaling (Beverly, MA). GAPDH and cytochrome C antibodies were obtained from Imgenex (San Diego, CA). FITC and Alexa-conjugated secondary antibodies were obtained from Molecular Probes/Invitrogen (Carlsbad, CA). Filamin, α-tubulin, and all other chemicals and reagents were obtained from Santa Cruz Biotechnology. All other chemicals and reagents were obtained from Sigma Chemical (St. Louis, MO) unless otherwise stated.

Cardiac myocyte (CM) Preparation. Adult male Sprague-Dawley rats (250-300 g, male) were anesthesized with ketamine (100mg/kg) and xylazine (10mg/kg), hearts were excised and retrograde-perfused with media containing collagenase II, as previously described [217]. Animals were heparinized (1,000-2000 units IP) 5 min prior to anesthesia. Hearts were removed and placed in ice-cold cardioplegic solution (containing in mM: 112 NaCl, 5.4 KCl, 1 $MgCl_2$, 9 NaH_2PO_4, 11.1 D-glucose; supplemented with 10 Hepes, 30 Taurine, 2 DL-carnitine, 2 creatine, pH. 7.4). The hearts were retrograde-perfused on a

Langendorff apparatus for 5 min at a rate of 5 ml/min at 37°C, followed by perfusion

with media containing collagenase II (250 units/mg; Worthington) for 20 min. Following

perfusion, ventricles were separated from atria and minced in collagenase II-containing

media for 10-15 min, washed several times and re-acclimated to 1.2 mM Ca^{2+} over 25 min

to produce calcium-tolerant CM. Myocytes were then plated in 4% fetal bovine serum on

laminin (2 $\mu g/cm^2$) coated plates for 1 h; followed by serum-free medium (1% bovine

serum albumin) to remove all non-myocytes; CM were incubated at 37°C in 5% CO_2 for

24 h prior to experiments.

Real-time PCR Analysis of Gene Expression. Total RNA was isolated using a RNeasy

Mini Kit (Qiagen). First strand cDNA synthesis (Superscript First Strand Synthesis

System for RT-PCR, Invitrogen) was performed using random hexamers on 1-2 μg of

total RNA. The concentration of cDNA was determined and adjusted to 50 ng/μl for real-

time PCR analysis, which was performed on a MJ Research Opticon 2 in triplicate using

the QPCR Mastermix Plus for SYBR Green Kit (Eurogentec) with 100 ng cDNA and 0.5

μM forward/reverse primer mix in 20 μl final reaction volume. Thermal cycle conditions

were as follows: 94°C-10 min (1 cycle); 94°C-20 sec, 55°C-20 sec, 72°C-30 sec (40

cycles). Resulting PCR products were confirmed by melt curve analysis and agarose gel

electrophoresis. Analysis of cycle threshold (C_t) was performed using Opticon 2

Analysis Software (MJ Research); normalized values were obtained for each group by

subtracting matched glyceraldehyde-3-phosphate dehyodrogenase (GAPDH) C_t values.

Membrane Fractionation. CM were fractionated using both detergent-free and detergent-containing (1% Triton X-100) methods [7, 122]. A buffer containing 10 mM KH_2PO_4, 5 mM $MgCl_2$, 5 mM EDTA, 1 mM EGTA was used to extract the contractile myofibrils, as described previously [218]. CM from a 15 cm plate were washed twice in ice-cold PBS and scraped in 3 ml of either 500 mM Na_2CO_3, pH 11.0, to extract peripheral membrane proteins, or TNE (25 mM Tris-HCl, 150 mM NaCl, 5 mM EDTA) containing Triton X-100 (1%). For detergent-free extraction cells were homogenized using three 10 sec bursts of a tissue grinder and then sonicated with three cycles of 20 sec bursts of sonication and 1 min incubation on ice. Approximately 2 ml of homogenate were mixed with 2 ml of 90% sucrose in 25 mM MES, 150 mM NaCl (MBS, pH 6.5) to form 45% sucrose and loaded at the bottom of an ultracentrifuge tube. A discontinuous sucrose gradient was generated by layering 4 ml of 35% sucrose prepared in MBS/250 mM Na_2CO_3 followed by 4 ml of 5% sucrose (in MBS/Na_2CO_3). Gradients were centrifuged at 280,000 g using a SW41Ti rotor (Beckman) for 16-20 h at 4°C. For subcellular fractionation using Triton X-100, 2 ml of homogenate were mixed with 2 ml of 90% sucrose in TNE. A discontinuous sucrose gradient was generated by layering 4 ml of 30% sucrose in TNE followed by layering 4 ml of 5% sucrose in TNE and centrifugation at 190,000 g using a SW41Ti rotor for 16-20 h at 4°C. Samples were removed in 1 ml aliquots to form 12 fractions.

Immunoprecipitation of BF and HF. Immunoprecipitations were performed using either protein A or protein G-agarose (Roche). BF and HF (in which pH was neutralized with HCl and treated with 1% Igepal CA-630) or Triton X-100 fractions were incubated with primary antibody for 1-3 h at 4°C, immunoprecipitated with protein-agarose overnight at 4°C and then centrifuged at 13,000 g for 5 min. Protein-agarose pellets were washed once in lysis buffer (50 mM Tris-HCl, pH 7.5, 500 mM NaCl, 1% Igepal CA-630) followed by subsequent washes in wash buffer 2 (50 mM Tris-HCl, pH 7.5, 500 mM NaCl, 0.2% Igepal CA-630) and wash buffer 3 (10 mM Tris-HCl, pH 7.5, 0.2% Igepal CA-630).

Immunoblot Analysis. Proteins in fractions and cell lysates were separated by SDS-polyacrylamide gel electrophoresis using 10 or 12% acrylamide precast gels (Invitrogen) and transferred to polyvinylidene difluoride membranes (Millipore) by electroelution. Membranes were blocked in 20 mM PBS Tween (1%) containing 1.5% nonfat dry milk and incubated with primary antibody overnight at 4°C. Primary antibodies were visualized using secondary antibodies conjugated with horseradish peroxidase (Santa Cruz Biotech, Santa Cruz, CA) and ECL reagent (Amersham Pharmacia Biotech, Piscataway, NJ). All displayed bands migrated at the appropriate size, as determined by comparison to molecular weight standards (Santa Cruz Biotech). The amount of protein per fraction was determined using a dye-binding protein assay (Bio-Rad, Hercules, PA).

Immunofluorescence Microscopy of adult CM and heart. Adult rat heart ventricles

and CM were prepared for immunofluorescence microscopy as described [219, 220]. CM

were plated on pre-coated laminin (2 μg/cm^2) glass coverslips and grown for 24 h. Rat

ventricles were freshly harvested, frozen and then mounted on a cryostat (–23°C) in order

to cut 10 mm semithin sections. Semithin sections and cells were fixed with 2%

paraformaldehyde in PBS for 10 min at room temperature, incubated with 100 mM

glycine (pH. 7.4) for 10 min to quench aldehyde groups, permeabilized in buffered Triton

X-100 (0.1%) for 10 min, blocked with 1% BSA/PBS/Tween (0.05%) for 20 min and then

incubated with primary antibodies (1:100) in 1% BSA/PBS/Tween (0.05%) for 24-48 h at

4°C. Excess antibody was removed by incubation with PBS/Tween (0.1%) for 15 min and

samples were then incubated with FITC or Alexa-conjugated secondary antibody (1:250)

for 1 h. To remove excess secondary antibody, semithin sections and cells were washed

6x at 5 min intervals with PBS/Tween (0.1%) and incubated for 20 min with the nuclear

stain Dapi (1:5000) diluted in PBS. Sections and cells were washed for 10 min with PBS

and mounted in gelvatol for microscopic imaging.

Deconvolution Image Analysis. Deconvolution images were obtained as described [221, 222] and captured with a DeltaVision deconvolution microscope system (Applied

Precision, Inc., Issaquah, WA.). The system includes a Photometrics CCD mounted on a

Nikon TE-200 inverted epi-fluorescence microscope. Between 30 and 80 optical sections

spaced by ~0.1-0.3 mm were generally taken. Exposure times were set such that the

camera response was in the linear range for each fluorophore. Lenses included 100x (NA 1.4), 60x (NA 1.4) and 40x (NA 1.3). The data sets were deconvolved and analyzed using SoftWorx software (Applied Precision, Inc) on a Silicon Graphics Octane workstation. Image analysis was performed with Data Inspector program in SoftWorx. Maximal projection volume views or single optical sections are shown as indicated**.**

Quantitation of colocalization analysis. Colocalization of pixels was assessed quantitatively by CoLocalizer Pro 1.0 software (http://www.home-page.mac.com/colocalizerpro). Overlap coefficient according to Manders (MOC) was used to determine the degree of colocalization on whole cells or sarcolemmal membrane regions of interest (ROI) after subtracting background through normalized threshold values [223]. The values are defined by 0 to 1 with 1 implying that 100% of both components overlap with the other part of the image. Statistics were performed with Prism.

Electron Microscopy. Cells were fixed with 2.5% glutaraldehyde in 0.1 M cacodylate buffer for 2 h at room temperature, postfixed in 1% OsO_4 in 0.1 M cacodylate buffer (1 hr) at room temperature, and embedded as monolayers in LX-112 (Ladd Research, Williston, VT), as described previously [224]. Sections were stained in uranyl acetate and lead citrate and observed with the use of an electron microscope (JEOL 1200 EX-II or Philips CM-10). Caveolae were quantitated on random images per length of membrane.

Immunoelectron Microscopy. Cells were fixed in 4% paraformaldehyde in 0.1 M

phosphate buffer, gently scraped and pelleted. The resuspended pellet was fixed for 1 h

at room temperature with 8% paraformaldehyde and then overnight with 4%

paraformaldehyde at 40°C. Cells were washed 3x with 0.1 M phosphate buffer,

embedded in 10% gelatin and cryoprotected in 2.3 M sucrose overnight at 40°C.

Cryosections were cut on a Leica UltraCut E; 80 nm ultrathin sections were mounted on

glow-discharged Ni grids and stored on 2% gelatin until labeled. Sections were blocked

with 1% goat serum/1% BSA, incubated with primary antibodies for 2 h to overnight,

followed by 5 or 10 nm gold-labeled goat-anti rabbit or goat anti-mouse IgG (Amersham).

Sections were then absorption-stained with uranyl acetate and embedded in 0.2% methyl

cellulose. For AC localization, cells were treated with an adenoviral construct containing

either LacZ (control; *Adv-LacZ*) or AC_6 (*Adv-AC_6*) for 24 h prior to fixation [97].

Measurement of AC Activity. AC activity was measured in Cav-3 immunoprecipitates

using a modification of a previously described method [14]. A 15 cm plate of adult CM was

homogenized on ice in a lysis buffer (50 mM Tris-HCl, pH 7.5, 150 mM NaCl, 5 mM

$MgCl_2$, 1 mM EGTA, 2 mM DTT, and 0.5% Igepal CA-630, plus mammalian protease

inhibitor cocktail from Sigma), pre-cleared with protein A-agarose for 1 h, and then

incubated with primary antibody for 1 h at 4°C. Antibody conjugates were

immunoprecipitated with protein G-agarose for 1 h at 4°C and then centrifuged at 13,000

g for 5 min. Agarose pellets were washed once in lysis buffer, subsequently in wash

buffers 2 and 3 and then resuspended in 30 mM Na-HEPES, 5 mM $MgCl_2$, 2 mM DTT,

pH 7.5. Protein (30 μl of immunoprecipitate) was added to tubes containing 30 mM Na-

HEPES pH 7.5, 100 mM NaCl, 1 mM EGTA, 10 mM $MgCl_2$, 1 mM

isobutylmethylxanthine (IBMX, a cyclic nucleotide phosphodiesterase inhibitor), 1 mM

ATP, 10 mM phosphocreatine, 5 μM GTP, 60 U/ml creatine phosphokinase, and 0.1%

BSA. After 5 min, naloxone (0.1 μM), an opioid receptor antagonist, or vehicle was

added, followed by addition of DAMGO (1 μM), a selective μ-opioid receptor agonist,

or vehicle 5 min later. After 5 min, forskolin (10 μM) was added and samples were

incubated for an additional 15 min. The reaction was stopped by boiling for 5 min and

cAMP content was assayed as previously described [13].

Measurement of cAMP production. Assay for cAMP accumulation was performed by

incubation with drugs of interest and 0.2 mM IBMX for 10 min. To terminate reaction,

assay medium was aspirated, and 250 ml of ice-cold trichloroacetic acid (7.5%, w/v) was

immediately added to each well. cAMP content in trichloroacetic acid extracts was

determined by radioimmunoassay. Production of cAMP was normalized to the amount

of protein per sample as determined using a dye-binding protein assay (Bio-Rad).

Terminal deoxynucleotidyl Transferase (TdT)-mediated dUTP Nick End-Labeling

(TUNEL). TUNEL staining was performed on cells plated on a 24 well plate with an R

& D Systems CardioTACS *in situ* apoptosis detection kit. Briefly, cells were fixed in

3.7% formaldehyde for 10 min at room temperature. Cells were then washed with PBS

and permeabilized with Triton X (0.1%) for 90 min at 37°C in a humidified chamber.

Cells are quenched with 3% H_2O_2 in methanol for 5 min at room temperature and

incubated with TUNEL reaction mixture for 100 min at 37°C in a humidified chamber.

As a positive control, fixed and permeabilized cells were treated with nuclease enzyme

and nuclease buffer to introduce double stranded breaks in genomic DNA. The percentage

of DNA nick end-labeling myocytes were determined by counting in triplicate 100 cells

from randomly chosen fields and compared across three samples (900 total cells).

APOPercentage Assay. Adult CM were treated with agents to induce or inhibit

apoptosis. Approximately 30 min prior to measuring apoptosis, media was removed and

fresh culture media containing 1:20 dilution of APOPercentage dye was added to the cells

for 30 min at 37°C/5% CO_2. Dye was then removed and the cells were washed twice

with PBS followed by the addition of 100 μl of APOPercentage dye (Biocolor,

Newtonabbey, Northern Ireland) release reagent for 10 min on a shaker. The cell bound

dye recovered in the solution was then measured using a microplate fluorimeter at

excitation and emission wavelengths of 530 nm and 580 nm, respectively.

Statistical Analysis. Data are expressed as mean ± SEM. Students unpaired *t* test was used to compare the number of groups as indicated. Significance was established at a level of *P*<0.05.

PROTOCOLS

<u>Preparation of Adult Rat Ventricular Myocytes</u>
Cardiac myocytes (CM) were be isolated from adult Sprague-Dawley rats (250-300 g, male) as previously described (Communal et al. 1998). Briefly, animals are heparinized (1,000-2000 units IP) 5 min prior to being anesthetized with ketamine (100mg/kg) and xylazine (10mg/kg), and their hearts removed and placed in ice-cold cardioplegic (20 mM KCl) heart media solution (in mmol/L: 112 NaCl, 5.4 KCl, 1 $MgCl_2$, 9 NaH_2PO_4. 11.1 D-glucose; supplemented with 10 Hepes, 30 Taurin, 2 DL-carnitine, 2 creatine, pH. 7.4). The hearts are retrograde-perfused on a Langendorff apparatus with Ca^{2+}-free heart media for 5 min at 5 ml/min at 37°C, followed by perfusion with a Ca^{2+}-free heart media containing collagenase II (250 units/mg; Worthington) for 20 min. Following perfusion, both ventricles are removed from the heart and minced in collagenase II containing heart media for 10-15 min. Cell solution are washed several times to remove collagenase II and re-acclimated to 1.2 mM Ca^{2+} over 25 min to produce calcium-tolerant CM. Myocytes are plated in 4% fetal bovine serum (FBS) on laminin (2 µg/cm^2) coated plates for 1 h. Plating media is changed to serum free media (1% BSA) to remove all non-myocytes, and CM are placed in an incubator set at 37°C and 5% CO_2 for 12-24 h prior to experiments.

Protocol steps are as follows:

1. Set flow rate to 5 ml/min
2. Set up cannula with 3 ml syringe containing heart media (HM)
3. Set up two 50 ml conical tubes with HM, one containing 20 mM KCl (plegic solution).
4. Heparinize rat with 0.3 ml of 10,000 unit/ml (total 3000 units), 5 min prior to anesthesia.
5. Anesthetize rat with 100 mg/kg of Ketamine (100 mg/ml) and 10 mg/kg of Xylazene (20mg/ml)
   a. Inject 0.7-0.9 ml IP from stock into 200-300 g rat.
   b. Stock: 10 ml of Ket + 5 ml of Xyl + 5 ml 0.8% NaCl.
6. Shave thoracic region and wipe down with 70% EtOH prior to incision.

7. Remove heart and place it in HM (without KCl) to remove blood, and then transfer heart to HM containing 20 mM KCl.
8. Place heart into dish with HM (KCl). Cannulate heart via aorta with 3-5 cc syringe containing HM with KCl. (IMPORTANT: No air bubbles in cannula! This will prevent perfusion of the myocardium).
9. Transfer heart with cannula to Langendorff apparatus and perfuse heart with calcium free HM for 5 min, at **6 ml/min**, at 35°C.
10. Following **5 min** perfusion, perfuse for **20 min** at the **same rate** with HM containing collagenase II.
11. Remove heart and place in dish containing 10 ml of collagenase II. Cut ventricles into smaller pieces. At this point the heart should fall apart easily and the myocardium should be flaccid, light-pink in appearance.
12. Transfer minced heart from dish into 50 ml conical tube and triturate for 6 min at 37°C.
13. Filter heart through 80-100 micron mesh into 50 ml conical tube and use washing solution to wash the excess cells through the mesh.
14. Let tube sit at 45° angle for 10 min to generate a loose pellet (cardiac myocytes). The supernatant can be drawn off and pelleted to produce cardiac fibroblasts.
15. Add 1:1 volume of washing solution to remove excess collagenase II, invert 2-4 times and let tube sit at 45° angle for 10 min to re-establish the pellet.
16. Aspirate supernatant and add 1:1 volume of washing solution. Let tube sit at 45° angle for 10 min to re-establish the pellet.
17. Aspirate supernatant and add 1:1 volume of washing solution. **Begin calcium re-introduction step.**
18. Introduce Ca^{2+} to myocytes by adding 0.25, 0.5, 0.75, 1, 1.25 mM Ca^{2+} in 4 min increments to slowly equilibrate the cells to 1.25 mM Ca^{2+}. Invert tube 2x after each calcium addition.
19. Let cells sediment again, remove 50% of washing solution and add 25% Plating Media (4% Fetal Bovine Serum). Make sure the media has a maximum of 1.25 mM Ca^{2+} (Media 199 Hanks Salts).
20. Let cells sediment again, aspirate supernatant, and add 50% Plating Media and mix cells.
21. Let cells sediment again, aspirate supernatant, and add 75% Plating Media and mix.
22. Let cells sediment again, aspirate supernatant, add 90% Plating Media and mix thoroughly. Cells are ready for plating on Laminin pre-coated plates (2 μg/cm^2).
23. Should yield between 3-5 x 10^6 cardiac myocytes.
24. Plate cells for 1 h and then remove Plate Media and add Maintenance Media (1% BSA).
25. Culture ACM in 37°C at 5% CO_2.

26. Cells die an average 10-24% per 24 h while in maintenance media (1% BSA in 199 Media with Hanks Salts).

Buffers and Media

Joklik Modified Media

NaCl	112 mM
KCl	5.4 mM
$MgCl_2$	1 mM
NaH_2PO_4	9 mM
D-glucose	11.1 mM

Add to Joklik

Hepes	2380 mg/L	10 mM
Taurin	3750 mg/L	30 mM
DL-carnitine	400 mg/L	2 mM
Creatine	300 mg/L	2 mM

Adjust pH to 7.4 with NaOH and then filtrate.

Collagenase Solution

Heart Media	150 mL
Collagenase II	150 mg of 251 units/mg*
	*(Units vary per collagenase stock, so adjust amount so that it is equal to 150 mg of 250units/mg)
BSA	150 mg (0.1%)
$CaCl_2$	20 µM (30 µl from 100 mM stock)

Washing Solution

Heart Media	100 mL
BSA	1000 mg (1%)
$CaCl_2$	20 µM (20 µl from 100 mM stock)

Adenylyl Cyclase Activity Assay

1. Thaw AC buffers Solution A (30 mM Na-HEPES, 5 mM $MgCl_2$, 2 mM DTT, pH 7.5) and Solution B (30 mM Na-HEPES, 100 mM NaCl, 1 mM EGTA, 10 mM $MgCl_2$, 1 mM IBMX, 1 mM ATP, 10 mM phosphocreatine, 5 μM GTP, 60 U/ ml creatine phosphokinase, and 0.1% bovine serum albumin, pH 7.5. The stock should be in the -80 unless you are making a new batch. A and B should be equal amounts.

2. Dilute drugs to proper concentrations from 10^{-2} M stock.

3. Depending on what the final volume is, mix the AC buffers in the 2 ml microcentrifuge tubes with the drugs.

4. Place the tubes at 30 degrees to equilibrate for a few minutes. Then add the tissue to start the assay (typically 10 min). Add the AC buffers and tissue together and placed in heat block for a few minutes.

5. Start the reaction by adding the drugs. First, add the antagonists for 5 min, then add the agonists to start the **10 minute** reaction time.

6. Finish by **boiling** for **5 min**.

7. For immunoprecpitation, re-suspend final 50 μl of agarose G (Cav-3 IP) in 300 μl of membrane buffer

8. Place in –20 degrees.

9. For RIA, use 30 ul for basal and 15 ul for drug-treated samples.

10. For example:

    - Total volume = 200 ul
    - AC Buffer solution (A & B mix) = 160 ul
    - Drug of interest = 20 ul
        i. Add antagonist 5 min prior to agonist
    - Add tissue (e.g., immunoprecipitation solution) = 20 ul
    - Incubate for 10 min
    - Boil for 5 min

Immunofluorescence Staining Protocol

1. Wash 2x with 1x PBS at room temperature (RT).

2. Fix in 2% paraformaldehyde/PBS for 10 min at RT.

3. Wash with 100 mM Glycine (pH 7.4) in PBS for 5 min.

4. Permeabilize in 0.1% Triton X/PBS for 10 min at RT.

5. Wash 2x with PBS/Tween 20 (0.1% Tween).

    *Can be stored overnight at 4°C if necessary.

6. Block in 1% BSA/PBS/0.05% Tween for 20 min at RT (make fresh every few times).

7. Dilute primary antibody **(1:100)** in 1%BSA/PBS/0.05% Tween and incubate for 48 h at 4°C.

8. Wash 3x at 5 min intervals with PBS/0.1% Tween (15 min).

9. Dilute secondary antibody **(1:250)** in 1%BSA/PBS/0.1% Tween for 1 h at RT.

10. Wash 6x at 5 min intervals with PBS/0.1% Tween.

11. Incubate with Heoscht **(1:2000)** for 20 min diluted in PBS on lab bench.

12. Wash 2x at 5 min with PBS, and 1x with D.I. H_2O.

13. Mount in mounting media and place in dark area.

Note: If the cells are on coverslips incubate in a humidified chamber for the antibodies and Hoescht.
Also, check with the antibodies being used, some require TBS instead of PBS, i.e. 10 mg/mL BSA in 1xTBS.

Reverse Transcriptase PCR and PCR

1. Amount of Oligo = X nmoles (of Primer) x 5 volume of molecular grade H_2O
    a. Add the X nmole + volume to get 200 μM of primer (Oligo)
        i. E.g. 28.15 x 5 = 140.8 μL = 200 μM of Oligo (frozen stock at −20°C)

2. Dilute the 200 μM Oligo → 5-10 μM
   a. E.g. 5 μL of both primers (200 μM) and add 90 μL → total 100 μL (10 μM; working stock)

3. Reverse transcription (rt)-PCR and PCR Mix
   a. Take **2 μL** of primer (10 μM Primer mix) +
   b. **5 μL** of mRNA +
   c. **25 μL** of 2x Mix +
   d. **17.5 μL** of H_2O +
   e. **0.5 μL** of SS II RT (reverse transcriptase)/Taq (DNA polymerase)
   f. **Total 50 μL**

4. PCR Machine
   a. 94°C to digest mRAN and inactivate SS II rt
   b. 94°C to break cDNA away from mRNA
   c. 55°C to allow primer to anneal to cDNA
   d. 74°C to initiate Taq to extend primer

5. Run on cDNA on Gel
   a. To Cast Gel: 25 mL of TBE pluse 0.25 g of Agarose (1%), heat until melts (30-60 s), let cool, add 1.5 mL of ethidium bromide
   b. Add Blue Juice 1 μL /10 μL of sample
   c. 10 μL of Standard of 1 kb
   d. Run @ 100 V for 25 min

Reverse Primer for Cav-3 (mouse) with EcoR1 Restriction Site

5'-CGGAATTCCGTTAGCCTTCCCTTCGCAGCA-3'

Plasmid Isolation: Mini and Max Prep

1. Take 1.9 mL of bacteria/LB media, leave the remainder at 4°C
   e. Spin at 10,000 rpm for 2 min
   f. Remove Media and add 250 μL of P1 buffer to re-suspend
   g. Vortex (last vortex in protocol, invert 4-6x from here on out)

2. Add 250 μL of P2 (lysis buffer), invert 4-6x

3. Add 350 μL of N3 buffer, invert 4-6x
    h. Spin @ 13,000 rpm for 10 min

4. Take Supernatant and add to spin column and spin @ 13,000 rpm for 1 min

5. Discard flow thru and wash column with 750 μL of PE Buffer (wash buffer) and Centrifuge for 1 min

6. Re-spin for an additional 1 min to remove residual wash buffer

7. Place column into new centrifuge tube (remove caps with scizzors) and add 50 μL of Elution Buffer, let stand for 1 min, and centrifuge for 1 min

8. To spec DNA, take 1 μL and mix with 99 μL of molecular grade water (1:100 dilution) and spec against water alone

9. After spec, take 150 μL of Bacteria/LB and mix with 100 mL of LB with 100 μL of Amp from 100 mg/ml stock; 1:1000 dilution) to generate large amounts of Plasmid for Maxi-prep.

Maxi-Prep for Plasmid Isolation

1. Harvest and Lyse bacteria
    a. Pellet 150 ml of an overnight culture at 5,000 g for 10 min, discard supernatant
    b. Resuspend cells in 12 mL of resuspension solution, pipet up and down, or vortex
    c. Add 12 mL of Lysis Solution and gently invert 6-8x to mix (**Do not vortex!**); allow to clear 3-5 min
    d. Remove the plunger from a filter syringe and place the barrel in an upright position

2. Prepare Cleared Lysate
    a. Add 12 mL of Neutralization Solution P to the lysed cells and gently invert 6-8x
    b. Add 9 mL of Binding Solution G and gently invert 1-2x
    c. Immediately add the mix to the barrel of the filter syringe and let sit for 5 min

3. Prepare Column
    a. Place the binding column into a collection tube

    b. Add 12 mL of Column Preparation Solution to the column and spin in a swinging bucket rotor at 3,000 g for 2 min, discard flow-through

4. Bind Plasmid DNA to column
    a. Hold the filter syringe over the column and gently insert plunger to expel half of the cleared lysate. Pull back slightly on the plunger to stop the flow from the syringe
    b. Spin in a swinging bucket rotor at 3,000 g for 2 min, discard flow-through
    c. Add the remainder of the cleared lysate to the column and repeat the spin, discard flow-through

5. Wash to remove contaminants
    a. Optional (EndA+ strains only): Add 12 mL of Wash Solution O and spin in a swinging bucket rotor at 3,000 g for 2 min. Discard flow-through
    b. Add 12 mL of Wash Solution and spin in a swinging bucket rotor at 3,000 g for 5 min. Discard flow-through

6. Elute Purified Plasmid DNA
    a. Transfer the column to a new collection tube.
    b. Add 3 ml of Elution Solution and spin in a swinging bucket rotor at 3,000 g for 5 min.

REFERENCES

1.   Singer SJ, Nicolson GL. The fluid mosaic model of the structure of cell membranes. *Science.* Feb 18 1972;175(23):720-731.

2.   Smart EJ, Graf GA, McNiven MA, et al. Caveolins, liquid-ordered domains, and signal transduction. *Mol Cell Biol.* Nov 1999;19(11):7289-7304.

3.   Palade G. Fine structure of blood capilaries. *J Appl Physiol.* 1953;24:1424-1436.

4.   Yamada E. The fine structure of the gall bladder epithelium of the mouse. *J Biophys Biochem Cytol.* Sep 25 1955;1(5):445-458.

5.   Pike LJ. Lipid rafts: bringing order to chaos. *J Lipid Res.* Apr 2003;44(4):655-667.

6.   Lisanti MP, Scherer PE, Vidugiriene J, et al. Characterization of caveolin-rich membrane domains isolated from an endothelial-rich source: implications for human disease. *Journal of Cell Biology.* 1994;126(1):111-126.

7.   Smart EJ, Ying YS, Mineo C, et al. A detergent-free method for purifying caveolae membrane from tissue culture cells. *Proc Natl Acad Sci U S A.* Oct 24 1995;92(22):10104-10108.

8.   Song SK, Li S, Okamoto T, et al. Co-purification and direct interaction of Ras with caveolin, an integral membrane protein of caveolae microdomains. Detergent-free purification of caveolae microdomains. *Journal of Biological Chemistry.* 1996;271(16):9690-9697.

9.   Rothberg KG, Heuser JE, Donzell WC, et al. Caveolin, a protein component of caveolae membrane coats. *Cell.* Feb 21 1992;68(4):673-682.

10.   Hnasko R, Lisanti MP. The biology of caveolae: lessons from caveolin knockout mice and implications for human disease. *Mol Interv.* Dec 2003;3(8):445-464.

11. Parton RG, Way M, Zorzi N, et al. Caveolin-3 associates with developing T-tubules during muscle differentiation. *J Cell Biol.* Jan 13 1997;136(1):137-154.

12. Chun M, Liyanage UK, Lisanti MP, et al. Signal transduction of a G protein-coupled receptor in caveolae: colocalization of endothelin and its receptor with caveolin. *Proceedings of the National Academy of Sciences of the United States of America.* 1994;91(24):11728-11732.

13. Ostrom RS, Gregorian C, Drenan RM, et al. Receptor number and caveolar co-localization determine receptor coupling efficiency to adenylyl cyclase. *J Biol Chem.* 2001;276(45):42063-42069.

14. Ostrom RS, Liu X, Head BP, et al. Localization of adenylyl cyclase isoforms and G protein-coupled receptors in vascular smooth muscle cells: expression in caveolin-rich and noncaveolin domains. *Mol Pharmacol.* Nov 2002;62(5):983-992.

15. Lisanti MP, Scherer PE, Tang Z, et al. Caveolae, caveolin and caveolin-rich membrane domains: a signaling hypothesis. *Trends Cell Biol.* Jul 1994;4(7):231-235.

16. Williams TM, Lisanti MP. The caveolin proteins. *Genome Biol.* 2004;5(3):214.

17. Dickson EW, Blehar DJ, Carraway RE, et al. Naloxone blocks transferred preconditioning in isolated rabbit hearts. *J Mol Cell Cardiol.* 2001;33:1751-1756.

18. Anderson RG. Potocytosis of small molecules and ions by caveolae. *Trends Cell Biol.* Mar 1993;3(3):69-72.

19. Fujimoto T. Calcium pump of the plasma membrane is localized in caveolae. *J Cell Biol.* Mar 1993;120(5):1147-1157.

20. Fujimoto T, Nakade S, Miyawaki A, et al. Localization of inositol 1,4,5-trisphosphate receptor-like protein in plasmalemmal caveolae. *J Cell Biol.* Dec 1992;119(6):1507-1513.

21. Scriven DR, Klimek A, Lee KL, et al. The molecular architecture of calcium microdomains in rat cardiomyocytes. *Ann N Y Acad Sci.* Nov 2002;976:488-499.

22. Steinberg SF, Brunton LL. Compartmentation of g protein-coupled signaling pathways in cardiac myocytes. *Annu Rev Pharmacol Toxicol.* 2001;41:751-773.

23. Ostrom RS, Insel PA. The evolving role of lipid rafts and caveolae in G protein-coupled receptor signaling: implications for molecular pharmacology. *Br J Pharmacol.* Sep 2004;143(2):235-245.

24. Insel PA, Head BP, Ostrom RS, et al. Caveolae and lipid rafts: G protein-coupled receptor signaling microdomains in cardiac myocytes. *Ann N Y Acad Sci.* Jun 2005;1047:166-172.

25. Heijnen HF, Waaijenborg S, Crapo JD, et al. Colocalization of eNOS and the catalytic subunit of PKA in endothelial cell junctions: a clue for regulated NO production. *J Histochem Cytochem.* Oct 2004;52(10):1277-1285.

26. Kim HP, Wang X, Galbiati F, et al. Caveolae compartmentalization of heme oxygenase-1 in endothelial cells. *Faseb J.* Jul 2004;18(10):1080-1089.

27. Feron O, Zhao YY, Kelly RA. The ins and outs of caveolar signaling. m2 muscarinic cholinergic receptors and eNOS activation versus neuregulin and ErbB4 signaling in cardiac myocytes. *Ann N Y Acad Sci.* Jun 30 1999;874:11-19.

28. Rybin VO, Pak E, Alcott S, et al. Developmental changes in beta2-adrenergic receptor signaling in ventricular myocytes: the role of Gi proteins and caveolae microdomains. *Mol Pharmacol.* Jun 2003;63(6):1338-1348.

29. Liu X, Ostrom RS, Insel PA. Enhanced cAMP production by drugs or adenylyl cyclase gene transfer blunts proliferation and function of pulmonary fibroblasts. *The Pharmacologist.* 2002;44:A230.

30. Fujita T, Toya Y, Iwatsubo K, et al. Accumulation of molecules involved in alpha1-adrenergic signal within caveolae: caveolin expression and the development of cardiac hypertrophy. *Cardiovasc Res.* Sep 2001;51(4):709-716.

31.   Oh P, Schnitzer JE. Segregation of heterotrimeric G proteins in cell surface microdomains. G(q) binds caveolin to concentrate in caveolae, whereas g(i) and g(s) target lipid rafts by default. *Mol Biol Cell.* 2001;12(3):685-698.

32.   Dessy C, Kelly RA, Balligand JL, et al. Dynamin mediates caveolar sequestration of muscarinic cholinergic receptors and alteration in NO signaling. *Embo J.* 2000;19(16):4272-4280.

33.   Shaul PW, Anderson RG. Role of plasmalemmal caveolae in signal transduction. *Am J Physiol.* 1998;275(5 Pt 1):L843-851.

34.   Rybin VO, Xu X, Lisanti MP, et al. Differential targeting of beta -adrenergic receptor subtypes and adenylyl cyclase to cardiomyocyte caveolae. A mechanism to functionally regulate the cAMP signaling pathway. *J Biol Chem.* 2000;275(52):41447-41457.

35.   Ostrom RS, Bundey RA, Insel PA. Nitric oxide inhibition of adenylyl cyclase type 6 activity is dependent upon lipid rafts and caveolin signaling complexes. *J Biol Chem.* May 7 2004;279(19):19846-19853.

36.   Bers DM. Cardiac excitation-contraction coupling. *Nature.* Jan 10 2002;415(6868):198-205.

37.   Gao T, Puri TS, Gerhardstein BL, et al. Identification and Subcellular localization of the subunits of L-type calcium channels and adenylyl cylcase in cardiac myocytes. *Journal of BIological Chemistry.* 1997;272:19401-19407.

38.   Laflamme MA, Becker PL. G(s) and adenylyl cyclase in transverse tubules of heart: implications for cAMP-dependent signaling. *Am J Physiol.* Nov 1999;277(5 Pt 2):H1841-1848.

39.   Yang J, Drazba JA, Ferguson DG, et al. A-kinase anchoring protein 100 (AKAP100) is localized in multiple subcellular compartments in the adult rat heart. *J Cell Biol.* Jul 27 1998;142(2):511-522.

40.   Head BP, Patel HH, Roth DM, et al. G-protein-coupled receptor signaling components localize in both sarcolemmal and intracellular caveolin-3-associated microdomains in adult cardiac myocytes. *J Biol Chem.* Sep 2 2005;280(35):31036-31044.

41.   Scriven DR, Klimek A, Asghari P, et al. Caveolin-3 is adjacent to a group of extradyadic ryanodine receptors. *Biophys J.* Sep 2005;89(3):1893-1901.

42.   Monier S, Parton RG, Vogel F, et al. VIP21-caveolin, a membrane protein constituent of the caveolar coat, oligomerizes in vivo and in vitro. *Mol Biol Cell.* Jul 1995;6(7):911-927.

43.   Parolini I, Sargiacomo M, Galbiati F, et al. Expression of caveolin-1 is required for the transport of caveolin-2 to the plasma membrane. Retention of caveolin-2 at the level of the golgi complex. *J Biol Chem.* Sep 3 1999;274(36):25718-25725.

44.   Li S, Galbiati F, Volonte D, et al. Mutational analysis of caveolin-induced vesicle formation. Expression of caveolin-1 recruits caveolin-2 to caveolae membranes. *FEBS Lett.* Aug 28 1998;434(1-2):127-134.

45.   Tang Z, Scherer PE, Okamoto T, et al. Molecular cloning of caveolin-3, a novel member of the caveolin gene family expressed predominantly in muscle. *Journal of Biological Chemistry.* 1996;271(4):2255-2261.

46.   Razani B, Woodman SE, Lisanti MP. Caveolae: from cell biology to animal physiology. *Pharmacol Rev.* Sep 2002;54(3):431-467.

47.   Ralston E, Ploug T. Caveolin-3 is associated with the T-tubules of mature skeletal muscle fibers. *Exp Cell Res.* Feb 1 1999;246(2):510-515.

48.   Ratajczak P, Damy T, Heymes C, et al. Caveolin-1 and -3 dissociations from caveolae to cytosol in the heart during aging and after myocardial infarction in rat. *Cardiovasc Res.* Feb 2003;57(2):358-369.

49.   Jasmin JF, Mercier I, Hnasko R, et al. Lung remodeling and pulmonary hypertension after myocardial infarction: pathogenic role of reduced caveolin expression. *Cardiovasc Res.* Sep 1 2004;63(4):747-755.

50.   Volonte D, Galbiati F, Pestell RG, et al. Cellular stress induces the tyrosine phosphorylation of caveolin-1 (Tyr(14)) via activation of p38 mitogen-activated protein kinase and c-Src kinase. Evidence for caveolae, the actin cytoskeleton, and focal adhesions as mechanical sensors of osmotic stress. *J Biol Chem.* Mar 16 2001;276(11):8094-8103.

51. Kimura A, Mora S, Shigematsu S, et al. The insulin receptor catalyzes the tyrosine phosphorylation of caveolin-1. *J Biol Chem.* Aug 16 2002;277(33):30153-30158.

52. Cao H, Sanguinetti AR, Mastick CC. Oxidative stress activates both Src-kinases and their negative regulator Csk and induces phosphorylation of two targeting proteins for Csk: caveolin-1 and paxillin. *Exp Cell Res.* Mar 10 2004;294(1):159-171.

53. Chen DB, Li SM, Qian XX, et al. Tyrosine Phosphorylation of Caveolin 1 by Oxidative Stress Is Reversible and Dependent on the c-src Tyrosine Kinase but Not Mitogen-Activated Protein Kinase Pathways in Placental Artery Endothelial Cells. *Biol Reprod.* Oct 2005;73(4):761-772.

54. Lee H, Park DS, Wang XB, et al. Src-induced phosphorylation of caveolin-2 on tyrosine 19. Phospho-caveolin-2 (Tyr(P)19) is localized near focal adhesions, remains associated with lipid rafts/caveolae, but no longer forms a high molecular mass hetero-oligomer with caveolin-1. *J Biol Chem.* Sep 13 2002;277(37):34556-34567.

55. Sowa G, Pypaert M, Fulton D, et al. The phosphorylation of caveolin-2 on serines 23 and 36 modulates caveolin-1-dependent caveolae formation. *Proc Natl Acad Sci U S A.* May 27 2003;100(11):6511-6516.

56. Wang XB, Lee H, Capozza F, et al. Tyrosine phosphorylation of caveolin-2 at residue 27: differences in the spatial and temporal behavior of phospho-Cav-2 (pY19 and pY27). *Biochemistry.* Nov 2 2004;43(43):13694-13706.

57. Razani B, Engelman JA, Wang XB, et al. Caveolin-1 null mice are viable, but show evidence of hyper- proliferative and vascular abnormalities. *J Biol Chem.* 2001;16:16.

58. Razani B, Wang XB, Engelman JA, et al. Caveolin-2-deficient mice show evidence of severe pulmonary dysfunction without disruption of caveolae. *Mol Cell Biol.* Apr 2002;22(7):2329-2344.

59. Drab M, Verkade P, Elger M, et al. Loss of caveolae, vascular dysfunction, and pulmonary defects in caveolin-1 gene-disrupted mice. *Science.* Sep 28 2001;293(5539):2449-2452.

60.   Mora R, Bonilha VL, Marmorstein A, et al. Caveolin-2 localizes to the golgi complex but redistributes to plasma membrane, caveolae, and rafts when co-expressed with caveolin-1. *J Biol Chem.* Sep 3 1999;274(36):25708-25717.

61.   Cohen AW, Park DS, Woodman SE, et al. Caveolin-1 null mice develop cardiac hypertrophy with hyperactivation of p42/44 MAP kinase in cardiac fibroblasts. *Am J Physiol Cell Physiol.* Feb 2003;284(2):C457-474.

62.   Chang L, Goldman RD. Intermediate filaments mediate cytoskeletal crosstalk. *Nat Rev Mol Cell Biol.* Aug 2004;5(8):601-613.

63.   Gundersen GG. Evolutionary conservation of microtubule-capture mechanisms. *Nat Rev Mol Cell Biol.* Apr 2002;3(4):296-304.

64.   Revenu C, Athman R, Robine S, et al. The co-workers of actin filaments: from cell structures to signals. *Nat Rev Mol Cell Biol.* Aug 2004;5(8):635-646.

65.   Herrmann H, Hesse M, Reichenzeller M, et al. Functional complexity of intermediate filament cytoskeletons: from structure to assembly to gene ablation. *Int Rev Cytol.* 2003;223:83-175.

66.   Goldman RD, Khuon S, Chou YH, et al. The function of intermediate filaments in cell shape and cytoskeletal integrity. *J Cell Biol.* Aug 1996;134(4):971-983.

67.   Goldman RD. The role of three cytoplasmic fibers in BHK-21 cell motility. I. Microtubules and the effects of colchicine. *J Cell Biol.* Dec 1971;51(3):752-762.

68.   Yoon KH, Yoon M, Moir RD, et al. Insights into the dynamic properties of keratin intermediate filaments in living epithelial cells. *J Cell Biol.* Apr 30 2001;153(3):503-516.

69.   Green KJ, Geiger B, Jones JC, et al. The relationship between intermediate filaments and microfilaments before and during the formation of desmosomes and adherens-type junctions in mouse epidermal keratinocytes. *J Cell Biol.* May 1987;104(5):1389-1402.

70.   Pyle WG, Solaro RJ. At the crossroads of myocardial signaling: the role of Z-discs in intracellular signaling and cardiac function. *Circ Res.* Feb 20 2004;94(3):296-305.

71.   Mineo C, Ying YS, Chapline C, et al. Targeting of protein kinase Calpha to caveolae. *Journal of Cell Biology.* 1998;141(3):601-610.

72.   Parton RG, Joggerst B, Simons K. Regulated internalization of caveolae. *J Cell Biol.* Dec 1994;127(5):1199-1215.

73.   Stahlhut M, van Deurs B. Identification of filamin as a novel ligand for caveolin-1: evidence for the organization of caveolin-1-associated membrane domains by the actin cytoskeleton. *Mol Biol Cell.* Jan 2000;11(1):325-337.

74.   Mundy DI, Machleidt T, Ying YS, et al. Dual control of caveolar membrane traffic by microtubules and the actin cytoskeleton. *J Cell Sci.* Nov 15 2002;115(Pt 22):4327-4339.

75.   Pelkmans L, Puntener D, Helenius A. Local actin polymerization and dynamin recruitment in SV40-induced internalization of caveolae. *Science.* Apr 19 2002;296(5567):535-539.

76.   Engqvist-Goldstein AE, Drubin DG. Actin assembly and endocytosis: from yeast to mammals. *Annu Rev Cell Dev Biol.* 2003;19:287-332.

77.   Thomsen P, Roepstorff K, Stahlhut M, et al. Caveolae are highly immobile plasma membrane microdomains, which are not involved in constitutive endocytic trafficking. *Mol Biol Cell.* Jan 2002;13(1):238-250.

78.   Kanzaki M, Pessin JE. Caveolin-associated filamentous actin (Cav-actin) defines a novel F-actin structure in adipocytes. *J Biol Chem.* Jul 19 2002;277(29):25867-25869.

79.   Tsutsui H, Ishihara K, Cooper Gt. Cytoskeletal role in the contractile dysfunction of hypertrophied myocardium. *Science.* Apr 30 1993;260(5108):682-687.

80.   Tagawa H, Wang N, Narishige T, et al. Cytoskeletal mechanics in pressure-overload cardiac hypertrophy. *Circ Res.* Feb 1997;80(2):281-289.

81.   Zile MR, Green GR, Schuyler GT, et al. Cardiocyte cytoskeleton in patients with left ventricular pressure overload hypertrophy. *J Am Coll Cardiol.* Mar 15 2001;37(4):1080-1084.

82.   Tagawa H, Koide M, Sato H, et al. Cytoskeletal role in the transition from compensated to decompensated hypertrophy during adult canine left ventricular pressure overloading. *Circ Res.* Apr 20 1998;82(7):751-761.

83.   Ishibashi Y, Tsutsui H, Yamamoto S, et al. Role of microtubules in myocyte contractile dysfunction during cardiac hypertrophy in the rat. *Am J Physiol.* Nov 1996;271(5 Pt 2):H1978-1987.

84.   Lampidis TJ, Kolonias D, Savaraj N, et al. Cardiostimulatory and antiarrhythmic activity of tubulin-binding agents. *Proc Natl Acad Sci U S A.* Feb 15 1992;89(4):1256-1260.

85.   Lampidis TJ, Trevorrow KW, Rubin RW. Effects of colchicine on cardiac cell function indicate possible role for membrane surface tubulin. *Exp Cell Res.* Jun 1986;164(2):463-470.

86.   Webster DR, Patrick DL. Beating rate of isolated neonatal cardiomyocytes is regulated by the stable microtubule subset. *Am J Physiol Heart Circ Physiol.* May 2000;278(5):H1653-1661.

87.   Kolodney MS, Elson EL. Contraction due to microtubule disruption is associated with increased phosphorylation of myosin regulatory light chain. *Proc Natl Acad Sci U S A.* Oct 24 1995;92(22):10252-10256.

88.   Paul RJ, Bowman PS, Kolodney MS. Effects of microtubule disruption on force, velocity, stiffness and [Ca(2+)](i) in porcine coronary arteries. *Am J Physiol Heart Circ Physiol.* Nov 2000;279(5):H2493-2501.

89.   Galli A, DeFelice LJ. Inactivation of L-type Ca channels in embryonic chick ventricle cells: dependence on the cytoskeletal agents colchicine and taxol. *Biophys J.* Dec 1994;67(6):2296-2304.

90.   Unno T, Komori S, Ohashi H. Microtubule cytoskeleton involvement in muscarinic suppression of voltage-gated calcium channel current in guinea-pig ileal smooth muscle. *Br J Pharmacol.* Aug 1999;127(7):1703-1711.

91.   Palmer BM, Valent S, Holder EL, et al. Microtubules modulate cardiomyocyte beta-adrenergic response in cardiac hypertrophy. *Am J Physiol.* Nov 1998;275(5 Pt 2):H1707-1716.

92.   Limas C, Limas CJ. Disparate effects of colchicine on thyroxine-induced cardiac hypertrophy and adrenoceptor changes. *Circ Res.* Jan 1991;68(1):309-313.

93.   Collins JF, Pawloski-Dahm C, Davis MG, et al. The role of the cytoskeleton in left ventricular pressure overload hypertrophy and failure. *J Mol Cell Cardiol.* Jul 1996;28(7):1435-1443.

94.   Bailey BA, Dipla K, Li S, et al. Cellular basis of contractile derangements of hypertrophied feline ventricular myocytes. *J Mol Cell Cardiol.* Jul 1997;29(7):1823-1835.

95.   Cicogna AC, Robinson KG, Conrad CH, et al. Direct effects of colchicine on myocardial function: studies in hypertrophied and failing spontaneously hypertensive rats. *Hypertension.* Jan 1999;33(1):60-65.

96.   Huang C, Hepler J, Chen L, et al. Organization of G proteins and adenylyl cyclase at the plasma membrane. *Mol Biol Cell.* 1997;8:2365-2378.

97.   Ostrom RS, Violin JD, Coleman S, et al. Selective enhancement of beta-adrenergic receptor signaling by overexpression of adenylyl cyclase type 6: colocalization of receptor and adenylyl cyclase in caveolae of cardiac myocytes. *Mol Pharmacol.* 2000;57(5):1075-1079.

98.   Stan RV, Roberts WG, Predescu D, et al. Immunoisolation and partial characterization of endothelial plasmalemmal vesicles (caveolae). *Molecular Biology of the Cell.* 1997;8(4):595-605.

99.   Ostrom RS, Post SR, Insel PA. Stoichiometry and compartmentation in G protein-coupled receptor signaling: implications for therapeutic interventions involving Gs. *Journal of Pharmacology and Experimental Therapeutics.* July 1, 2000 2000;294(2):407-412.

100. Mitcheson JS, Hancox JC, Levi AJ. Cultured adult cardiac myocytes: future applications, culture methods, morphological and electrophysiological properties. *Cardiovasc Res.* Aug 1998;39(2):280-300.

101. Song KS, Li S, Okamoto T, et al. Co-purification and direct interaction of Ras with caveolin, an integral membrane protein of caveolae microdomains. Detergent-free purification of caveolae microdomains. *J Biol Chem.* Apr 19 1996;271(16):9690-9697.

102. Feron O, Smith TW, Michel T, et al. Dynamic targeting of the agonist-stimulated m2 muscarinic acetylcholine receptor to caveolae in cardiac myocytes. *Journal of Biological Chemistry.* 1997;272(28):17744-17748.

103. Carozzi AJ, Ikonen E, Lindsay MR, et al. Role of cholesterol in developing T-tubules: analogous mechanisms for T-tubule and caveolae biogenesis. *Traffic.* Apr 2000;1(4):326-341.

104. Brette F, Orchard C. T-tubule function in mammalian cardiac myocytes. *Circ Res.* Jun 13 2003;92(11):1182-1192.

105. Costantin LL. The role of sodium current in the radial spread of contraction in frog muscle fibers. *J Gen Physiol.* Jun 1970;55(6):703-715.

106. Gonzalez-Serratos H. Inward spread of activation in vertebrate muscle fibers. *J Physiol.* Feb 1971;212(3):777-799.

107. Nakajima S, Gilai A. Radial propagation of muscle action potential along the tubular system examined by potential-sensitive dyes. *J Gen Physiol.* Dec 1980;76(6):751-762.

108. Soeller C, Cannell MB. Examination of the transverse tubular system in living cardiac rat myocytes by 2-photon microscopy and digital image-processing techniques. *Circ Res.* Feb 19 1999;84(3):266-275.

109. Scriven DR, Dan P, Moore ED. Distribution of proteins implicated in excitation-contraction coupling in rat ventricular myocytes. *Biophys J.* Nov 2000;79(5):2682-2691.

110. Fryer RM, Hsu AK, Nagase H, et al. Opioid-induced cardioprotection against myocardial infarction and arrhythmias: mitochondrial versus sarcolemmal ATP-sensitive potassium channels. *J Pharmacol Exp Ther.* 2000;294:451-457.

111. Schultz JE, Rose E, Yao Z, et al. Evidence for involvement of opioid receptors in ischemic preconditioning in rat hearts. *American Journal of Physiology.* 1995;268:H2157-2161.

112. Yu X-C, Wang H-X, Pei J-M, et al. Anti-arrhythmic effect of κ-opioid receptor stimulation in the perfused rat heart: involvement of a cAMP-dependent pathway. *J Mol Cell Cardiol.* 1999;31:1809-1819.

113. Ventura C, Bastagli L, Bernardi P, et al. Opioid receptors in rat cardiac sarcolemma: effect of phenylephrine and isoproterenol. *Biochim Biophys Acta.* 1989;987:69-74.

114. Wittert G, Hope P, Pyle D. Tissue distribution of opioid receptor gene expression in the rat. *Biochemical and Biophysical Research Communications.* 1996;218:877-881.

115. Jung NH, Kim HP, Kim BR, et al. Evidence for heme oxygenase-1 association with caveolin-1 and -2 in mouse mesangial cells. *IUBMB Life.* Sep 2003;55(9):525-532.

116. Garcia-Cardena G, Oh P, Liu J, et al. Targeting of nitric oxide synthase to endothelial cell caveolae via palmitoylation: implications for nitric oxide signaling. *Proc Natl Acad Sci U S A.* Jun 25 1996;93(13):6448-6453.

117. Venema VJ, Ju H, Zou R, et al. Interaction of neuronal nitric-oxide synthase with caveolin-3 in skeletal muscle. Identification of a novel caveolin scaffolding/inhibitory domain. *J Biol Chem.* Nov 7 1997;272(45):28187-28190.

118. Feron O, Dessy C, Opel DJ, et al. Modulation of the endothelial nitric-oxide synthase-caveolin interaction in cardiac myocytes. Implications for the autonomic regulation of heart rate. *J Biol Chem.* Nov 13 1998;273(46):30249-30254.

119. Goligorsky MS, Li H, Brodsky S, et al. Relationships between caveolae and eNOS: everything in proximity and the proximity of everything. *Am J Physiol Renal Physiol.* Jul 2002;283(1):F1-10.

120. Shaul PW. Regulation of endothelial nitric oxide synthase: location, location, location. *Annu Rev Physiol.* 2002;64:749-774.

121. Szabadkai G, Horváth A, Spat A, et al. Expression of voltage-dependent calcium channel alpha1 subunits in rat adrenal capsular tissue and single glomerulosa cells. *Endocrine Research.* 1998;24(3-4):425-426.

122. Song KS, Scherer PE, Tang Z, et al. Expression of caveolin-3 in skeletal, cardiac, and smooth muscle cells. Caveolin-3 is a component of the sarcolemma and co-fractionates with dystrophin and dystrophin-associated glycoproteins. *J Biol Chem.* 1996;271(25):15160-15165.

123. Segal SS, Brett SE, Sessa WC. Codistribution of NOS and caveolin throughout peripheral vasculature and skeletal muscle of hamsters. *Am J Physiol.* Sep 1999;277(3 Pt 2):H1167-1177.

124. Rybin VO, Grabham PW, Elouardighi H, et al. Caveolae-associated proteins in cardiomyocytes: caveolin-2 expression and interactions with caveolin-3. *Am J Physiol Heart Circ Physiol.* Jul 2003;285(1):H325-332.

125. Capozza F, Cohen AW, Cheung MW, et al. Muscle-specific interaction of caveolin isoforms: differential complex formation between caveolins in fibroblastic vs. muscle cells. *Am J Physiol Cell Physiol.* Mar 2005;288(3):C677-691.

126. Fryer RM, Eells JT, Hsu AK, et al. Ischemic preconditioning in rats: role for the mitochondrial K_{ATP} channel in the preservation of mitochondrial function. *American Journal of Physiology.* 2000;278:H305-H312.

127. Yabe K-i, Nasa Y, Sato M, et al. Preconditioning preserves mitochondrial function and glycolytic flux during an early period of reperfusion in perfused rat hearts. *Cardiovascular Research.* 1997;33:677-685.

128. Gross GJ, Fryer RM. Mitochondrial K_{ATP} channels triggers or distal effectors of ischemic or pharmacological preconditioning? *Circulation Research.* 2000;87:431-433.

129. Sato T, Sasaki N, Seharaseyon J, et al. Selective pharmacological agents implicate mitochondrial but not sarcolemmal K_{ATP} channels in ischemic cardioprotection. *Circulation.* 2000;101:2418-2423.

130. Taggart MJ. Smooth muscle excitation-contraction coupling: a role for caveolae and caveolins? *News Physiol Sci.* 2001;16:61-65.

131. Park DS, Woodman SE, Schubert W, et al. Caveolin-1/3 double-knockout mice are viable, but lack both muscle and non-muscle caveolae, and develop a severe cardiomyopathic phenotype. *Am J Pathol.* Jun 2002;160(6):2207-2217.

132. Zhao Y-Y, Liu Y, Stan R-V, et al. Defects in caveolin-1 cause dilated cardiomyopathy and pulmonary hypertension in knockout mice. *PNAS.* August 20, 2002 2002;99(17):11375-11380.

133. Vepa S, Scribner WM, Natarajan V. Activation of protein phosphorylation by oxidants in vascular endothelial cells: identification of tyrosine phosphorylation of caveolin. *Free Radic Biol Med.* 1997;22(1-2):25-35.

134. Sanguinetti AR, Cao H, Corley Mastick C. Fyn is required for oxidative- and hyperosmotic-stress-induced tyrosine phosphorylation of caveolin-1. *Biochem J.* Nov 15 2003;376(Pt 1):159-168.

135. Paradies G, Ruggiero FM, Petrosillo G, et al. Age-dependent decline in the cytochrome c oxidase activity in rat heart mitochondria: role of cardiolipin. *FEBS Letters.* 1997;406:136-138.

136. Wagner BA, Buettner GR, Burnes CP. Free radical-mediated lipid peroxidation in cells: oxidizability is a function of cell lipid bis-allylic hydrogen content. *Biochemistry.* 1994;33:4449-4453.

137. Cabiscol E, Levine RL. Carbonic anhydrase III: oxidative modification in vivo and loss of phosphatase activity during aging. *Journal of Biological Chemistry.* 1995;270:14742-14747.

138. Dean RT, Fu S, Stocker R, et al. Biochemistry and pathology of radical-mediated protein oxidation. *Biochemical Journal.* 1997;324:1-18.

139. Starke PE, Oliver CN, Stadtman ER. Modification of hepatic proteins in rats exposed to high oxygen concentration. *FASEB Journal.* 1987;1:36-39.

140. Jackson JH, Schraufstatter IU, Hyslop PA, et al. Role of oxidants in DNA damage: hydroxyl radical mediates the synergistic DNA damaging effects of asbestos and cigarette smoke. *Journal of Clinical Investigation.* 1987;80:1090-1095.

141. Schraufstatter IU, Hyslop PA, Jackson J, et al. Oxidant injury of cells. *International Journal of Tissue Reactions.* 1987;9:317-324.

142. Chen YH, Yet SF, Perrella MA. Role of heme oxygenase-1 in the regulation of blood pressure and cardiac function. *Exp Biol Med (Maywood).* May 2003;228(5):447-453.

143. Fang FC. Perspectives series: host/pathogen interactions. Mechanisms of nitric oxide-related antimicrobial activity. *J Clin Invest.* Jun 15 1997;99(12):2818-2825.

144. Moncada S, Higgs EA. Molecular mechanisms and therapeutic strategies related to nitric oxide. *FASEB Journal.* 1995;9:1319-1330.

145. Sass G, Seyfried S, Parreira Soares M, et al. Cooperative effect of biliverdin and carbon monoxide on survival of mice in immune-mediated liver injury. *Hepatology.* Nov 2004;40(5):1128-1135.

146. Nakao A, Neto JS, Kanno S, et al. Protection against ischemia/reperfusion injury in cardiac and renal transplantation with carbon monoxide, biliverdin and both. *Am J Transplant.* Feb 2005;5(2):282-291.

147. Stocker R. Antioxidant activities of bile pigments. *Antioxid Redox Signal.* Oct 2004;6(5):841-849.

148. Sasaki N, Sato T, Ohler A, et al. Activation of mitochondrial ATP-dependent potassium channels by nitric oxide. *Circulation.* 2000;101:439-445.

149. Carroll R, Gant VA, Yellon DM. Mitochondrial K (ATP) channel opening protects a human atrial-derived cell line by a mechanism involving free radical generation. *Cardiovascular Research.* 2001;51:691-700.

150. Lakkisto P, Palojoki E, Backlund T, et al. Expression of heme oxygenase-1 in response to myocardial infarction in rats. *J Mol Cell Cardiol.* Oct 2002;34(10):1357-1365.

151. Katori M, Buelow R, Ke B, et al. Heme oxygenase-1 overexpression protects rat hearts from cold ischemia/reperfusion injury via an antiapoptotic pathway. *Transplantation.* Jan 27 2002;73(2):287-292.

152. Clark JE, Foresti R, Sarathchandra P, et al. Heme oxygenase-1-derived bilirubin ameliorates postischemic myocardial dysfunction. *Am J Physiol Heart Circ Physiol.* Feb 2000;278(2):H643-651.

153. Li WP, Liu P, Pilcher BK, et al. Cell-specific targeting of caveolin-1 to caveolae, secretory vesicles, cytoplasm or mitochondria. *J Cell Sci.* 2001;114(Pt 7):1397-1408.

154. Parton RG, Richards AA. Lipid rafts and caveolae as portals for endocytosis: new insights and common mechanisms. *Traffic.* Nov 2003;4(11):724-738.

155. Isshiki M, Anderson RG. Function of caveolae in Ca2+ entry and Ca2+-dependent signal transduction. *Traffic.* Nov 2003;4(11):717-723.

156. van der Heyden MA, Wijnhoven TJ, Opthof T. Molecular aspects of adrenergic modulation of cardiac L-type Ca2+ channels. *Cardiovasc Res.* Jan 1 2005;65(1):28-39.

157. Insel PA, Kennedy MS. Colchicine potentiates beta-adrenoreceptor-stimulated cyclic AMP in lymphoma cells by an action distal to the receptor. *Nature.* Jun 8 1978;273(5662):471-473.

158. Rasenick MM, Stein PJ, Bitensky MW. The regulatory subunit of adenylate cyclase interacts with cytoskeletal components. *Nature.* Dec 10 1981;294(5841):560-562.

159. Donati RJ, Rasenick MM. Chronic antidepressant treatment prevents accumulation of gsalpha in cholesterol-rich, cytoskeletal-associated, plasma membrane domains (lipid rafts). *Neuropsychopharmacology.* Jul 2005;30(7):1238-1245.

160. Mons S, Veretout F, Carlier M, et al. The interaction between lipid derivatives of colchicine and tubulin: consequences of the interaction of the alkaloid with lipid membranes. *Biochim Biophys Acta.* Sep 29 2000;1468(1-2):381-395.

161. van Deurs B, von Bulow F, Vilhardt F, et al. Destabilization of plasma membrane structure by prevention of actin polymerization. Microtubule-dependent tubulation of the plasma membrane. *J Cell Sci.* Jul 1996;109 (Pt 7):1655-1665.

162. Jasper JR, Post SR, Desai KH, et al. Colchicine and cytochalasin B enhance cyclic AMP accumulation via postreceptor actions. *J Pharmacol Exp Ther.* 1995;274(2):937-942.

163. Goto Y, Yoshikane H, Honda M, et al. Three-dimensional observation on sarcoplasmic reticulum and caveolae in myocardium of spontaneously hypertensive rats. *J Submicrosc Cytol Pathol.* Oct 1990;22(4):535-542.

164. Howarth FC, Calaghan SC, Boyett MR, et al. Effect of the microtubule polymerizing agent taxol on contraction, Ca2+ transient and L-type Ca2+ current in rat ventricular myocytes. *J Physiol.* Apr 15 1999;516 (Pt 2):409-419.

165.   Deng L, Fairbank NJ, Cole DJ, et al. Airway smooth muscle tone modulates mechanically induced cytoskeletal stiffening and remodeling. *J Appl Physiol.* Aug 2005;99(2):634-641.

166.   Chaldakov GN, Nabika T, Nara Y, et al. Cyclic AMP- and cytochalasin B-induced arborization in cultured aortic smooth muscle cells: its cytopharmacological characterization. *Cell Tissue Res.* Feb 1989;255(2):435-442.

167.   Naito M, Hayashi T, Kuzuya M, et al. Vascular endothelial cell migration in vitro roles of cyclic nucleotides, calcium ion and cytoskeletal system. *Artery.* 1989;17(1):21-31.

168.   Birukova AA, Birukov KG, Adyshev D, et al. Involvement of microtubules and Rho pathway in TGF-beta1-induced lung vascular barrier dysfunction. *J Cell Physiol.* Sep 2005;204(3):934-947.

169.   Zor U. Role of cytoskeletal organization in the regulation of adenylate cyclase-cyclic adenosine monophosphate by hormones. *Endocr Rev.* Winter 1983;4(1):1-21.

170.   Georget M, Mateo P, Vandecasteele G, et al. Cyclic AMP compartmentation due to increased cAMP-phosphodiesterase activity in transgenic mice with a cardiac-directed expression of the human adenylyl cyclase type 8 (AC8). *Faseb J.* Aug 2003;17(11):1380-1391.

171.   Baillie GS, Scott JD, Houslay MD. Compartmentalisation of phosphodiesterases and protein kinase A: opposites attract. *FEBS Lett.* Jun 13 2005;579(15):3264-3270.

172.   Bacskai BJ, Hochner B, Mahaut-Smith M, et al. Spatially resolved dynamics of cAMP and protein kinase A subunits in Aplysia sensory neurons. *Science.* Apr 9 1993;260(5105):222-226.

173.   Hempel CM, Vincent P, Adams SR, et al. Spatio-temporal dynamics of cyclic AMP signals in an intact neural circuitm. *Nature.* Nov 14 1996;384(6605):166-169.

174.   Zaccolo M, Pozzan T. Discrete microdomains with high concentration of cAMP in stimulated rat neonatal cardiac myocytes. *Science.* Mar 1 2002;295(5560):1711-1715.

175. **del Pozo MA, Balasubramanian N, Alderson NB, et al. Phospho-caveolin-1 mediates integrin-regulated membrane domain internalization.** *Nat Cell Biol.* **Sep 2005;7(9):901-908.**

176. **Kuppuswamy D, Kerr C, Narishige T, et al. Association of tyrosine-phosphorylated c-Src with the cytoskeleton of hypertrophying myocardium.** *J Biol Chem.* **Feb 14 1997;272(7):4500-4508.**

177. **Fox JE, Lipfert L, Clark EA, et al. On the role of the platelet membrane skeleton in mediating signal transduction. Association of GP IIb-IIIa, pp60c-src, pp62c-yes, and the p21ras GTPase-activating protein with the membrane skeleton.** *J Biol Chem.* **Dec 5 1993;268(34):25973-25984.**

178. **Caselli A, Taddei ML, Manao G, et al. Tyrosine-phosphorylated caveolin is a physiological substrate of the low M(r) protein-tyrosine phosphatase.** *J Biol Chem.* **Jun 1 2001;276(22):18849-18854.**

179. **Haunstetter A, Izumo S. Apoptosis: basic mechanisms and implications for cardiovascular disease.** *Circ Res.* **Jun 15 1998;82(11):1111-1129.**

180. **Communal C, Singh K, Pimentel DR, et al. Norepinephrine stimulates apoptosis in adult rat ventricular myocytes by activation of the beta-adrenergic pathway.** *Circulation.* **Sep 29 1998;98(13):1329-1334.**

181. **Communal C, Singh K, Sawyer DB, et al. Opposing effects of beta(1)- and beta(2)-adrenergic receptors on cardiac myocyte apoptosis: role of a pertussis toxin-sensitive G protein.** *Circulation.* **Nov 30 1999;100(22):2210-2212.**

182. **Schultz JEJ, Hsu AK, Barbieri JT, et al. Pertussis toxin abolishes the cardioprotective effect of ischemic preconditioning in intact rat heart.** *Am J Physiol Heart Circ Physiol.* **1998;275:H495-H500.**

183. **Liu H, Zhang HY, McPherson BC, et al. Role of opioid delta1 receptors, mitochondrial K(ATP) channels, and protein kinase C during cardiocyte apoptosis.** *J Mol Cell Cardiol.* **Nov 2001;33(11):2007-2014.**

184. **Narula J, Haider N, Virmani R, et al. Apoptosis in myocytes in end-stage heart failure.** *N Engl J Med.* **Oct 17 1996;335(16):1182-1189.**

185. Olivetti G, Abbi R, Quaini F, et al. Apoptosis in the failing human heart. *N Engl J Med.* Apr 17 1997;336(16):1131-1141.

186. Blankenberg F, Narula J, Strauss HW. In vivo detection of apoptotic cell death: a necessary measurement for evaluating therapy for myocarditis, ischemia, and heart failure. *J Nucl Cardiol.* Sep-Oct 1999;6(5):531-539.

187. Olivetti G, Quaini F, Sala R, et al. Acute myocardial infarction in humans is associated with activation of programmed myocyte cell death in the surviving portion of the heart. *J Mol Cell Cardiol.* Sep 1996;28(9):2005-2016.

188. Gottlieb RA, Burleson KO, Kloner RA, et al. Reperfusion injury induces apoptosis in rabbit cardiomyocytes. *J Clin Invest.* Oct 1994;94(4):1621-1628.

189. Saraste A, Pulkki K, Kallajoki M, et al. Apoptosis in human acute myocardial infarction. *Circulation.* Jan 21 1997;95(2):320-323.

190. Schultz JEJ, Hsu AK, Gross GJ. Ischemic preconditioning in the intact rat heart is mediated by δ_1- but not μ- or κ- opioid receptors. *Circulation.* 1998;97:1282-1289.

191. Pugsley MK. The diverse molecular mechanisms responsible for the actions of opioids on the cardiovascular system. *Pharmacol Ther.* Jan 2002;93(1):51-75.

192. Zunkin R, Zunkin, SR. Multiple opiate receptors: emerging concepts. *Life Sciences.* 1981;29:2681-2690.

193. Zhang WM, Jin WQ, Wong TM. Multiplicity of kappa opioid receptor binding in the rat cardiac sarcolemma. *J Mol Cell Cardiol.* 1996;28:1547-1554.

194. Singh K, Xiao L, Remondino A, et al. Adrenergic regulation of cardiac myocyte apoptosis. *J Cell Physiol.* Dec 2001;189(3):257-265.

195. Hasking GJ, Esler MD, Jennings GL, et al. Norepinephrine spillover to plasma in patients with congestive heart failure: evidence of increased overall and cardiorenal sympathetic nervous activity. *Circulation.* Apr 1986;73(4):615-621.

196. Bristow MR. beta-adrenergic receptor blockade in chronic heart failure. *Circulation.* Feb 8 2000;101(5):558-569.

197. Fliss H, Gattinger D. Apoptosis in ischemic and reperfused rat myocardium. *Circ Res.* Nov 1996;79(5):949-956.

198. Zhao ZQ, Nakamura M, Wang NP, et al. Reperfusion induces myocardial apoptotic cell death. *Cardiovasc Res.* Feb 2000;45(3):651-660.

199. Sugden PH, Clerk A. "Stress-responsive" mitogen-activated protein kinases (c-Jun N-terminal kinases and p38 mitogen-activated protein kinases) in the myocardium. *Circ Res.* Aug 24 1998;83(4):345-352.

200. Wang Y, Huang S, Sah VP, et al. Cardiac muscle cell hypertrophy and apoptosis induced by distinct members of the p38 mitogen-activated protein kinase family. *J Biol Chem.* Jan 23 1998;273(4):2161-2168.

201. Nishihara H, Hwang M, Kizaka-Kondoh S, et al. Cyclic AMP promotes cAMP-responsive element-binding protein-dependent induction of cellular inhibitor of apoptosis protein-2 and suppresses apoptosis of colon cancer cells through ERK1/2 and p38 MAPK. *J Biol Chem.* Jun 18 2004;279(25):26176-26183.

202. Communal C, Colucci WS, Singh K. p38 mitogen-activated protein kinase pathway protects adult rat ventricular myocytes against beta -adrenergic receptor-stimulated apoptosis. Evidence for Gi-dependent activation. *J Biol Chem.* Jun 23 2000;275(25):19395-19400.

203. Mastick CC, Brady MJ, Saltiel AR. Insulin stimulates the tyrosine phosphorylation of caveolin. *J Cell Biol.* Jun 1995;129(6):1523-1531.

204. Lee H, Volonte D, Galbiati F, et al. Constitutive and growth factor-regulated phosphorylation of caveolin-1 occurs at the same site (Tyr-14) in vivo: identification of a c-Src/Cav-1/Grb7 signaling cassette. *Mol Endocrinol.* Nov 2000;14(11):1750-1775.

205. Haddock PS, Coetzee WA, Cho E, et al. Subcellular [Ca2+]i gradients during excitation-contraction coupling in newborn rabbit ventricular myocytes. *Circ Res.* Sep 3 1999;85(5):415-427.

206. Chen F, Mottino G, Klitzner TS, et al. Distribution of the Na+/Ca2+ exchange protein in developing rabbit myocytes. *Am J Physiol.* May 1995;268(5 Pt 1):C1126-1132.

207. Clark WA, Decker, R. S., Borg, T. K. *Biology of Isoalted Adult Cardiac Myocytes.* Vol 1. New York, New York: Elsevier Publishing Co., Inc.; 1988.

208. Gabella G. Inpocketings of the cell membrane (caveolae) in the rat myocardium. *J Ultrastruct Res.* Nov 1978;65(2):135-147.

209. Gabella G, Blundell D. Effect of stretch and contraction on caveolae of smooth muscle cells. *Cell Tissue Res.* Jul 5 1978;190(2):255-271.

210. Somlyo AP. Excitation-contraction coupling and the ultrastructure of smooth muscle. *Circ Res.* Oct 1985;57(4):497-507.

211. Ishikawa H. Formation of elaborate networks of T-system tubules in cultured skeletal muscle with special reference to the T-system formation. *J Cell Biol.* Jul 1968;38(1):51-66.

212. Franzini-Armstrong C. Simultaneous maturation of transverse tubules and sarcoplasmic reticulum during muscle differentiation in the mouse. *Dev Biol.* Aug 1991;146(2):353-363.

213. Nixon GF, Mignery GA, Somlyo AV. Immunogold localization of inositol 1,4,5-trisphosphate receptors and characterization of ultrastructural features of the sarcoplasmic reticulum in phasic and tonic smooth muscle. *J Muscle Res Cell Motil.* Dec 1994;15(6):682-700.

214. Sharma VK, Ramesh V, Franzini-Armstrong C, et al. Transport of Ca2+ from sarcoplasmic reticulum to mitochondria in rat ventricular myocytes. *J Bioenerg Biomembr.* Feb 2000;32(1):97-104.

215. Dohm GL, Dudek RW. Role of transverse tubules (T-tubules) in muscle glucose transport. *Adv Exp Med Biol.* 1998;441:27-34.

216. Heinzel FR, Bito V, Volders PG, et al. Spatial and temporal inhomogeneities during Ca2+ release from the sarcoplasmic reticulum in pig ventricular myocytes. *Circ Res.* Nov 29 2002;91(11):1023-1030.

217. **Ander AN, Duggirala SK, Drumm JD, et al. Natriuretic peptide gene expression after beta-adrenergic stimulation in adult mouse cardiac myocytes.** *DNA Cell Biol.* **Oct 2004;23(9):586-591.**

218. **Roth DA, Urasawa K, Leiber D, et al. A substantial proportion of cardiac Gs is not associated with the plasma membrane.** *FEBS Letters.* **1992;296:46-50.**

219. **Page E, Winterfield J, Goings G, et al. Water channel proteins in rat cardiac myocyte caveolae: osmolarity-dependent reversible internalization.** *Am J Physiol.* **Jun 1998;274(6 Pt 2):H1988-2000.**

220. **Sedarat F, Xu L, Moore ED, et al. Colocalization of dihydropyridine and ryanodine receptors in neonate rabbit heart using confocal microscopy.** *Am J Physiol Heart Circ Physiol.* **Jul 2000;279(1):H202-209.**

221. **Agard DA, Hiraoka Y, Shaw P, et al. Fluorescence microscopy in three dimensions.** *Methods Cell Biol.* **1989;30:353-377.**

222. **Agard DA, Sedat JW. Three-dimensional architecture of a polytene nucleus.** *Nature.* **Apr 21 1983;302(5910):676-681.**

223. **Zinchuk O, Fukushima A, Hangstefer E. Dynamics of PAF-induced conjunctivitis reveals differential expression of PAF receptor by macrophages and eosinophils in the rat.** *Cell Tissue Res.* **Sep 2004;317(3):265-277.**

224. **De Vries L, Elenko E, McCaffery JM, et al. RGS-GAIP, a GTPase-activating protein for Galphai heterotrimeric G proteins, is located on clathrin-coated vesicles.** *Mol Biol Cell.* **1998;9(5):1123-1134.**